UNIVERSIDADE FEDERAL DE PERNAMBUCO
DEPARTAMENTO DE FÍSICA-CCEN
PROGRAMA DE PÓS-GRADUAÇÃO EM FÍSICA

FÁBIO GOMES RIBEIRO

STRONGLY CORRELATED ELECTRONS ON THE HONEYCOMB LATTICE: MAGNETISM AND SUPERCONDUCTIVITY

Recife
2015

FÁBIO GOMES RIBEIRO

STRONGLY CORRELATED ELECTRONS ON THE HONEYCOMB LATTICE: MAGNETISM AND SUPERCONDUCTIVITY

Tese apresentada ao Programa de Pós-Graduação em Física da Universidade Federal de Pernambuco, como requisito parcial para a obtenção do título de Doutor em Física.

Orientador:
Prof. Dr. Maurício Domingues Coutinho-Filho
Universidade Federal de Pernambuco

Recife
2015

Catalogação na fonte
Bibliotecário Jefferson Luiz Alves Nazareno CRB 4-1758

R484s Ribeiro, Fábio Gomes.
Strongly correlated electrons on the honeycombb lattice: magnetism and superconductivity / Fábio Gomes Ribeiro . – 2015.
117 f.: fig.

Orientador: Maurício Domingues Coutinho-Filho.
Tese (Doutorado) – Universidade Federal de Pernambuco. CCEN. Física, Recife, 2015.
Inclui referências e apêndices.

1. Física da matéria condensada. 2. Elétrons fortemente correlacionados. I. Coutinho-Filho, Maurício Domingues (Orientador). II. Título.

530.41 CDD (22. ed.) UFPE-FQ 2017-34

FÁBIO GOMES RIBEIRO

STRONGLY CORRELATED ELECTRONS ON THE HONEYCOMB LATTICE: MAGNETISM AND SUPERCONDUCTIVITY

Tese apresentada ao Programa de Pós-Graduação em Física da Universidade Federal de Pernambuco, como requisito parcial para a obtenção do título de Doutor em Física.

Aprovada em: 28/08/2015.

BANCA EXAMINADORA

Prof. Dr. Maurício Domingues Coutinho Filho
Orientador
Universidade Federal de Pernambuco

Prof. Dr. Ernesto Carneiro Pessoa Raposo
Examinador Interno
Universidade Federal de Pernambuco

Prof. Dr. Flávio Menezes de Aguiar
Examinador Interno
Universidade Federal de Pernambuco

Prof. Dr. Fernando Jorge Sampaio Moraes
Examinador Externo
Universidade Federal da Paraíba

Prof. Dr. Mucio Amado Continentino
Examinador Externo
Centro Brasileiro de Pesquisas Físicas

"I dedicate this thesis to my honey mother, Elzani Gomes de Oliveira, for all that she means in my life."

Acknowledgements

I thank God for being with me all the time. God and I know how hard was to face this huge challenge of making this Ph.D. Thesis together with a job in Caruaru (140 km far away).

This work could not reach this form without the expertise of my Ph. D. supervisor Prof. Maurício Coutinho. During these five years and six months, I have had the opportunity of learning how to make research in physics by observing his way of doing it. I really enjoyed, mainly, because he taught me throughout my Ph. D. time by the most effective way: the example. In special, I always keep in my mind his support in 2011.

I really appreciate several discussions with Prof. Renê Montenegro-Filho on various topics of this Thesis. I also thank his friendship.

I thank Prof. Sandra Sampaio for her pretty good hospitality every time that I have been at her house, working with my Ph. D. supervisor.

The strongly support of my honey mother, Elzani de Oliveira, was decisive for me to arrive at this point. During the last years, her guidance have been so much important for me. Certainly, she has a great contribution for this work.

The support of my second mother, Evany Oliveira, in several moments was really significant.

I would like to thank my honey sister, Rayra Ribeiro, for our harmonious friendship and also for her many stimulating words.

My thanks also go to my lovely Manu. She knows why.

Since I began my Ph.D. course, I have spent few days in Teresina. However, every time I have been there I have had nice days together with my mother's family. I thank all of you.

In the Centro Acadêmico do Agreste, I have had the pleasure of meeting nice people. In the Laboratory of Physics (LabPhys), I have shared a nice work environment with Elder Vasconcelos (so far, the most gentle person who I have ever met), Eduardo Novais, Cléssio Leão, Gustavo Camelo and Pedro Henrique. Outside the LabPhys, I really enjoyed the conversations (also the friendship) with Luana Leite, Neide Menezes and Simoninha Xavier.

Sometimes, we really do great friends. I actually thank the friendship of Washington Lima, Jehan Fonseca, Agilson Souza, Saulo Oliveira and Lenival José.

During the years that I spent in LFTC, I met nice guys: Leonardo, Hugo, Plinio, Elizane, Victor, Luiz, Fernando, Aldo. Further, I thank the good friendship of Welington Moreira, Anderson Amaral and Murilo Sodré.

"Perhaps you will not only have some appreciation of this culture; it is even possible that you may want to join in the greatest adventure that the human mind has ever begun." (Richard Feynman)

"Nunca desista do seu sonho. Se acabou numa padaria, procure em outra!" (Aparício Torelly - Barão de Itararé)

Resumo

Diante dos recentes resultados experimentais sobre propriedades magnéticas e supercontudoras de materias compostos com estruturas cristalinas "rede colmeia" (*honeycomb*) e hexagonal, nesta tese utilizamos métodos da teoria de campos e da teoria quântica de muitos corpos para investigar as propriedades magnéticas e supercondutoras do modelo de Hubbard no limite de acoplamento forte na rede *honeycomb*, incluindo os regimes de banda semi-cheia e dopada (buracos). No âmbito do formalismo de integração funcional, obtivemos uma densidade de lagrangiana associada aos graus de liberdade de carga (campos de Grassmann) e de *spin* [campos de calibre SU(2)]. O hamiltoniano relacionado aos graus de liberdade de carga é exatamente diagonalizado. No regime de acoplamento forte, derivamos uma teoria perturbativa de baixa energia adequada para descrever as fases (quânticas) magnéticas e supercondutoras nos regimes de banda semi-cheia e dopada por buracos. No regime de banda semi-cheia investigamos os efeitos das flutuações quânticas de *spin* na fase antiferromagnética (AF) no contexto do modelo de Heisenberg, utilizando uma teoria perturbativa de ondas de *spin* até $\mathcal{O}\left(1/S^2\right)$, onde S é a magnitude do *spin*. Com efeito, calculamos a energia do estado fundamental e a magnetização por sítio, cujos resultados estão em boa concordância com estudos anteriores. Além disso, analisamos a competição AF-VBS (estado cristalino de ligação de valência) por meio do modelo σ não-linear com a presença do termo topológico de Hopf. No desafiante regime dopado por buracos, nossa abordagem possibilitou a derivação de um hamiltoniano t-J e a análise do papel desempenhado pelas flutuações quânticas de carga e de *spin* na energia do estado fundamental da fase AF e, principalmente, no colapso da fase AF para uma dopagem crítica; os resultados são aferidos com recentes simulações de *Grassmann tensor product state*. Em adição, realizamos um estudo extensivo das estruturas eletrônicas do sistema dopado para cada fase competidora, na ausência de flutuações quânticas de *spin*: AF, ferromagnética (FM) e supercondutora (SC) induzida por efeitos puramente eletrônicos com simetria (pareamento tipo singleto) s, $d_{x^2-y^2}$ ou d_{xy}. Neste contexto, uma análise energética do estado fundamental dessas fases revela que a fase AF prevalece no regime de baixa dopagem, enquanto que o estado supercondutor com simetria quiral $d_{x^2-y^2} + id_{xy}$ predomina nas proximidades da singularidade de Van Hove (regime de alta dopagem). Destacamos ainda que uma análise termodinâmica da fase supercondutora demonstra que a temperatura crítica está diretamente relacionada à constante de troca $J = 4t^2/U$, onde t é a amplitude de *hopping* e U é a repulsão coulombiana intra-sítio do modelo de Hubbard (origem puramente eletrônica). Finalmente, ressaltamos que a competição entre as fases AF - $d_{x^2-y^2} + id_{xy}$ SC se manifesta pela ocorrência de uma transição de primeira ordem acompanhada da separação espacial das referidas fases.

Palavras-chave: Fases magnéticas e supercondutoras. Rede *honeycomb*. Modelo de Hubbard no limite de acoplamento forte. Modelo de Heisenberg. Modelo t-J. Modelo σ não-linear.

Abstract

In view of quite recent experimental activities on magnetic and superconducting properties of honeycomb and hexagonal lattice based materials, in this thesis we have used field-theoretic and many-body methods to investigate magnetic and superconducting properties of the large-U Hubbard model on the honeycomb lattice at half-filling and in the hole-doped regime. Within the framework of a functional-integral approach, we obtain the Lagrangian density associated with the charge (Grassmann fields) and spin [SU(2) gauge fields] degrees of freedom. The Hamiltonian related to the charge degrees of freedom is exactly diagonalized. In the strong-coupling regime, we derive a perturbative low-energy theory suitable to describe the (quantum) magnetic and superconducting phases at half-filling and in the hole-doped regime. At half-filling, we deal with the underlying spin degrees of freedom of the quantum antiferromagnetic (AF) Heisenberg model by employing a second-order spin-wave analysis, in which case we have calculated the ground-state energy and the staggered magnetization; the results are in very good agreement with previous studies. Further, in the continuum, we derive a nonlinear σ-model with a topological Hopf term that describes the AF-VBS (valence bond solid) competition. In the challenging hole-doped regime, our approach allows the derivation of a t-J Hamiltonian, and the analysis of the role played by charge and spin quantum fluctuations on the ground-state energy and, particularly, on the breakdown of the AF order at a critical hole doping; the results are benchmarked against recent Grassmann tensor product state simulations. In addition, we have performed an extensive study of the electronic structure of the doped system for each competing phase: AF, ferromagnetic (FM), and (spin-singlet pairing) s-, $d_{x^2-y^2}$ - and d_{xy} -wave superconducting (SC) state induced by purely electronic effects. In this context, an energetic analysis of the ground state of these phases reveal that the AF order prevails for low hole doping, while a dominantly chiral $d_{x^2-y^2} + id_{xy}$ superconducting state was found in the vicinity of the Van Hove singularity (high hole doping). We also stress that a thermodynamic analysis of the superconducting phase shows that the critical temperature is directly related to the exchange constant $J = 4t^2/U$, in which t denotes the hopping amplitude and U the on-site Coulomb repulsion of the Hubbard model (purely electronic origin). Remarkably, the competition between the AF and $d_{x^2-y^2} + id_{xy}$ SC phases takes place by the occurrence of a first-order transition accompanied by a spatial phase separation of the referred phases.

Keywords: Superconducting and magnetic phases. Honeycomb lattice. Large-U Hubbard model. Heisenberg model. t-J model. Nonlinear σ-model.

List of Figures

List of Tables

Contents

1. Introduction

1.1. Strongly Correlated Electrons in Two Dimensions

The advent of quantum mechanics has revolutionized the physicist's view of the world. Together with Einstein's theory of relativity and gravitation, they constitute the most celebrated events in the physics of the twentieth century. After almost a century of intensive research, its laws continue to surprise us. Indeed, its impact has been significant both on the scientific and technological realm. For instance, neither the transistor nor the laser could have been constructed without quantum mechanics. In fact, the two main phenomena that motivate this thesis, magnetism and superconductivity, are only explained using quantum mechanics concepts.

In the beginning of quantum mechanics, Paul Dirac commented in his paper on "Quantum Mechanics of Many-Electron Systems" [1]:

> " The underlying physical laws necessary for the mathematical theory of a large part of physics and the whole of chemistry are thus completely known, and the difficulty is only that the exact application of these laws leads to equations much too complicated to be soluble. It therefore becomes desirable that approximate practical methods of applying quantum mechanics should be developed, which can lead to an explanation of the main features of complex atomic systems without too much computation."

Notwithstanding, despite the fact that quantum mechanics correctly describes electrons and atoms (molecules), a straightforward application of these laws is probably pointless without the development of clever theoretical methods and new concepts, which share common insights with many areas of physics, chemistry, biology, and the so-called complex systems.

On the other hand, Philip W. Anderson, in his brilliant article "More is Different" [2], remarked:

> “ The ability to reduce everything to simple fundamental laws does not imply the ability to start from those laws and reconstruct the universe. At each new level of complexity, entirely new laws, concepts and generalizations are necessary, requiring inspiration and creativity to just as great a degree as in the previous one. The understanding of these behaviors requires research which I think is as fundamental in its nature as any other. ”

Current research in condensed matter physics, particularly that associated with strongly correlated electron systems, is intimately connected with the point of view advocate by Philip W. Anderson.

Nowadays, one among the big challenges in many-body physics is high T_c (transition temperature) superconductivity [3,4]. Since its discovery in the cuprates in 1986 [5], steady progress has been achieved in the understanding of these strongly interacting systems. Notwithstanding, a fully consistent theory is still lacking. It is generally believed that the strong Coulomb repulsion inside the two dimensional CuO_2 planes plays an important role as illustrated in Fig. 1.1 (i.e., the CuO_2 planes are primarily responsible for superconductivity.) The model that is pertinent to this research is the Hubbard model on a square lattice [6].

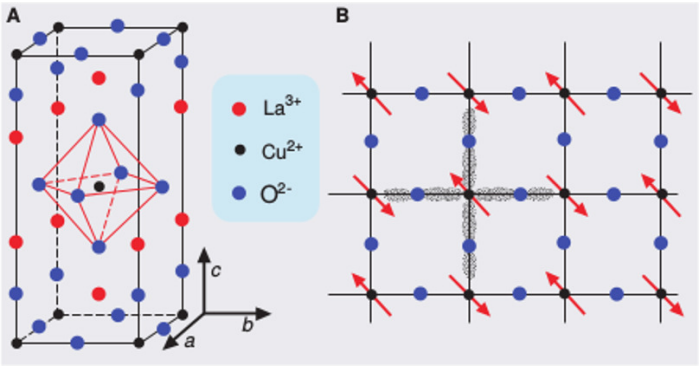

Figure 1.1: (A) Crystal structure of La_2CuO_4, the “parent compound” of the $La_{2-x}Sr_xCuO_4$ family of high-temperature superconductors. The crucial structural subunit is the Cu-O_2 plane, which extends in the $a-b$ direction; parts of three Cu-O_2 planes are shown. Electronic couplings in the interplane (c) direction are very weak. (B) Schematic of Cu-O_2 plane, the crucial structural subunit for high-T_c superconductivity. Red arrows indicate a possible alignment of spins in the antiferromagnetic ground state of La_2CuO_4. Speckled shading indicates oxygen “p_σ orbitals”; coupling through these orbitals leads to superexchange in the insulator and carrier motion in the doped, metallic state. Figure and caption taken from [3].

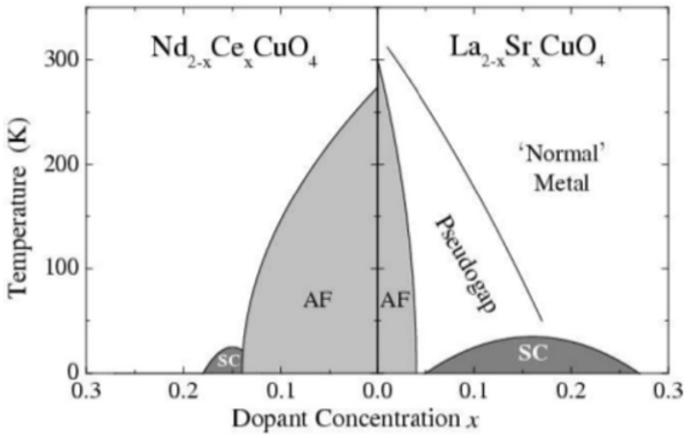

Figure 1.2: Phase diagram of n- and p-type superconductors, showing superconductivity (SC), antiferromagnetic (AF), pseudogap, and normal-metal regions. Figure and caption taken from [7].

The wide range of phenomena displayed in the phase diagram of Fig. 1.2 explain the difficulty of constructing a consistent theory of the cuprate materials. Parts of the phase diagram are well comprehended in their respective framework; however, these cease to be valid for other regions. The undoped system is a good example of a Mott insulator (an insulating state induced by Coulomb interaction and correlation effects) and exhibits antiferromagnetic long range order (AF). This AF order is destroyed by doping, and a superconducting phase emerges. Upon further doping the critical temperature T_c of the superconducting phase raises to its maximum value and beyond the optimal doping T_c decreases, such that the system turns into a normal metal at high enough doping.

The origin of superconductivity is always the main goal, i.e., the mechanism underlying the attraction between electrons. The widely successful Bardeen-Cooper-Schrieffer (BCS) theory of superconductivity [8] provides a good description of many "conventional" superconductors. Within the BCS framework, the two electrons effectively attract each other by an interaction mediated by phonon (quanta of lattice vibrations). A schematic version of this conventional scenario is shown in the upper panel of Fig. 1.3. On the other hand, there are classes of "unconventional" superconductors that can not be understood within the standard (phonon-mediated) BCS framework, but rather the binding of electrons into Cooper pairs might occur via the repulsive Coulomb interaction, without significant help from the lattice vibrations. The unconventional scenario for superconductivity is depicted in the lower panel of Fig. 1.3 [9]. The understanding of these pairing mechanisms in unconventional superconductors has been the focus of extensive theoretical and experimental investigations.

Another topical subject associated with strongly correlated systems is quantum magnetism. Magnetic materials, arising due to itinerant or localized electrons, is ubiquitous in nature and in the laboratory. In the insulating phase a great number

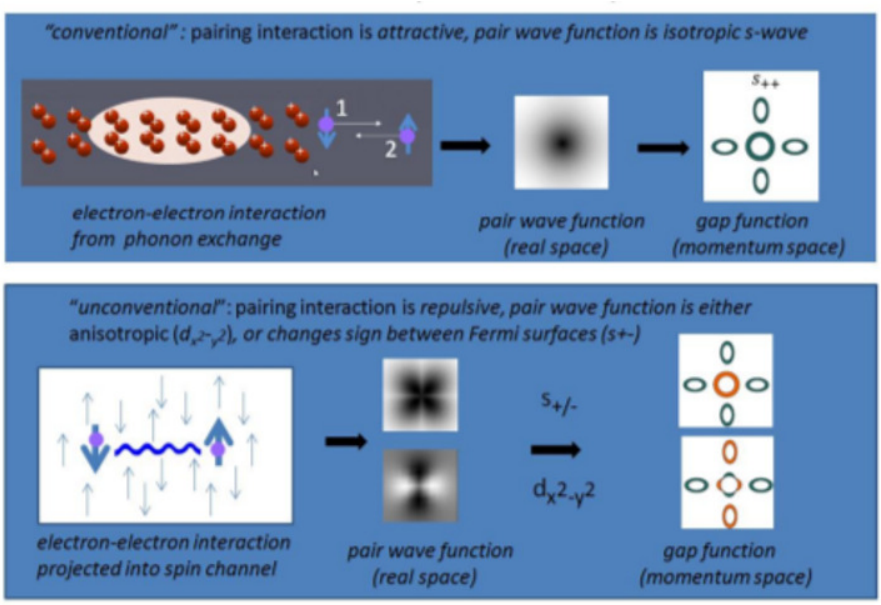

Figure 1.3: **Two routes to superconductivity.** Upper panel: two electrons attract each other when the first (1) polarizes the lattice, and the second (2) is attracted to this region. The pair wave function $\phi(r)$ of the relative electronic coordinate r, has the full symmetry of the crystal and gives rise to a gap function of the same sign everywhere on the Fermi surface (green= +). Lower panel: electrons interact with each other via Coulomb interaction. Shown is an example where the dominant interaction is the magnetic exchange arising between opposite spin electrons due to Coulomb forces. The first electron polarizes the conduction electron gas antiferromagnetically, and an opposite spin electron can lower its energy in this locally polarized region. In this case $\phi(r)$ has a node at the origin, helping to avoid the Coulomb interaction, and can have either s+/- or $d_{x^2-y^2}$ form, as shown. These two possibilities lead to gap functions of opposite sign on the Fermi surface (orange= -). Figure and caption taken from [9].

of these materials are governed by the spins (only degree of freedom) of magnetic ions, coupled via the exchange interaction J; in the context of the Hubbard model $J = 4t^2/U$, where t is the nearest-neighbor hopping amplitude and U is the on-site Coulomb repulsion. In a two dimensional spin systems, strong enough values of U imply in a antiferromagnetic structure, i.e., Néel order. However, for small values of U quantum fluctuations may destroy the Néel order or to turn valence bond solid (VBS) more stable than the Néel phase. The occurrence of a VBS phase and of a quantum critical point separating the referred phases requires the existence of competing exchange interactions, special anisotropies interactions, such as Dzyaloshinskii-Moriya interaction, and topological arguments, as depicted in Fig. 1.4.

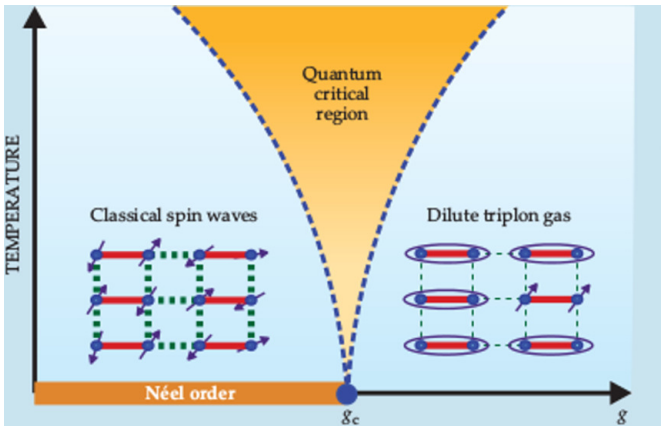

Figure 1.4: Quantum criticality extends to nonzero temperatures. In the blue region for small g, thermal effects induce spin waves that distort the Néel antiferromagnetic ordering. For large g, thermal fluctuations break dimers in the blue region and from quasiparticles called triplon. The dynamics of both types of excitations can be described quasi-classically. Quantum criticality appears in the intermediate orange region, where there is no description of the dynamics in terms of nontrivial entangled quantum excitations of the quantum critical point g_c. Figure and caption taken from [10].

Honeycomb and hexagonal lattice materials has attracted considerable scientific interest in the last decade, due to their remarkable electronic, magnetic and superconducting properties [11]. In the next Sections, we shall discuss magnetism and superconductivity in honeycomb materials.

1.2. Magnetism

In view of quite recent experimental activities on magnetic properties, it has been reported that the undoped Cu^2 ($3d^9$) spin-$\frac{1}{2}$ ($S = 1/2$) compound $In_3Cu_2VO_9$ displays an antiferromagnetic Néel (AF) ground state [12–14]. The magnetic Cu^{2+} (S=1/2) network in the c-plane is expected to take a honeycomb structure with the nonmagnetic V^{5+} ions in the center, as depicted in bottom right-hand side of Fig. 1.5. As each honeycomb layer is well separated from other honeycomb layers by nonmagnetic In^{3+} ions (along the c-axis), this compound can be considered a quasi 2D system. Likewise, experimental evidence has been provided that the undoped materials $Na_3T_2SbO_6$ [15], with T=Cu^{2+}; T=Ni^{2+} ($3d^9 4s^1$; $S = 1$) and T=Co^{2+} ($3d^7$; $S = 3/2$) also exhibit AF order.

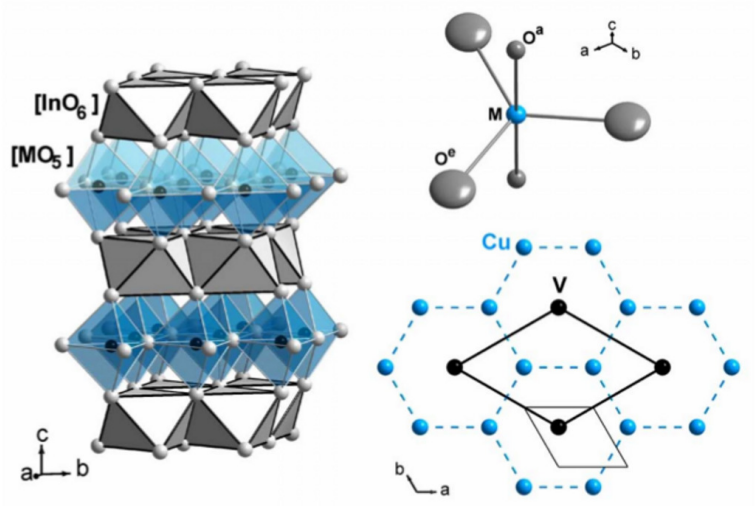

Figure 1.5: Perspective view of the crystal structure of $InCu_{2/3}V_{1/3}O_3$ with $[InO_6]$ and $[MO_5]$ polyhedra (left). On the right (top), a $[MO_5]$ entity is shown with the thermal ellipsoids. Below the in-plane Cu/V order representing in the honeycomb structure (dashed lines) without the oxygen atoms is given with the respective unit cell. Note that there are two distinct crystallographic sites for copper and vanadium. Figure and caption taken from [13].

In addition, it was experimentally observed [16] that the Ru-Ru bonds in the honeycomb lattice material Li_2RuO_3 have a strong tendency to form local dimers with covalent bonds via direct overlap of Ru $4d$ orbitals at temperatures below 270 °C. This signals the formation of a valence bond crystal (VBS), as sketched in Fig. 1.6. Moreover, experimental data have also indicated that the compound Na_2IrO_3 (see Fig. 1.7) displays an AF Mott-insulating ground state [17].

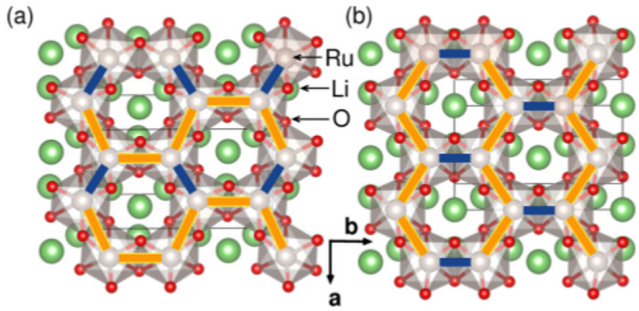

Figure 1.6: Armchair (a) and parallel (b) dimerized structures of Li_2RuO_3. Shorter (dimerized) Ru-Ru bonds are marked with a dark bar, longer bonds with a light bar. Figure and caption taken from [16].

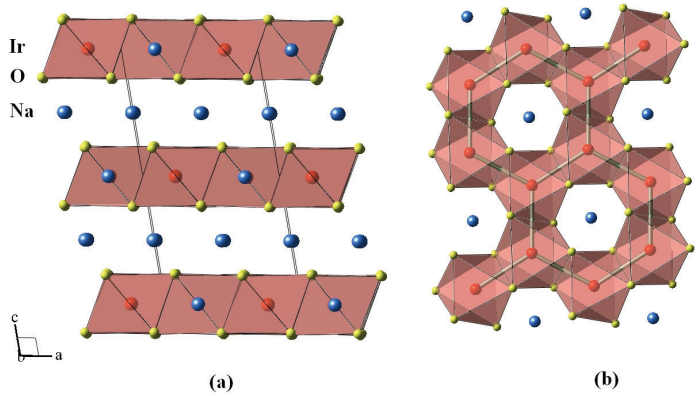

Figure 1.7: The crystallographic structure of Na_2IrO_3. The Na, Ir, and O atoms are shown as blue (black), red (dark gray) , and yellow (light gray) spheres, respectively. (a) The view perpendicular to the c axis showing the layered structure with layers containing only Na atoms alternating slabs of $NaIr_2O_6$ stacked along the c axis. The IrO_6 octahedra are shown in pink with the (red) Ir atoms sitting in the middle. (b) One of the $NaIr_2O_6$ slabs viewed down the c axis to highlight the honeycomb lattice of Ir atoms within the layer. The Na atoms occupy voids between the IrO_6. Figure and caption taken from [17].

In addition, it worth mentioning that the authors in Ref. [18] used polarized neutron spectroscopy to fully characterize the magnetic fluctuations in the metal-organic compound $Cu(DCOO)_2.4D_2O$ (CFTD), a known realization of the quantum square-lattice Heisenberg antiferromagnetic model . In Fig. 1.8 (upper panel), the authors compared the experimental CFTD data, spin-wave theory with first-order and third-order $1/S$ corrections, series expansion, and quantum Monte Carlo. The spin-wave theories described very well the low-energy branches. Effects of fractional excitations (S=1/2) are detected at high energies for $k = (\pi, 0)$ (magnetic zone boundary), as shown in the lower panel of Fig. 1.8.

The physics of electronic correlation in honeycomb and hexagonal lattice materials has been the issue of extensive theoretical investigations [11]. Several attempts have been undertaken with the purpose of describing the underlying mechanisms governing the physical properties of materials mentioned above.

In the context of the Heisenberg model, the occurrence of an AF ground state on the honeycomb lattice at half filling has been studied via quantum Monte Carlo (QMC) simulations [19, 20], second-order spin-wave perturbation theory [21, 22], series expansion [23], and tensor product state (TPS) numerical calculations [24,25] and Grassmann tensor product state (GTPS) [26].

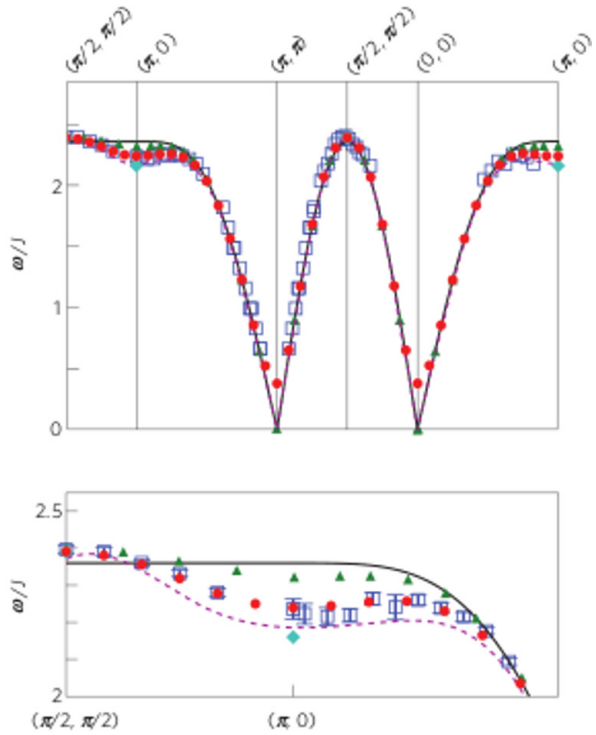

Figure 1.8: Upper panel: The magnon-like dispersion extracted from a (red points) compared to the experimental CFTD data, spin-wave theory with first-order (solid black line) and third-order (green triangles) $1/S$ corrections, series expansion (dashed purple line) and quantum Monte Carlo (cyan diamonds). Lower panel: Zoom-in on the magnon-like mode dispersion along the magnetic zone boundary. Figure and caption taken from [18].

The Hubbard model at half filling and generalized (competitive interactions) Heisenberg models [27] have been used with the aim of describing the possible occurrence of a VBS ground state [28–31]. We remark that in the context of the Hubbard model, QMC simulations have indicated a spin liquid ground state in a wide region of the phase diagram, between a semi-metal (SM) and an antiferromagnetic insulator [32], as shown in Fig. 1.9. However, very recently, Sorella *et al.* [33], by performing detailed QMC calculations, have reexamined the ground-state phase diagram of this model and did not find the occurrence of a VBS or liquid phase. Indeed, they predicted a robust AF phase to occur in the strong-coupling regime (Heisenberg limit), as shown in Fig. 1.10. On the other hand, it has been shown that the AF-VBS competition takes place within the framework of the theory of unconventional quantum critical points [34–37]. Senthil *et. al* [35] have proposed that the AF-VBS transition do not fit into the Landau-Ginzburg-Wilson (LGW) paradigm, since it is a continuous phase transition between two ordered states with different symmetries.

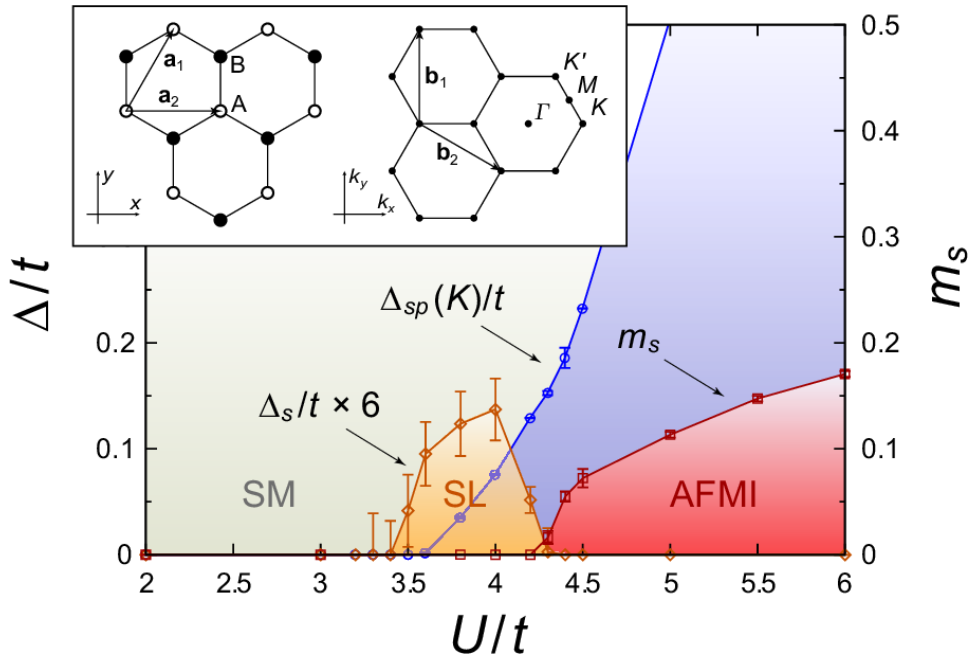

Figure 1.9: **Phase diagram for the Hubbard model on the honeycomb lattice at half-filling**. The semimetal (SM) and the antiferromagnetic Mott insulator (AFMI) are separated by a gapped spin-liquid (SL) phase in an intermediate-coupling regime. $\Delta_{sp}(K)$ denotes the single-particle gap and Δ_s denotes the spin gap; m_s denotes the staggered magnetization, whose saturation value is 1/2. Inset: the honeycomb lattice with primitive vectors $\boldsymbol{a}_1$ and $\boldsymbol{a}_2$, and the reciprocal lattice with primitive vectors $\boldsymbol{b}_1$ and $\boldsymbol{b}_2$. Open and filled sites, respectively, indicate two different sublattices. The Dirac points K and $K^{'}$ and the M and Γ points are marked. Figure and caption taken from Ref. [32].

The crucial elements responsible for this continuous transition are topological objects called hedgehogs.

In a broader perspective, the t-J model has provided a comprehensive framework for investigating the effect of charge and spin quantum fluctuations on doped Mott insulators [38–41]. Recently, a numerical analysis through GTPS [26] calculations of the t-J model on the honeycomb lattice has been reported, in particular the data concerning the breakdown of the AF order due to hole doping, as shown in Fig. 1.11.

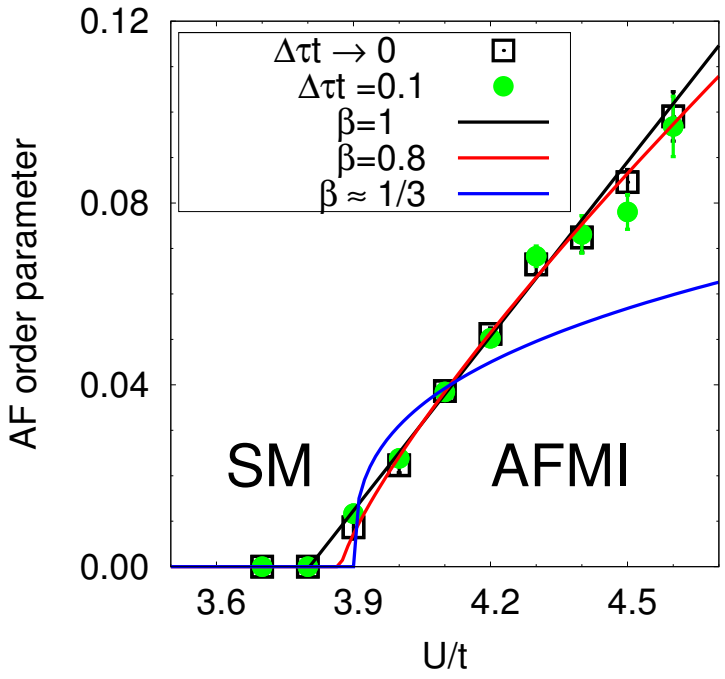

Figure 1.10: **The ground state phase diagram for the half-filled Hubbard model on the honeycomb lattice**. Antiferromagnetic order parameter m_s (open squares) as a function of U/t. The antiferromagnetic order parameter m_s is obtained by finite-size extrapolating the square root of S_{AF}/N, $m_s = \lim_{L\to\infty} \sqrt{S_{AF}/N}$. For comparison, m_s estimated by finite-size extrapolating S_{AF} for $\Delta\tau t$= 0.1 without the $\Delta\tau$ correction is also plotted (solid circles). SM and AFMI stand for semi-metal and antiferromagnetic insulator, respectively. Solid lines are fit of m_s with the critical behavior $m_s = (U_c - U)^{\beta}$, for selected critical exponents β. In any case, the critical U_c ranges from $U_c/t = 3.8 \quad (\beta = 1)$ to $U_c/t = 3.9 \quad (\beta = 0.3362)$. Our best estimate is $U_c/t = 3.869 \pm 0.013$. Figure and caption taken from Ref. [33].

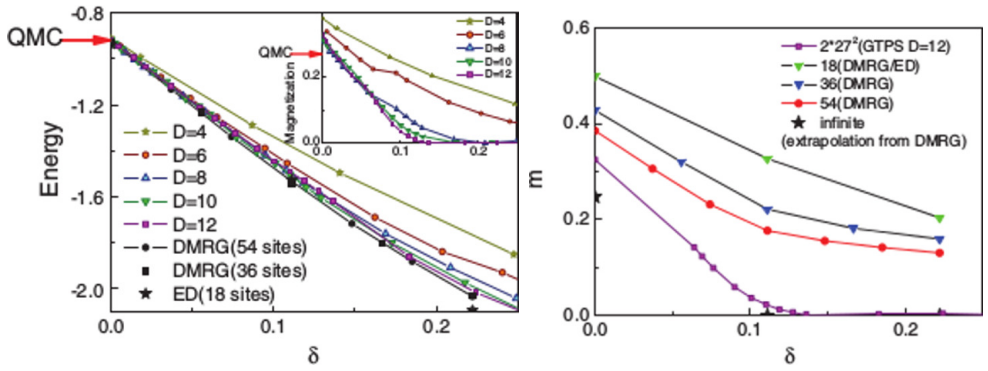

Figure 1.11: Left: ground-state energy as a function of doping. Inset: Stagger magnetization as a function of doping. Right: The comparison of DMRG/ED and GTPS calculations for stagger magnetization m. Figure and caption taken from [26].

1.3. Unconventional Superconductivity

Several experiments have provided evidence of unconventional superconductivity in honeycomb and hexagonal lattice materials. For instance, angle-resolved photoemission spectroscopy (ARPES) measurements have suggested that doped graphene (see Fig. 1.12) might exhibits a purely electronically mediated superconductivity close to the van Hove singularity [42].

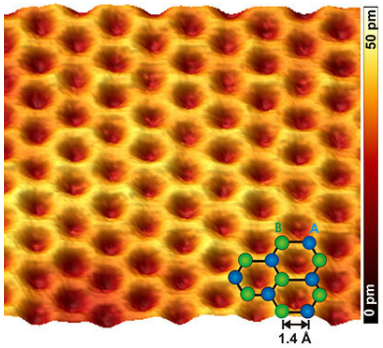

Figure 1.12: STM topography revealing atomically resolved graphene lattice. The blue and green spheres indicate two carbon atoms of the unit cell labeled by A and B. Tunneling parameters are $I = 10$ pA and $U = 50$ mV. Figure and caption taken from [43].

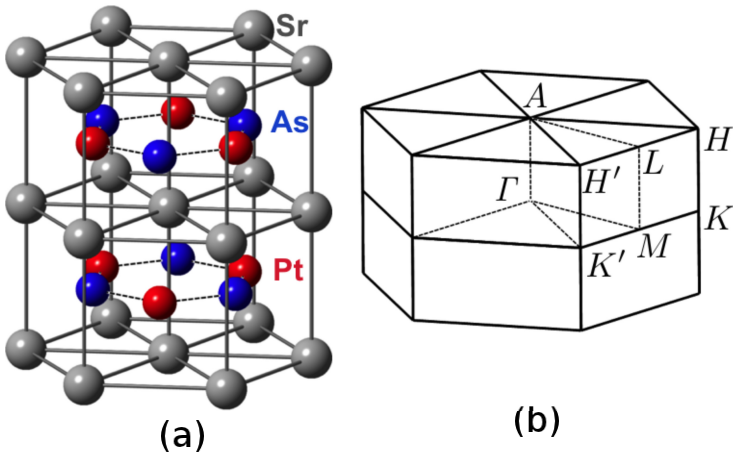

Figure 1.13: (a) Crystal structure of SrPtAs, where red, blue, and grey spheres denote Pt, As, and Sr atoms, respectively. (b) Brillouin zone of SrPtAs and high symmetry points. Figure and caption taken from [44].

Another example is the recently discovered superconducting pnictide, SrPtAs. This compound displays a hexagonal structure with weakly coupled PtAs layers forming a honeycomb lattice, as decipted in Fig. 1.13. Further, it has an interesting physics associated with its hexagonal crystal structure. For example, it exhibits strong spin-orbit coupling at the Pt ions and the PtAs layers break inversion symmetry. Indeed, experimental data have indicated that this material exhibits a chiral d-wave state [44, 45].

Several theoretical attempts have been made to describe the emergence of superconductivity in the above mentioned materials. It was shown by means of functional renormalization group techniques that in the *weak-coupling regime* the purely on-site repulsive Hubbard interaction U can lead to a $d_{x^2-y^2} + id_{xy}$ superconducting state [46], as shown in Figs. 1.14 and 1.15.

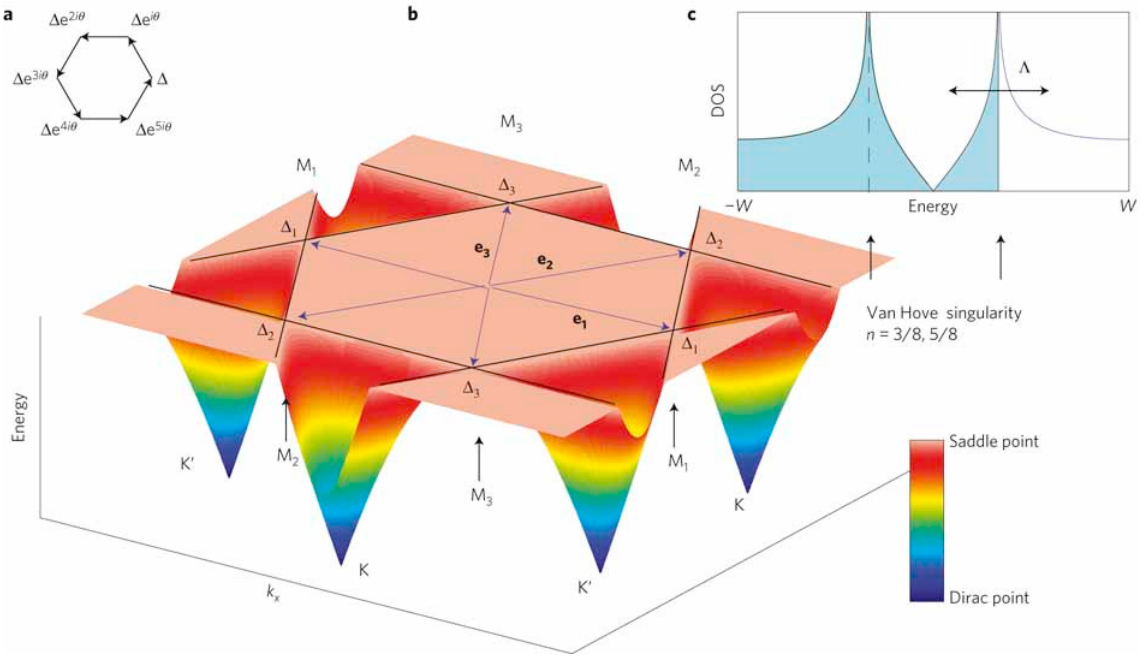

Figure 1.14: **Chiral superconductivity arises when graphene is doped to the van Hove singularity at the saddle point (M points of the Brillouin zone).**(a) $d + id$ pairing exhibiting phase winding around the hexagonal Fermi surface, which breaks TRS and parity ($\theta = 2\pi/3$). (b) Conduction band for monolayer graphene. At 5/8 filling of the π band, the Fermi surface is hexagonal, and the DOS strongly enhances the effect of interactions, driving the system into a chiral superconducting state (a). As the Fermi surface is nested, superconductivity competes with density-wave instabilities, and a full renormalization group treatment is required to establish the dominance of superconductivity. A hexagonal Fermi surface and log divergent density of states also arise at 3/8 filling, giving rise to analogous physics. Figure and caption taken from [46].

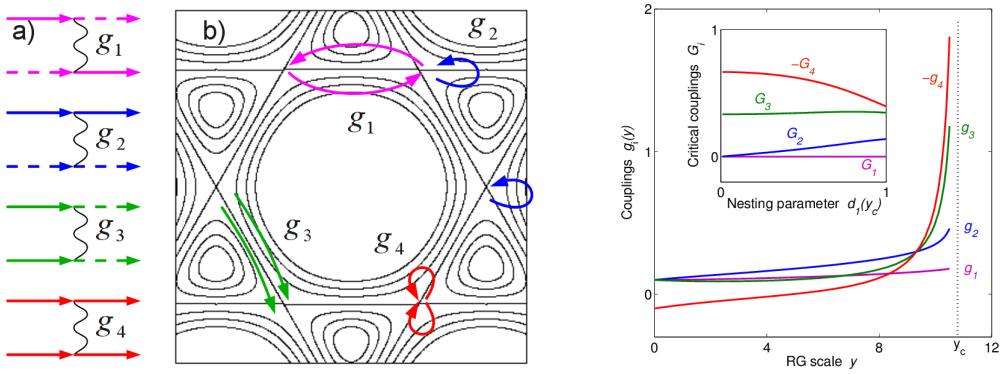

Figure 1.15: **Possible interactions in the patch model.** (a) Feynman diagrams representing allowed two-particle scattering processes among different patches. Solid and dashed lines represent fermions on different patches, whereas wavy lines represent interactions. (b) Pictorial representation of these scattering processes, superimposed on a contour plot of the energy dispersion. Each scattering process comes in three flavours, according to the patches involved. However, it follows by symmetry that the scattering amplitudes are independent of the patches involved, and therefore we suppress the flavour labels. **Flow of coupling with renormalization group scale y, starting from repulsive interactions.** Note that the coupling g_4 changes sign and becomes attractive, leading to a (superconducting) instability at the energy scale y_c. Inset: Critical couplings G_i near y_c as a function of the nesting parameter at the ordering energy scale $d(y_c)$. The dominance of superconductivity over spin-density-wave order arises because $-G_4 > G_2$ for all values of $d_1(y_c)$. The renormalization group flow is obtained of the β-functions with the initial conditions $g_i(0) = 0.1$ and modeling the nesting parameter as $d_1\left(1/\sqrt{1+y}\right)$. The qualitative features of the flow are insensitive to the initial conditions and to how we model d_1. The critical coupling (inset) are universal and independent of the initial conditions. Figure and caption taken form [46].

We also mention that the chiral $d_{x^2-y^2} + id_{xy}$ superconducting state has also been found in the strong-coupling regime using renormalized mean-field theory (RIFT) [47] and GTPS [26]. Notice that in Ref. [47] the calculated values for both s-wave and d-wave pairing parameters are nonzero, even for values of doping above the critical percolation threshold of the honeycomb lattice ($\delta = 0.42 \pm 0.01$; see Chapter 4), as shown in Fig. 1.16. Lastly, we would like to stress that the authors of Ref. [26] did not succeeded in evaluating the pairing superconducting order parameter Δ for doping values higher than $\delta = 0.15$, as shown in Fig. 1.17.

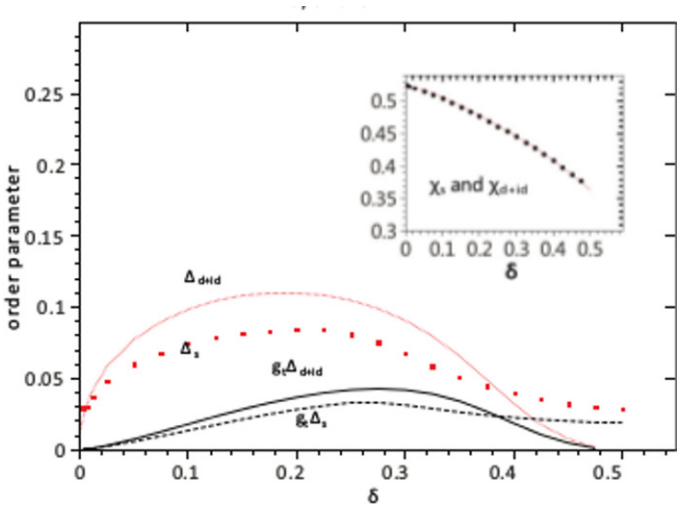

Figure 1.16: Spin gap Δ_{d+id} and Δ_s at $T = 0$ and superconducting transition temperature ($T_c \sim gt$) when $J_2 = 0$ for the $d \pm id$ and ES scenarios as a function of the hole doping parameter $\delta = 1 - n$. The order parameters are taken in units of $3g_sJ/4$. Inset: one can observe that the particle-hole order parameters behave identically for the $d \pm id$ and ES situations. Figure and caption taken from [47].

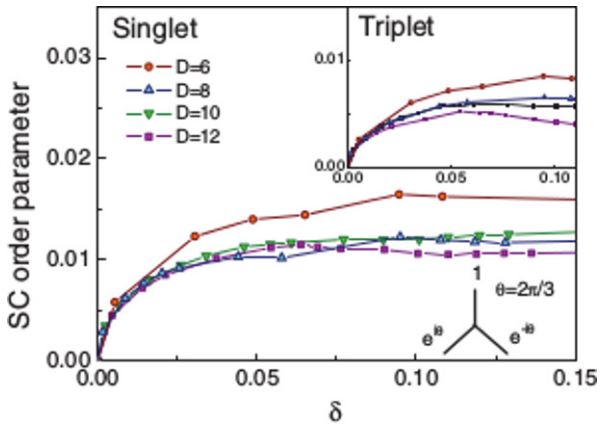

Figure 1.17: SC order parameters as a function of doping. Figure and caption taken from [26].

1.4. Outline of the Thesis

In Chapter 2, we shall use field-theoretic and many-body methods to establish a low-energy perturbative theory suitable to describe the magnetic and superconducting properties of the large-U Hubbard model on the honeycomb lattice at half-filling and in the hole-doped regime. In Chapter 3, we shall deal with the application of the low-energy perturbative Lagrangian density in investigating the effects of charge and spin quantum fluctuations in the breakdown of the AF order on the honeycomb lattice. In Chapter 4, we shall present a systematic study of the competition between superconducting and magnetic phases, using the strong-coupling low-energy effective Lagrangian density. Finally, in Chapter 5, we expose our conclusions.

2. Low-Energy Perturbative Functional Integral Approach of the Hubbard Model

In this chapter, we shall use field-theoretic and many-body methods to establish a low-energy perturbative theory suitable to describe the magnetic and superconducting properties of the large-U Hubbard model on the honeycomb lattice at half-filling and in the hole-doped regime. In Section 2.1, within the framework of a functional-integral approach, we present the Lagrangian density associated with the charge (Grassmann fields) and spin [SU(2) gauge fields] degrees of freedom. Further, in Section 2.2, the Hamiltonian related to the charge degrees of freedom is exactly diagonalized. The electronic dispersion exhibits a gap due to the Coulomb repulsive interaction, while in the tight-binding case we obtain the well known Dirac-like spectrum. Section 2.3 is devoted to the analysis of the strong-coupling regime within a controllable quantitative perturbative scheme, in which case we derive a perturbative low-energy Lagrangian density appropriated to describe both the half-filling and doped regimes. Lastly, in Section 2.4, we draw some final remarks.

2.1. Functional-Integral Representation

The Hamiltonian of the Hubbard model on the honeycomb lattice reads:

$$\mathcal{H} = -t \sum_{\langle \boldsymbol{i}\alpha,\boldsymbol{j}\beta\rangle\sigma} \left(\hat{c}^{\dagger}_{\boldsymbol{i}\alpha\sigma} \hat{c}_{\boldsymbol{j}\beta\sigma} + \hat{c}^{\dagger}_{\boldsymbol{j}\beta\sigma} \hat{c}_{\boldsymbol{i}\alpha\sigma} \right) + U \sum_{\boldsymbol{i}\alpha} \hat{n}_{\boldsymbol{i}\alpha\uparrow} \hat{n}_{\boldsymbol{i}\alpha\downarrow}, \tag{2.1}$$

where $\hat{c}^{\dagger}_{\boldsymbol{i}\alpha\sigma}$ ($\hat{c}_{\boldsymbol{i}\alpha\sigma}$) denotes the creation (annihilation) fermion operator of spin σ ($=\uparrow,\downarrow$) on one of the inequivalent site α=A or B of a unit cell $\boldsymbol{i} = 1, ..., N_c$, with N_c ($N/2$) being the number of unit cells (sites) [see Fig. 2.1(a)]; $\hat{n}_{\boldsymbol{i}\alpha\sigma} = \hat{c}^{\dagger}_{\boldsymbol{i}\alpha\sigma} \hat{c}_{\boldsymbol{i}\alpha\sigma}$ is the electron number operator with spin σ at the position $\boldsymbol{i}\alpha$. The first term describes hopping of electrons with kinetic energy t between nearest-neighbor sites of distinct sublattices, and the second one is the on-site repulsive Coulombian interaction $U > 0$.

Usually the interaction term in Eq.(2.1) is treated by means of the so-called Hubbard-Stratonovich transformation [48], which has been used to develop the functional-integral representation of the Hubbard model suitable to describe di-

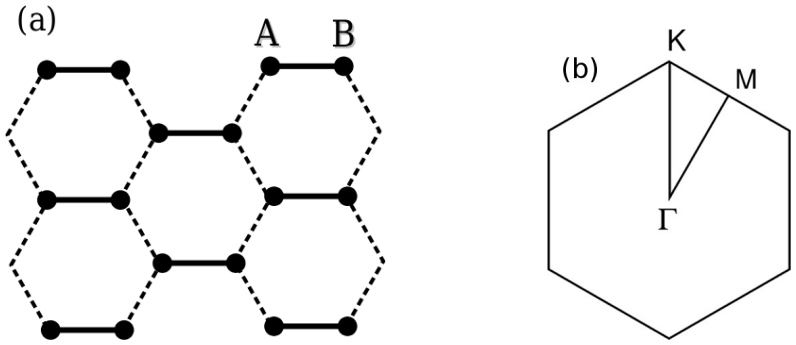

Figure 2.1: (a) Honeycomb lattice in real space with the two inequivalent A and B lattice sites of a unit cell. (b) Conventional representation of the Brillouin zone of the honeycomb lattice with high symmetry points: Γ (center), M (van Hove saddle point) and K.

agrammatic perturbation theory [49], critical phenomena [50] in 3D, and magnetic [51, 52] and superconducting [53] properties in 2D.

On the other hand, in the context of the large-U Hubbard model in 1D [54] and quasi-1D [55], it has been shown that this term can also be treated through the use of a decomposition procedure. Hence, we handle the particle density product in Eq. (2.1) by means of such a decomposition procedure [54, 55], which consist in expressing $\hat{n}_{\boldsymbol{i}\alpha\uparrow}\hat{n}_{\boldsymbol{i}\alpha\downarrow}$ in terms of charge and spin operators:

$$\hat{n}_{\boldsymbol{i}\alpha\uparrow}\hat{n}_{\boldsymbol{i}\alpha\downarrow} = \frac{1}{2}\hat{\rho}_{\boldsymbol{i}\alpha} - 2\left(\hat{\boldsymbol{S}}_{\boldsymbol{i}\alpha}\cdot\boldsymbol{n}_{\boldsymbol{i}\alpha}\right)^2, \tag{2.2}$$

where

$$\hat{\rho}_{\boldsymbol{i}\alpha} = \hat{n}_{\boldsymbol{i}\alpha\uparrow} + \hat{n}_{\boldsymbol{i}\alpha\downarrow}, \tag{2.3}$$

and

$$\hat{\boldsymbol{S}}_{\boldsymbol{i}\alpha} = 1/2\sum_{\sigma\sigma'}\hat{c}^{\dagger}_{\boldsymbol{i}\alpha\sigma'}\boldsymbol{\sigma}_{\sigma'\sigma}\hat{c}_{\boldsymbol{i}\alpha\sigma}, \tag{2.4}$$

are the charge-density and the spin-1/2 operators, respectively, $\boldsymbol{\sigma}_{\sigma'\sigma}$ denotes the Pauli matrix elements ($\hbar \equiv 1$), and $\boldsymbol{n}_{\boldsymbol{i}\alpha}$ is a unit vector field along the spin-quantization axis of an electron at site $\boldsymbol{i}\alpha$. In addition, since the expectation value of the local charge-density operator is 0, 1 or 2, we can write down the formal relation:

$$\left(\hat{\boldsymbol{S}}_{\boldsymbol{i}\alpha}\cdot\boldsymbol{n}_{\boldsymbol{i}\alpha}\right)^2 = \frac{\rho_{\boldsymbol{i}\alpha}(2-\rho_{\boldsymbol{i}\alpha})}{4}, \tag{2.5}$$

which is consistent with the fact that the expectation value of the operator on the left-hand side of the above equation is

$$\langle(\hat{\boldsymbol{S}}_{\boldsymbol{i}\alpha}\cdot\boldsymbol{n}_{\boldsymbol{i}\alpha})^2\rangle = (\pm 1/2)^2 = 1/4. \tag{2.6}$$

Hence, we have formally establish that

$$\hat{\boldsymbol{S}}_{\boldsymbol{i}\alpha} \cdot \boldsymbol{n}_{\boldsymbol{i}\alpha} = p_{\boldsymbol{i}\alpha} \frac{\rho_{\boldsymbol{i}\alpha}(2-\rho_{\boldsymbol{i}\alpha})}{2}, \tag{2.7}$$

where the staggered factor $p_{\boldsymbol{i}\alpha}$ is conveniently chosen to be $p_{\boldsymbol{i}\alpha} = 1$ at the A-sites with spin-up ($\sigma =\uparrow$), and $p_{\boldsymbol{i}\alpha} = -1$ at the B-sites with spin-down ($\sigma =\downarrow$). This choice anticipates the occurrence of a long-range AF ground state at half-filled band. Furthermore, let us define the normalized weight function:

$$\int \prod_{i\alpha} d^2\boldsymbol{n}_{\boldsymbol{i}\alpha} W(\boldsymbol{n}_{\boldsymbol{i}\alpha}) = 1, \tag{2.8}$$

where

$$W(\boldsymbol{n}_{\boldsymbol{i}\alpha}) = \sqrt{\frac{\varphi}{\pi}} \exp\left\{-\varphi\left[\boldsymbol{S}_{\boldsymbol{i}\alpha} \cdot \boldsymbol{n}_{\boldsymbol{i}\alpha} - \frac{p_{\boldsymbol{i}\alpha}}{2}\rho_{\boldsymbol{i}\alpha}(2-\rho_{\boldsymbol{i}\alpha})\right]^2\right\}, \tag{2.9}$$

and $\varphi \to \infty$ (delta-like limit).

In order to determine the partition function

$$\mathcal{Z} = \mathrm{Tr}\left[\exp\left(-\beta\mathcal{H}\right)\right], \tag{2.10}$$

at a temperature $k_B T = 1/\beta$, we are going to use the standard procedure [56–58], i.e., we formally slice the continuous imaginary-time $\tau \in [0, \beta)$ into M finite discrete intervals $[\tau_r, \tau_{r+1})$ of equal size $\delta\tau$, where $r = 0, 1, ..., M-1$, $\tau_0 = 0$, $\tau_M = \beta$ and $\beta = M\delta\tau$, in the limits $M \to \infty$ and $\delta\tau \to 0$. Thus, by using the Trotter formula, we can write down $\mathcal{Z}$ as

$$\mathcal{Z} = \mathrm{Tr}\left\{\hat{T}\prod_{r=0}^{M-1} \exp\left[-\delta\tau\mathcal{H}(\tau_r)\right]\right\}, \tag{2.11}$$

where $\hat{T}$ is the time-ordering operator. We now introduce, between each time interval, an overcomplete basis of fermionic coherent states,

$$1 = \int \prod_{\boldsymbol{i}\alpha\sigma} dc^{\dagger}_{\boldsymbol{i}\alpha\sigma} dc_{\boldsymbol{i}\alpha\sigma} \exp\left(-c^{\dagger}_{\boldsymbol{i}\alpha\sigma} c_{\boldsymbol{i}\alpha\sigma}\right) |c_{\boldsymbol{i}\alpha\sigma}\rangle\langle c_{\boldsymbol{i}\alpha\sigma}|, \tag{2.12}$$

where $\{c^{\dagger}_{\boldsymbol{i}\alpha\sigma}, c_{\boldsymbol{i}\alpha\sigma}\}$ denotes a set of Grassmann fields. Hence, by inserting Eqs. (2.9) and (2.12) into Eq. (2.11), we can rewrite the partition function in the form:

$$\begin{aligned}
\mathcal{Z} \;=\; & \lim_{M\to\infty,\delta\tau\to 0} \mathrm{Tr}\left\{\int \prod_{ir\alpha} d^2\boldsymbol{n}_{\boldsymbol{i}\alpha}(\tau_r)\, W\left[\boldsymbol{n}_{\boldsymbol{i}\alpha}(\tau_r)\right] \exp\left[-\delta\tau U \sum_{\boldsymbol{i}\alpha}\left(\frac{\rho_{\boldsymbol{i}\alpha}}{2}\right.\right.\right. \\
& \left.\left.\left. -2\left(\boldsymbol{S}_{\boldsymbol{i}\alpha} \cdot \boldsymbol{n}_{\boldsymbol{i}\alpha}\right)^2\right)\right]\right\}\left\{\int \prod_{ir\alpha\sigma} dc^{\dagger}_{\boldsymbol{i}\alpha\sigma}(\tau_r)\, dc_{\boldsymbol{i}\alpha\sigma}(\tau_r) \exp\left[-c^{\dagger}_{\boldsymbol{i}\alpha\sigma}(\tau_r)\, c_{\boldsymbol{i}\alpha\sigma}(\tau_r)\right]\right. \\
& \left.\times\langle c_{\boldsymbol{i}\alpha\sigma}(\tau_{r-1}) \mid \exp\left[t\delta\tau \sum_{\langle \boldsymbol{i}\alpha,\boldsymbol{j}\beta\rangle\sigma}\left(c^{\dagger}_{\boldsymbol{i}\alpha\sigma} c_{\boldsymbol{j}\beta\sigma} + \mathrm{H.c.}\right)\right] \mid c_{\boldsymbol{i}\alpha\sigma}(\tau_r)\rangle\right\}.
\end{aligned} \tag{2.13}$$

Let us mention that the above expression is written in terms of the Grassmann fields only. Technically, upon the assessment of the matrix elements entailing coherent states, the set of normally ordered creation ($\hat{c}^{\dagger}_{\boldsymbol{i}\alpha\sigma}$) and annihilation ($\hat{c}_{\boldsymbol{i}\alpha\sigma}$) operators and the set of Grassmann fields ($c^{\dagger}_{\boldsymbol{i}\alpha\sigma}$ and $c_{\boldsymbol{i}\alpha\sigma}$) are formally connected through the map: $\{\hat{c}^{\dagger}_{\boldsymbol{i}\alpha\sigma}, \hat{c}_{\boldsymbol{i}\alpha\sigma}\} \longleftrightarrow \{c^{\dagger}_{\boldsymbol{i}\alpha\sigma}, c_{\boldsymbol{i}\alpha\sigma}\}$. Accordingly, we can formally replace the operators $\hat{\rho}_{\boldsymbol{i}\alpha}$ and $\hat{\boldsymbol{S}}_{\boldsymbol{i}\alpha}$ by their related Grassmann fields $\rho_{\boldsymbol{i}}$ and $\boldsymbol{S}_{\boldsymbol{i}\alpha}$, respectively.

Next, it is important to use the auxiliary result:

$$\begin{aligned}
&\langle c_{\boldsymbol{i}\alpha\sigma}\left(\tau_{r-1}\right) \mid \exp\left[t\delta\tau \sum_{\langle \boldsymbol{i}\alpha,\boldsymbol{j}\beta\rangle\sigma}\left(c^{\dagger}_{\boldsymbol{i}\alpha\sigma}c_{\boldsymbol{j}\beta\sigma}+\text{H.c.}\right)\right] \mid c_{\boldsymbol{i}\alpha\sigma}\left(\tau_{r}\right)\rangle \\
&\times \exp\left[-\sum_{\boldsymbol{i}\alpha\sigma} c^{\dagger}_{\boldsymbol{i}\alpha\sigma}\left(\tau_{r}\right) c_{\boldsymbol{i}\alpha\sigma}\left(\tau_{r}\right)\right] = \exp\left[t\delta\tau \sum_{\langle \boldsymbol{i}\alpha,\boldsymbol{j}\beta\rangle\sigma}\left(c^{\dagger}_{\boldsymbol{i}\alpha\sigma}c_{\boldsymbol{j}\beta\sigma}+\text{H.c.}\right)\right] \\
&\times \exp\left\{-\sum_{\boldsymbol{i}\alpha\sigma} c^{\dagger}_{\boldsymbol{i}\alpha\sigma}\left(\tau_{r}\right)\left[c_{\boldsymbol{i}\alpha\sigma}\left(\tau_{r}\right)-c_{\boldsymbol{i}\alpha\sigma}\left(\tau_{r-1}\right)\right]\right\}, \qquad (2.14)
\end{aligned}$$

in which one should note that in the second exponential of the right-hand side the first and second terms derive from the exponential term in Eq. (2.12) and the factor introduced by the time-ordered matrix element associated with the coherent states $\mid c_{\boldsymbol{i}\alpha\sigma}\left(\tau_{r}\right)\rangle$ and $\mid c_{\boldsymbol{i}\alpha\sigma}\left(\tau_{r-1}\right)\rangle$, respectively.

Bearing in mind that the set of Grassmann fields satisfy anti-periodic boundary conditions in the imaginary-time domain: $c^{\dagger}_{\boldsymbol{i}\alpha\sigma}(0) = -c^{\dagger}_{\boldsymbol{i}\alpha\sigma}(\beta)$ and $c_{\boldsymbol{i}\alpha\sigma}(0) = -c_{\boldsymbol{i}\alpha\sigma}(\beta)$, while the unit vector field satisfies periodic ones: $\boldsymbol{n}_{\boldsymbol{i}\alpha}(0) = \boldsymbol{n}_{\boldsymbol{i}\alpha}(\beta)$, and by considering the limits $M \to \infty$, $\delta\tau \to 0$ together with the Eq. (2.14), we obtain that the partition function takes the form:

$$\mathcal{Z} = \int \prod_{\boldsymbol{i}\alpha} \mathcal{D}^{2}\boldsymbol{n}_{\boldsymbol{i}\alpha} \prod_{\boldsymbol{i}\alpha} \mathcal{D}c^{\dagger}_{\boldsymbol{i}\alpha}\mathcal{D}c_{\boldsymbol{i}\alpha} \exp\left[-\int_{0}^{\beta} \mathcal{L}(\tau)d\tau\right], \qquad (2.15)$$

where the measures are defined by

$$\begin{aligned}
\mathcal{D}^{2}\boldsymbol{n}_{\boldsymbol{i}\alpha} &\equiv \lim_{M\to\infty} \prod_{r=0}^{M-1} d^{2}\boldsymbol{n}_{\boldsymbol{i}\alpha}(\tau_{r}) W[\boldsymbol{n}_{\boldsymbol{i}\alpha}(\tau_{r})]; \\
\mathcal{D}c^{\dagger}_{\boldsymbol{i}\alpha\sigma}\mathcal{D}c_{\boldsymbol{i}\alpha\sigma} &\equiv \lim_{M\to\infty} \prod_{r=0}^{M-1} dc^{\dagger}_{\boldsymbol{i}\alpha\sigma}(\tau_{r}) dc_{\boldsymbol{i}\alpha\sigma}(\tau_{r}), \qquad (2.16)
\end{aligned}$$

and $\mathcal{L}(\tau)$ reads:

$$\begin{aligned}
\mathcal{L}(\tau) \;=\; & \sum_{\boldsymbol{i}\alpha\sigma} c^{\dagger}_{\boldsymbol{i}\alpha\sigma}\partial_{\tau}c_{\boldsymbol{i}\alpha\sigma} - t \sum_{\langle \boldsymbol{i}\alpha,\boldsymbol{j}\beta\rangle\sigma}\left(c^{\dagger}_{\boldsymbol{i}\alpha\sigma}c_{\boldsymbol{j}\beta\sigma} + c^{\dagger}_{\boldsymbol{j}\beta\sigma}c_{\boldsymbol{i}\alpha\sigma}\right) \\
& + U \sum_{\boldsymbol{i}\alpha}\left[\frac{1}{2}\rho_{\boldsymbol{i}\alpha} - p_{\boldsymbol{i}\alpha}\left(\boldsymbol{S}_{\boldsymbol{i}\alpha}\cdot\boldsymbol{n}_{\boldsymbol{i}\alpha}\right)\right]. \qquad (2.17)
\end{aligned}$$

At this stage, it is interesting to consider the symmetry exhibited by the AF order. Here, we shall use a SU(2) matrix [59], where the group space parameter is the surface of the unit S^3-sphere, parametrized according to the symmetry displayed by the AF phase. As the unit vector $\boldsymbol{n}_{\boldsymbol{i}\alpha}$, i.e., the Néel order parameter, lies in the manifold S^2, the corresponding SU(2) matrix, $U_{\boldsymbol{i}\alpha}$, assumes the form [$\det(U_{\boldsymbol{i}\alpha})$=1]:

$$U_{\boldsymbol{i}\alpha} = \begin{bmatrix} \cos\left(\frac{\theta_{\boldsymbol{i}\alpha}}{2}\right) & -\sin\left(\frac{\theta_{\boldsymbol{i}\alpha}}{2}\right) e^{-i\phi_{\boldsymbol{i}\alpha}} \\ \sin\left(\frac{\theta_{\boldsymbol{i}\alpha}}{2}\right) e^{i\phi_{\boldsymbol{i}\alpha}} & \cos\left(\frac{\theta_{\boldsymbol{i}\alpha}}{2}\right) \end{bmatrix}, \tag{2.18}$$

where $\theta_{\boldsymbol{i}\alpha}$ is the polar angle between the z-axis and the unit vector $\boldsymbol{n}_{\boldsymbol{i}\alpha}$, and $\phi_{\boldsymbol{i}\alpha}$ is an arbitrary azimuth angle due to the U(1) gauge freedom. Moreover, it obeys the relation:

$$U^{\dagger}_{\boldsymbol{i}\alpha}(\hat{\sigma}\cdot\boldsymbol{n}_{\boldsymbol{i}\alpha})U_{\boldsymbol{i}\alpha} = \sigma^z, \tag{2.19}$$

which explicitly manifest the rotationally broken symmetry along the z-axis. Notice also that by taking $\theta_{\boldsymbol{i}A} = \theta_{\boldsymbol{i}B} = 0$, together with the proper choice of the staggered factor $p_{\boldsymbol{i}\alpha}$, one obtains the representation for the classical Néel order. In this context, it will prove very useful to introduce a new set of Grassmann fields, $\{a^{\dagger}_{\boldsymbol{i}\alpha\sigma}, a_{\boldsymbol{i}\alpha\sigma}\}$, according to the transformation:

$$a_{\boldsymbol{i}\alpha\sigma} = \sum_{\sigma'} (U_{\boldsymbol{i}\alpha})^{\dagger}_{\sigma\sigma'} c_{\boldsymbol{i}\alpha\sigma'}, \tag{2.20}$$

whose associated spins point along the global z-axis.

Correspondingly, with the help of Eqs. (2.18) and (2.20), the Lagrangian density in Eq. (2.17) is transformed into the following form:

$$\begin{aligned} \mathcal{L}(\tau) &= \sum_{\boldsymbol{i}\alpha\sigma} a^{\dagger}_{\boldsymbol{i}\alpha\sigma}\partial_\tau a_{\boldsymbol{i}\alpha\sigma} + \sum_{\boldsymbol{i}\alpha\sigma\sigma'} a^{\dagger}_{\boldsymbol{i}\sigma'}(U_{\boldsymbol{i}\alpha})^{\dagger}_{\sigma'\sigma}\partial_\tau (U_{\boldsymbol{i}\alpha})_{\sigma'\sigma} a_{\boldsymbol{i}\alpha\sigma} \\ &\quad -t\sum_{\langle \boldsymbol{i}\alpha,\boldsymbol{j}\beta\rangle\sigma}\left(a^{\dagger}_{\boldsymbol{i}\alpha\sigma}a_{\boldsymbol{j}\beta\sigma} + \text{H.c.}\right) + \frac{U}{2}\sum_{\boldsymbol{i}\alpha\sigma}(1 - p_{\boldsymbol{i}\alpha}\sigma)a^{\dagger}_{\boldsymbol{i}\alpha\sigma}a_{\boldsymbol{i}\alpha\sigma} \\ &\quad -t\sum_{\langle \boldsymbol{i}\alpha,\boldsymbol{j}\beta\rangle\sigma\sigma'}\left[a^{\dagger}_{\boldsymbol{i}\alpha\sigma'}\left(U^{\dagger}_{\boldsymbol{i}\alpha}U_{\boldsymbol{j}\beta} - 1\right)_{\sigma'\sigma} a_{\boldsymbol{j}\beta\sigma} + \text{H.c.}\right]. \end{aligned} \tag{2.21}$$

Remarkably, $\mathcal{L}(\tau)$ can be split up into two parts:

$$\mathcal{L}(\tau) = \mathcal{L}_0 + \mathcal{L}_n. \tag{2.22}$$

One with only charge degrees of freedom:

$$\mathcal{L}_0 = \sum_{\boldsymbol{i}\alpha\sigma} a^{\dagger}_{\boldsymbol{i}\alpha\sigma}\partial_\tau a_{\boldsymbol{i}\alpha\sigma} - t\sum_{\langle \boldsymbol{i}\alpha,\boldsymbol{j}\beta\rangle\sigma}\left(a^{\dagger}_{\boldsymbol{i}\alpha\sigma}a_{\boldsymbol{j}\beta\sigma} + \text{H.c.}\right) + \frac{U}{2}\sum_{\boldsymbol{i}\alpha\sigma}(1 - p_{\boldsymbol{i}\alpha}\sigma)a^{\dagger}_{\boldsymbol{i}\alpha\sigma}a_{\boldsymbol{i}\alpha\sigma}, \tag{2.23}$$

and the other describes the coupling between the charge (Grassmann fields $a^{\dagger}_{\boldsymbol{i}\alpha\sigma}$ and $a_{\boldsymbol{i}\alpha\sigma}$) and spin degrees of freedom [SU(2) gauge fields $U_{\boldsymbol{i}\alpha}$]:

$$\begin{aligned}\mathcal{L}_n &= \sum_{\boldsymbol{i}\alpha\sigma\sigma'} a^{\dagger}_{\boldsymbol{i}\alpha\sigma'}(U_{\boldsymbol{i}\alpha})^{\dagger}_{\sigma'\sigma}\partial_\tau(U_{\boldsymbol{i}\alpha})_{\sigma'\sigma}a_{\boldsymbol{i}\alpha\sigma} \\ &\quad -t\sum_{\langle \boldsymbol{i}\alpha,\boldsymbol{j}\beta\rangle\sigma\sigma'}\left[a^{\dagger}_{\boldsymbol{i}\alpha\sigma'}\left(U^{\dagger}_{\boldsymbol{i}\alpha}U_{\boldsymbol{j}\beta}-1\right)_{\sigma'\sigma}a_{j\beta\sigma}+\text{H.c.}\right]. \qquad (2.24)\end{aligned}$$

It should be noted that the Hubbard repulsion U is present only in $\mathcal{L}_0$ [see Eq. (2.23)], while the SU(2) gauge fields $U_{\boldsymbol{i}\alpha}$ only appear in $\mathcal{L}_n$ [see Eq. (2.24)].

2.2. Analysis of Charge Degrees of Freedom in $\mathcal{L}_0$

We now turn our attention to $\mathcal{L}_0$ in Eq. (2.23). By performing the Legendre transform:

$$\mathcal{H}_0 = -\sum_{\boldsymbol{i}\alpha\sigma}\frac{\partial\mathcal{L}_0}{\partial\left(\partial_\tau a_{\boldsymbol{i}\alpha\sigma}\right)}\partial_\tau a_{\boldsymbol{i}\alpha\sigma}+\mathcal{L}_0; \qquad (2.25)$$

where

$$\frac{\partial\mathcal{L}_0}{\partial\left(\partial_\tau a_{\boldsymbol{i}\alpha\sigma}\right)} = a^{\dagger}_{\boldsymbol{i}\alpha\sigma}, \qquad (2.26)$$

we get the Hamiltonian associated with the charge degrees of freedom:

$$\mathcal{H}_0 = -t\sum_{\langle \boldsymbol{i}\alpha,\boldsymbol{j}\beta\rangle\sigma}\left(a^{\dagger}_{\boldsymbol{i}\alpha\sigma}a_{\boldsymbol{j}\beta\sigma}+\text{H.c.}\right)+\frac{U}{2}\sum_{\boldsymbol{i}\alpha\sigma}(1-p_{\boldsymbol{i}\alpha}\sigma)a^{\dagger}_{\boldsymbol{i}\alpha\sigma}a_{\boldsymbol{i}\alpha\sigma}. \qquad (2.27)$$

In order to diagonalize $\mathcal{H}_0$ we need a two step procedure. Initially, we perform a Fourier transform:

$$\begin{aligned}a_{\boldsymbol{k}\sigma} &= \frac{1}{\sqrt{N_c}}\sum_{\boldsymbol{i}}e^{i\boldsymbol{k}\cdot\boldsymbol{i}}a_{\boldsymbol{i}\sigma}; \\ b_{\boldsymbol{k}\sigma} &= \frac{1}{\sqrt{N_c}}\sum_{\boldsymbol{j}}e^{-i\boldsymbol{k}\cdot\boldsymbol{j}}b_{\boldsymbol{j}\sigma}, \qquad (2.28)\end{aligned}$$

where $a_{\boldsymbol{k}\sigma}$ ($b_{\boldsymbol{k}\sigma}$) is the Fourier transform of the Grassmann fields associated with the A (B) sublattice, i.e., for notation convenience we have replaced $a_{\boldsymbol{j}\beta\sigma}\rightarrow b_{\boldsymbol{j}\sigma}$. Inserting Eq. (2.28) into Eq. (2.27) leads to

$$\mathcal{H}_0 = -t\sum_{\boldsymbol{k}\sigma}\left(w^{*}_{\boldsymbol{k}}a^{\dagger}_{\boldsymbol{k}\sigma}b_{\boldsymbol{k}\sigma}+\text{H.c.}\right)+\frac{U}{2}\sum_{\boldsymbol{k}\sigma}(1-\sigma)a^{\dagger}_{\boldsymbol{k}\sigma}a_{\boldsymbol{k}\sigma}, \qquad (2.29)$$

in which

$$w^{*}_{\boldsymbol{k}} = e^{-ik_x}+2e^{i\frac{k_x}{2}}\cos\left(\frac{\sqrt{3}\,k_y}{2}\right). \qquad (2.30)$$

In addition, it is worthwhile to introduce the new set of Grassmann fields [60]:

$$A_{\boldsymbol{k}\sigma} = \frac{a_{\boldsymbol{k}\sigma}}{\sqrt{2}} + \frac{w^*_{\boldsymbol{k}}}{\sqrt{2}|w_{\boldsymbol{k}}|} b_{\boldsymbol{k}\sigma}; \tag{2.31}$$

$$B_{\boldsymbol{k}\sigma} = \frac{a_{\boldsymbol{k}\sigma}}{\sqrt{2}} - \frac{w^*_{\boldsymbol{k}}}{\sqrt{2}|w_{\boldsymbol{k}}|} b_{\boldsymbol{k}\sigma}, \tag{2.32}$$

such that, by substituting Eqs. (2.31) and (2.32) into Eq. (2.29), one finds:

$$\begin{aligned}\mathcal{H}_0 = &-\sum_{\boldsymbol{k}\sigma} \epsilon_{\boldsymbol{k}} \left(A^\dagger_{\boldsymbol{k}\sigma} A_{\boldsymbol{k}\sigma} - B^\dagger_{\boldsymbol{k}\sigma} B_{\boldsymbol{k}\sigma} \right) + \frac{U}{4} \sum_{\boldsymbol{k}\sigma} (1-\sigma) \\ &\left(A^\dagger_{\boldsymbol{k}\sigma} A_{\boldsymbol{k}\sigma} + A^\dagger_{\boldsymbol{k}\sigma} B_{\boldsymbol{k}\sigma} + B^\dagger_{\boldsymbol{k}\sigma} A_{\boldsymbol{k}\sigma} + B^\dagger_{\boldsymbol{k}\sigma} B_{\boldsymbol{k}\sigma} \right),\end{aligned} \tag{2.33}$$

where

$$\epsilon_{\boldsymbol{k}} = t \sqrt{3 + 2\cos\left(\sqrt{3}k_y\right) + 4\cos\left(\frac{3k_x}{2}\right)\cos\left(\frac{\sqrt{3}k_y}{2}\right)}. \tag{2.34}$$

Now, we can diagonalize $\mathcal{H}_0$ in Eq. (2.33) by means of the Bogoliubov transformation [61]:

$$\begin{aligned} A_{\boldsymbol{k}\sigma} &= u_{\boldsymbol{k}} \alpha_{\boldsymbol{k}\sigma} - \sigma v_{\boldsymbol{k}} \beta_{\boldsymbol{k}\sigma}; \\ B_{\boldsymbol{k}\sigma} &= \sigma v_{\boldsymbol{k}} \alpha_{\boldsymbol{k}\sigma} + u_{\boldsymbol{k}} \beta_{\boldsymbol{k}\sigma}, \end{aligned} \tag{2.35}$$

restricted by the canonical constraint

$$(u_{\boldsymbol{k}})^2 + (v_{\boldsymbol{k}})^2 = 1. \tag{2.36}$$

Thus, by plugging Eq. (2.35) into Eq. (2.33), we obtain:

$$\begin{aligned}\mathcal{H}_0 \;=\; &\sum_{\boldsymbol{k}\sigma} \Bigg\{ \left[\epsilon_{\boldsymbol{k}} \left(v^2_{\boldsymbol{k}} - u^2_{\boldsymbol{k}} \right) + \frac{U}{2} - U u_{\boldsymbol{k}} v_{\boldsymbol{k}} \right] \alpha^\dagger_{\boldsymbol{k}\sigma} \alpha_{\boldsymbol{k}\sigma} - \left[2u_{\boldsymbol{k}} v_{\boldsymbol{k}} \epsilon_{\boldsymbol{k}} - \frac{U}{2} \left(u^2_{\boldsymbol{k}} - v^2_{\boldsymbol{k}} \right) \right] \\ &\times \alpha^\dagger_{\boldsymbol{k}\sigma} \beta_{\boldsymbol{k}\sigma} - \left[2u_{\boldsymbol{k}} v_{\boldsymbol{k}} \epsilon_{\boldsymbol{k}} - \frac{U}{2} \left(u^2_{\boldsymbol{k}} - v^2_{\boldsymbol{k}} \right) \right] \beta^\dagger_{\boldsymbol{k}\sigma} \alpha_{\boldsymbol{k}\sigma} + \Bigg[\epsilon_{\boldsymbol{k}} \left(u^2_{\boldsymbol{k}} - v^2_{\boldsymbol{k}} \right) + \frac{U}{2} \\ &+ U u_{\boldsymbol{k}} v_{\boldsymbol{k}} \Bigg] \beta^\dagger_{\boldsymbol{k}\sigma} \beta_{\boldsymbol{k}\sigma} \Bigg\}.\end{aligned} \tag{2.37}$$

Further, with the help of Eq. (2.36) and imposing that the off-diagonal terms in Eq. (2.37) must vanish; we get the diagonal form of $\mathcal{H}_0$:

$$\mathcal{H}_0 = \sum_{\boldsymbol{k}\sigma} \left(E^\alpha_{\boldsymbol{k}} \alpha^\dagger_{\boldsymbol{k}\sigma} \alpha_{\boldsymbol{k}\sigma} + E^\beta_{\boldsymbol{k}} \beta^\dagger_{\boldsymbol{k}\sigma} \beta_{\boldsymbol{k}\sigma} \right), \tag{2.38}$$

where

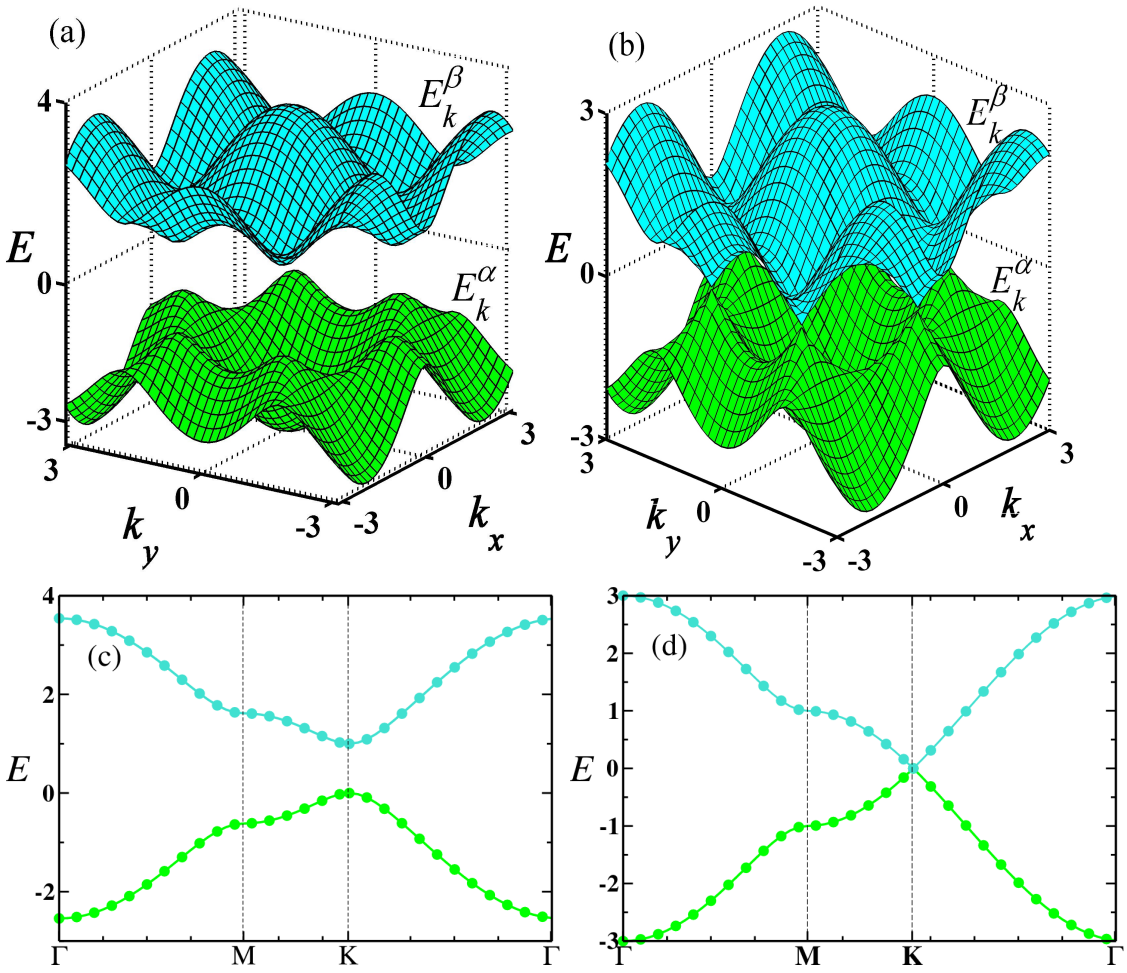

Figure 2.2: Energy spectrum (in units of t) of the charge Hamiltonian [Eq. (2.38)] on the honeycomb lattice (a) with a Hubbard charge gap U, and (b) the tight-binding ($U = 0$) case. Energy spectrum along the lines connecting points of high symmetry: (c) interacting case for $U = t$; (d) tight-binding approach.

$$u_{\boldsymbol{k}} = \frac{1}{\sqrt{2}}\sqrt{1 + \frac{|\epsilon_{\boldsymbol{k}}|}{E_{\boldsymbol{k}}}}\,;$$
$$v_{\boldsymbol{k}} = \frac{1}{\sqrt{2}}\sqrt{1 - \frac{|\epsilon_{\boldsymbol{k}}|}{E_{\boldsymbol{k}}}}\,, \tag{2.39}$$

with

$$E_{\boldsymbol{k}} = \sqrt{\epsilon_{\boldsymbol{k}}^2 + \frac{U^2}{4}}\,;$$
$$E_{\boldsymbol{k}}^{\alpha,\beta} = \mp E_{\boldsymbol{k}} + U/2. \tag{2.40}$$

The Hamiltonian in Eq. (2.38) presents two dispersive bands: the low-energy ($\alpha_{\boldsymbol{k}\sigma}$) and the high-energy one ($\beta_{\boldsymbol{k}\sigma}$), split up by the Hubbard gap U, as shown in Fig. 2.2(a). Further, it should be noted that the non-interacting tight-binding spectrum of $\mathcal{H}_0$ can be recast by setting $U = 0$, as shown in Fig. 2.2(b). In fact, these two dispersive bands meet in the so-called Dirac points. As it is well known, close to the Dirac points the system can be mapped onto free massless Dirac fermions [11].

In order to clarify the above discussion, in Figs. 2.2(c) and (d) we also plotted the energy spectrum along the lines which connects the high symmetry points Γ-M-K-Γ of the first Brillouin zone (BZ), as illustrated in Fig. 2.1(b). Indeed, one clearly sees in Fig. 2.2(c) that the two dispersive bands are split up by the Hubbard gap U, while in Fig. 2.2(d) the two bands meet in the Dirac points (K) in the non-interacting tight-binding case. Additionally, we emphasize that the M and the K points are of particular importance for the physics of electronic correlation in honeycomb materials [the $\Gamma = (0, 0)$ point is located at the center of the first BZ]. The M point indicates the position of the van Hove singularities, at which the density of states is logarithmically divergent [11,46], and the K point specifies where the two bands meet, and the density of states vanishes linearly [11].

2.3. Effective Lagrangian Density in the Strong-Coupling Regime

In this section, we shall build a strong-coupling ($U/t \gg 1$) perturbative low-energy theory (effective Lagrangian density) suitable to describe the system in the half-filled and doped regimes. Our aim is to investigate the relevant processes that characterize the magnetic and superconducting phases in the large-U regime in terms of the lower α band and the upper β band (see Fig. 2.2).

Let us start by expanding the auxiliary functions $u_{\boldsymbol{k}}$ and $v_{\boldsymbol{k}}$ in Eq. (2.39) in powers of t/U as follows:

$$\begin{aligned} u_{\boldsymbol{k}} &= \frac{1}{\sqrt{2}}\left[1+\frac{t|w_{\boldsymbol{k}}|}{U}-\frac{t^2|w_{\boldsymbol{k}}|^2}{2U^2}+\mathcal{O}\left(\frac{t^3}{U^3}\right)\right]; \\ v_{\boldsymbol{k}} &= \frac{1}{\sqrt{2}}\left[1-\frac{t|w_{\boldsymbol{k}}|}{U}-\frac{t^2|w_{\boldsymbol{k}}|^2}{2U^2}+\mathcal{O}\left(\frac{t^3}{U^3}\right)\right], \end{aligned} \tag{2.41}$$

where

$$\epsilon_{\boldsymbol{k}} = t|w_{\boldsymbol{k}}| \quad \text{[see Eq. (2.30)]}. \tag{2.42}$$

In the sequence, by using Eqs. (2.28)-(2.32) and (2.35), we can express the Grassmann field $a_{\boldsymbol{i}\alpha\sigma}$ in terms of the Bogoliubov fields $\alpha_{\boldsymbol{k}\sigma}$ and $\beta_{\boldsymbol{k}\sigma}$:

$$a_{\boldsymbol{i}\alpha\sigma} = \frac{1}{\sqrt{N_c}}\sum_{\boldsymbol{k}\sigma} e^{i\boldsymbol{k}\cdot\boldsymbol{i}}\left[\left(u_{\boldsymbol{k}}+\sigma v_{\boldsymbol{k}}\right)\alpha_{\boldsymbol{k}\sigma}+\left(u_{\boldsymbol{k}}-\sigma v_{\boldsymbol{k}}\right)\beta_{\boldsymbol{k}\sigma}\right]. \tag{2.43}$$

Now, by substituting Eq. (2.41) into Eq. (2.43), we can obtain a perturbative expression for the Grassmann field $a_{\boldsymbol{i}\alpha\sigma}$ in terms of the spinless Grassmann fields $\alpha_{\boldsymbol{i}}$ and $\beta_{\boldsymbol{i}}$ (see below), up to $\mathcal{O}\left(t^2/U^2\right)$, as follows:

$$\begin{aligned} a_{\boldsymbol{i}\alpha\sigma} &= \theta(\sigma)\alpha_{\boldsymbol{i}}+\theta(-\sigma)\beta_{\boldsymbol{i}}+\theta(-\sigma)\frac{t}{U}\alpha_{\boldsymbol{i}}+\theta(\sigma)\frac{t}{U}\beta_{\boldsymbol{i}} \\ &-\frac{t^2}{U^2}\left[\theta(-\sigma)\sum_j\left(\alpha_{\boldsymbol{i}+\hat{\boldsymbol{e}}_j}+\alpha_{\boldsymbol{i}-\hat{\boldsymbol{e}}_j}\right)+3\theta(\sigma)\alpha_{\boldsymbol{i}}\right] \\ &+\frac{t^2}{U^2}\left[\theta(\sigma)\sum_j\left(\beta_{\boldsymbol{i}+\hat{\boldsymbol{e}}_j}+\beta_{\boldsymbol{i}-\hat{\boldsymbol{e}}_j}\right)+3\theta(-\sigma)\beta_{\boldsymbol{i}}\right], \end{aligned} \tag{2.44}$$

where $\alpha_{\boldsymbol{i}}$ and $\beta_{\boldsymbol{i}}$ are defined by [54]

$$\begin{aligned} \alpha_{\boldsymbol{i}} &= \sqrt{\frac{1}{N_c}}\sum_\sigma \theta(\sigma)\sum_{\boldsymbol{k}} e^{i\boldsymbol{k}\cdot\boldsymbol{i}}\alpha_{\boldsymbol{k}\sigma}; \\ \beta_{\boldsymbol{i}} &= \sqrt{\frac{1}{N_c}}\sum_\sigma \theta(-\sigma)\sum_{\boldsymbol{k}} e^{i\boldsymbol{k}\cdot\boldsymbol{i}}\beta_{\boldsymbol{k}\sigma}, \end{aligned} \tag{2.45}$$

$\theta(\sigma)$ is the Heaviside function, with $\theta(\sigma)\theta(-\sigma') = \theta(\sigma)\delta_{\sigma,-\sigma'}$, and $\hat{\boldsymbol{e}}_j$ are the standard three unit vectors of the honeycomb lattice [11]. This representation is appropriated to describe the magnetic and superconducting orders, in the large-U regime, in the context of the referred α and β bands. For example, to $\mathcal{O}(t/U)$, Eq. (2.44) yields: $a_{\boldsymbol{i}A\uparrow} \approx \alpha_{\boldsymbol{i}}$ and $a_{\boldsymbol{i}B\downarrow} \approx \alpha_{\boldsymbol{i}}$, which is consistent with the situation of spins up present at A sublattice sites and spins down being at B sublattice sites in a given unit-cell $\boldsymbol{i}$ (low-energy spin configuration), while for the high-energy β band one finds an opposite spin configuration: $a_{\boldsymbol{i}A\downarrow} \approx \beta_{\boldsymbol{i}}$ and $a_{\boldsymbol{i}B\uparrow} \approx \beta_{\boldsymbol{i}}$. (Notice that this physical picture of low-energy configuration is compatible with both AF ordering and spin-singlet pairing.)

At this stage, it should be noted, on the grounds of the previous physical picture, that only single occupancy (in each site) is allowed. In fact, mathematically speaking, our perturbative scheme will be consistent with the preceding physical scenario, only if after inserting Eq. (2.44) into Eq. (2.27) [the latter contains the hopping term, t, and the Coulombian repulsion, U] one keeps terms of $\mathcal{O}(U)$ and $\mathcal{O}\left(t^2/U^2\right)$; subsequently, straightforward algebraic manipulations will lead to the superexchange $J \equiv 4t^2/U$ [52–55, 61]. By doing so, one can write $\mathcal{H}_0$ in terms of the spinless Grassmann fields $\alpha_{\boldsymbol{i}}$ and $\beta_{\boldsymbol{i}}$ in direct space:

$$\begin{aligned}\mathcal{H}_0 &= -J\sum_{\boldsymbol{i}}\left(\alpha^{\dagger}_{\boldsymbol{i}}\alpha_{\boldsymbol{i}} - \beta^{\dagger}_{\boldsymbol{i}}\beta_{\boldsymbol{i}}\right) + U\sum_{\boldsymbol{i}}\beta^{\dagger}_{\boldsymbol{i}}\beta_{\boldsymbol{i}} \\ &\quad -\frac{J}{8}\sum_{\boldsymbol{i}j}\left(\alpha^{\dagger}_{\boldsymbol{i}}\alpha_{\boldsymbol{i}+\hat{\boldsymbol{e}}_j} \;-\beta^{\dagger}_{\boldsymbol{i}}\beta_{\boldsymbol{i}+\hat{\boldsymbol{e}}_j} + \text{H.c.}\right). \qquad (2.46)\end{aligned}$$

The charge Hamiltonian above correctly exhibits the phenomenon of band shrinking [62] in the large-U regime. Notwithstanding, we stress that $\mathcal{H}_0$ describes only processes in the charge sector, i.e., no spin dynamics is involved. Therefore, in our study of the magnetic and superconducting properties of the system these processes play no role and, after a Legendre transform, the Lagrangian density can be taken simply as:

$$\mathcal{L}_0 = \sum_{\boldsymbol{i}}\alpha^{\dagger}_{\boldsymbol{i}}\partial_{\tau}\alpha_{\boldsymbol{i}}, \qquad (2.47)$$

where the dynamic (kinetic) term signals the background of the charge degrees of freedom.

We now employ the same perturbative scheme to $\mathcal{L}_n$, i.e., we insert Eq. (2.44) into Eq. (2.24), such that, by keeping terms which incorporates only the most relevant low-energy processes, i.e., quantum charge and spin dynamics between

nearest-neighbor sites, we obtain the following perturbative expansion for $\mathcal{L}_n$:

$$\begin{aligned}\mathcal{L}_n &= \sum_{\boldsymbol{i}\alpha\sigma}\theta(\sigma)\left(U^{\dagger}_{\boldsymbol{i}\alpha}\partial_\tau U_{\boldsymbol{i}\alpha}\right)_{\sigma\sigma}\alpha^{\dagger}_{\boldsymbol{i}}\alpha_{\boldsymbol{i}} - t\sum_{\boldsymbol{ij}\alpha\beta\sigma}\Big[\theta(-\sigma)\left(U^{\dagger}_{\boldsymbol{i}\alpha}U_{\boldsymbol{i}+\hat{\boldsymbol{e}}_j\beta}-1\right)_{\sigma,-\sigma}\alpha^{\dagger}_{\boldsymbol{i}}\alpha_{\boldsymbol{i}+\hat{\boldsymbol{e}}_j} \\ &\quad +\text{H.c.}\Big] + \frac{t}{2U}\sum_{\boldsymbol{ij}\alpha\sigma}\left[\theta(-\sigma)(U^{\dagger}_{\boldsymbol{i}\alpha}\partial_\tau U_{\boldsymbol{i}\alpha})_{\sigma,-\sigma}\left(\alpha^{\dagger}_{\boldsymbol{i}+\hat{\boldsymbol{e}}_j}+\alpha^{\dagger}_{\boldsymbol{i}-\hat{\boldsymbol{e}}_j}\right)\alpha_{\boldsymbol{i}}+\text{H.c.}\right] \\ &\quad - t\sum_{\boldsymbol{ij}\alpha\beta\sigma}\left\{\left(U^{\dagger}_{\boldsymbol{i}\alpha}U_{\boldsymbol{i}+\hat{\boldsymbol{e}}_j\beta}-1\right)_{\sigma\sigma}\left[\theta(\sigma)\alpha^{\dagger}_{\boldsymbol{i}}\beta_{\boldsymbol{i}+\hat{\boldsymbol{e}}_j}-\theta(\sigma)\beta^{\dagger}_{\boldsymbol{i}}\alpha_{\boldsymbol{i}+\hat{\boldsymbol{e}}_j}\right]+\text{H.c.}\right\}.\end{aligned} \tag{2.48}$$

It should be noted that the last term in Eq. (2.48) contains hopping between α and β bands. This term must be treated perturbatively, so that $\mathcal{L}_n$ appears as dependent on the low-energy α band only. We thus consider the perturbing Hamiltonian below:

$$\mathcal{H}_1 = -t\sum_{\boldsymbol{ij}\alpha\beta\sigma}\left\{\left(U^{\dagger}_{\boldsymbol{i}\alpha}U_{\boldsymbol{i}+\hat{\boldsymbol{e}}_j\beta}-1\right)_{\sigma\sigma}\left[\theta(\sigma)\beta^{\dagger}_{\boldsymbol{i}}\alpha_{\boldsymbol{i}+\hat{\boldsymbol{e}}_j}\ -\theta(\sigma)\alpha^{\dagger}_{\boldsymbol{i}}\beta_{\boldsymbol{i}+\hat{\boldsymbol{e}}_j}\right]+\text{H.c.}\right\}. \tag{2.49}$$

It can be handled by means of standard second-order perturbation theory [55,61], which is consistent with the strong-coupling expansion up to $\mathcal{O}\left(t^2/U\right)$:

$$\Delta E \equiv \mathcal{H}_{\text{eff}} = \sum_{\boldsymbol{k}\sigma}\frac{|\langle\alpha_{\boldsymbol{k}\sigma}|\mathcal{H}_1|\beta_{\boldsymbol{k}\sigma}\rangle|^2}{E^{\alpha}_{\boldsymbol{k}}-E^{\beta}_{\boldsymbol{k}}}, \tag{2.50}$$

where the unperturbed state is the system at half filling: the low-energy α band is filled, while the β band is empty. In other words, $|\alpha_{\boldsymbol{k}\sigma}\rangle$ corresponds to the unperturbed state, with N electrons filling completely the low-energy α band, whereas $|\beta_{\boldsymbol{k}\sigma}\rangle$ denotes the virtual perturbative states, in which these virtual states represent a situation that one electron with spin σ is removed from α band and it occupies the β band with energy $E^{\beta}_{\boldsymbol{k}}$ [see Eq. (2.40)] and spin σ.

From the above discussion, as well as with the help of Eq. (2.45), we obtain the following auxiliary results:

$$\begin{aligned}&\alpha^{\dagger}_{\boldsymbol{i}}|\alpha_{\boldsymbol{k}\sigma}\rangle = \beta_{\boldsymbol{i}}|\alpha_{\boldsymbol{k}\sigma}\rangle = 0; \\ &\theta\left(-\sigma\right)\beta_{\boldsymbol{i}}|\beta_{\boldsymbol{k}\sigma}\rangle = \frac{1}{\sqrt{N_c}}e^{i\boldsymbol{k}\cdot\boldsymbol{i}}|\alpha_{\boldsymbol{k}\sigma}\left(N-1\right)\rangle.\end{aligned} \tag{2.51}$$

Consequently, by inserting Eqs. (2.49) and (2.51) into Eq. (2.50), we find that ΔE becomes:

$$\begin{aligned}\Delta E &= t^2\langle\alpha_{\boldsymbol{k}\sigma}|\sum_{\boldsymbol{i}\alpha\sigma}\theta\left(-\sigma\right)\Big[\left(U^{\dagger}_{\boldsymbol{i}+\hat{\boldsymbol{e}}_j\beta}U_{\boldsymbol{i}\alpha}-1\right)_{\sigma\sigma}\alpha^{\dagger}_{\boldsymbol{i}+\hat{\boldsymbol{e}}_j}+\left(U^{\dagger}_{\boldsymbol{i}-\hat{\boldsymbol{e}}_j\beta}U_{\boldsymbol{i}\alpha}-1\right)_{\sigma\sigma} \\ &\quad\times\alpha^{\dagger}_{\boldsymbol{i}-\hat{\boldsymbol{e}}_j}\Big]\left[\frac{1}{N_c}\sum_{\boldsymbol{k}}\frac{1}{E^{\alpha}_{\boldsymbol{k}}-E^{\beta}_{\boldsymbol{k}}}\right]P_0\left(N-1\right)\Big[\left(U^{\dagger}_{\boldsymbol{i}\alpha}U_{\boldsymbol{i}+\hat{\boldsymbol{e}}_j\beta}-1\right)_{\sigma\sigma}\alpha_{\boldsymbol{i}+\hat{\boldsymbol{e}}_j} \\ &\quad+\left(U^{\dagger}_{\boldsymbol{i}\alpha}U_{\boldsymbol{i}-\hat{\boldsymbol{e}}_j\beta}-1\right)_{\sigma\sigma}\alpha_{\boldsymbol{i}-\hat{\boldsymbol{e}}_j}\Big]|\alpha_{\boldsymbol{k}\sigma}\rangle,\end{aligned} \tag{2.52}$$

where $P_0 = |\alpha_{\boldsymbol{k}\sigma}\rangle\langle\alpha_{\boldsymbol{k}\sigma}|$ denotes the projector operator onto the state $|\alpha_{\boldsymbol{k}\sigma}\rangle$.

At this point, it is worthwhile to use the following lemma of Quantum Mechanics [63]:

Lemma. Let A and B be two Hermitian operators, $|\psi\rangle$ an arbitrary state in Hilbert space and P_0 the projector operator onto the state $|\phi_0\rangle$. Then, if $P_0|\psi\rangle = \phi_0|\phi_0\rangle$, we have:

$$\langle\phi_0|AP_0B|\phi_0\rangle = \langle\psi|C|\psi\rangle \longleftrightarrow C = AB. \tag{2.53}$$

Therefore, by means of the above Lemma [Eq. (2.53)], we can express the effective Hamiltonian in terms of the α band only:

$$\mathcal{H}_{\text{eff}} = t^2 \sum_{\boldsymbol{ij}\alpha\beta\sigma} \theta\left(-\sigma\right) \left[\left(U^{\dagger}_{\boldsymbol{i}+\hat{\boldsymbol{e}}_j\beta} U_{\boldsymbol{i}\alpha} - 1\right)_{\sigma\sigma} \alpha^{\dagger}_{\boldsymbol{i}+\hat{\boldsymbol{e}}_j} + \left(U^{\dagger}_{\boldsymbol{i}-\hat{\boldsymbol{e}}_j\beta} U_{\boldsymbol{i}\alpha} - 1\right)_{\sigma\sigma} \alpha^{\dagger}_{\boldsymbol{i}-\hat{\boldsymbol{e}}_j}\right]$$
$$\left[\frac{1}{N_c}\sum_{\boldsymbol{k}} \frac{1}{E^{\alpha}_{\boldsymbol{k}} - E^{\beta}_{\boldsymbol{k}}}\right] \left[\left(U^{\dagger}_{\boldsymbol{i}\alpha} U_{\boldsymbol{i}+\hat{\boldsymbol{e}}_j\beta} - 1\right)_{\sigma\sigma} \alpha_{\boldsymbol{i}+\hat{\boldsymbol{e}}_j} + \left(U^{\dagger}_{\boldsymbol{i}\alpha} U_{\boldsymbol{i}-\hat{\boldsymbol{e}}_j\beta} - 1\right)_{\sigma\sigma} \alpha_{\boldsymbol{i}-\hat{\boldsymbol{e}}_j}\right]. \tag{2.54}$$

Keeping in mind that we are interested in the thermodynamic limit, we can turn the sum in $\boldsymbol{k}$ in Eq. (2.54) into an integral:

$$\frac{1}{N_c}\sum_{\boldsymbol{k}} \frac{1}{E^{\alpha}_{\boldsymbol{k}} - E^{\beta}_{\boldsymbol{k}}} \approx -\frac{1}{4\pi^2}\int_{BZ} \frac{d^2\boldsymbol{k}}{E^{\alpha}_{\boldsymbol{k}} - E^{\beta}_{\boldsymbol{k}}}, \tag{2.55}$$

so that, by using Eqs. (2.34) and (2.40), in the strong-coupling regime ($U \gg t$), we find

$$\frac{1}{4\pi^2}\int_{BZ} \frac{d^2\boldsymbol{k}}{E^{\alpha}_{\boldsymbol{k}} - E^{\beta}_{\boldsymbol{k}}} = -\frac{1}{U}\left[1 + \mathcal{O}\left(\frac{t^2}{U^2}\right)\right]. \tag{2.56}$$

The above result [Eq. (2.56)] allows us to express the effective Hamiltonian $\mathcal{H}_{\text{eff}}$ in Eq. (2.54), after a slightly rearrangement of the terms, in the form:

$$\mathcal{H}_{\text{eff}} = -\frac{t^2}{2U}\sum_{\boldsymbol{ij}\alpha\beta\sigma} \theta(\sigma) \left[\left|\left(U^{\dagger}_{\boldsymbol{i}\alpha} U_{\boldsymbol{i}+\hat{\boldsymbol{e}}_j\beta}\right)_{\sigma\sigma}\right|^2 + \left|\left(U^{\dagger}_{\boldsymbol{i}\alpha} U_{\boldsymbol{i}-\hat{\boldsymbol{e}}_j\beta}\right)_{\sigma\sigma}\right|^2\right] \alpha^{\dagger}_{\boldsymbol{i}}\alpha_{\boldsymbol{i}}. \tag{2.57}$$

Indeed, with this result, we have reached a perturbative expression of $\mathcal{L}_n$, up to $\mathcal{O}\left(t^2/U\right)$, in terms of the low-energy α band only [we plug Eq. (2.57) into

Eq.(2.48)]:

$$\begin{aligned}\mathcal{L}_n &= \sum_{\boldsymbol{i}\alpha\sigma}\theta(\sigma)\left(U^{\dagger}_{\boldsymbol{i}\alpha}\partial_\tau U_{\boldsymbol{i}\alpha}\right)_{\sigma\sigma}\alpha^{\dagger}_{\boldsymbol{i}}\alpha_{\boldsymbol{i}} - t\sum_{\boldsymbol{i}j\alpha\beta\sigma}\Big[\theta(-\sigma)\left(U^{\dagger}_{\boldsymbol{i}\alpha}U_{\boldsymbol{i}+\hat{\boldsymbol{e}}_j\beta}-1\right)_{\sigma,-\sigma}\alpha^{\dagger}_{\boldsymbol{i}}\alpha_{\boldsymbol{i}+\hat{\boldsymbol{e}}_j} \\ &\quad +\text{H.c.}\Big] + \frac{t}{2U}\sum_{\boldsymbol{i}j\alpha\sigma}\Big[\theta(-\sigma)(U^{\dagger}_{\boldsymbol{i}\alpha}\partial_\tau U_{\boldsymbol{i}\alpha})_{\sigma,-\sigma}\left(\alpha^{\dagger}_{\boldsymbol{i}+\hat{\boldsymbol{e}}_j}+\alpha^{\dagger}_{\boldsymbol{i}-\hat{\boldsymbol{e}}_j}\right)\alpha_{\boldsymbol{i}}+\text{H.c.}\Big] \\ &\quad -\frac{t^2}{2U}\sum_{\boldsymbol{i}j\alpha\beta\sigma}\theta(\sigma)\left[\left|\left(U^{\dagger}_{\boldsymbol{i}\alpha}U_{\boldsymbol{i}+\hat{\boldsymbol{e}}_j\beta}\right)_{\sigma\sigma}\right|^2+\left|\left(U^{\dagger}_{\boldsymbol{i}\alpha}U_{\boldsymbol{i}-\hat{\boldsymbol{e}}_j\beta}\right)_{\sigma\sigma}\right|^2\right]\alpha^{\dagger}_{\boldsymbol{i}}\alpha_{\boldsymbol{i}}.\end{aligned} \tag{2.58}$$

Correspondingly, by adding $\mathcal{L}_0$ [see Eq. (2.47)] to the perturbation expression of $\mathcal{L}_n$ [see Eq. (2.58)], we find that the effective low-energy Lagrangian density of the honeycomb Hubbard model in the large-U regime, up to $\mathcal{O}\left(J\equiv 4t^2/U\right)$, is given by

$$\begin{aligned}\mathcal{L} &= \sum_{\boldsymbol{i}}\alpha^{\dagger}_{\boldsymbol{i}}\partial_\tau\alpha_{\boldsymbol{i}}+\sum_{\boldsymbol{i}\alpha\sigma}\theta(\sigma)\left(U^{\dagger}_{\boldsymbol{i}\alpha}\partial_\tau U_{\boldsymbol{i}\alpha}\right)_{\sigma\sigma}\alpha^{\dagger}_{\boldsymbol{i}}\alpha_{\boldsymbol{i}} - t\sum_{\boldsymbol{i}j\alpha\beta\sigma}\Big[\theta(-\sigma)\left(U^{\dagger}_{\boldsymbol{i}\alpha}U_{\boldsymbol{i}+\hat{\boldsymbol{e}}_j\beta}\right)_{\sigma,-\sigma} \\ &\quad \times\alpha^{\dagger}_{\boldsymbol{i}}\alpha_{\boldsymbol{i}+\hat{\boldsymbol{e}}_j}+\text{H.c.}\Big] + \frac{J}{8t}\sum_{\boldsymbol{i}j\alpha\sigma}\left(U^{\dagger}_{\boldsymbol{i}\alpha}\ \partial_\tau U_{\boldsymbol{i}\alpha}\right)_{\sigma,-\sigma}\Big[\theta(-\sigma)\alpha^{\dagger}_{\boldsymbol{i}}\left(\alpha_{\boldsymbol{i}+\hat{\boldsymbol{e}}_j}+\alpha_{\boldsymbol{i}-\hat{\boldsymbol{e}}_j}\right) \\ &\quad +\text{H.c.}\Big] - \frac{J}{8}\sum_{\boldsymbol{i}j\alpha\beta\sigma}\theta(\sigma)\left[\left|\left(U^{\dagger}_{\boldsymbol{i}\alpha}U_{\boldsymbol{i}+\hat{\boldsymbol{e}}_j\beta}\right)_{\sigma\sigma}\right|^2+\left|\left(U^{\dagger}_{\boldsymbol{i}\alpha}U_{\boldsymbol{i}-\hat{\boldsymbol{e}}_j\beta}\right)_{\sigma\sigma}\right|^2\right]\alpha^{\dagger}_{\boldsymbol{i}}\alpha_{\boldsymbol{i}}.\end{aligned} \tag{2.59}$$

We emphasize that the above low-energy Lagrangian density incorporates only quadratic terms in $\alpha^{\dagger},\alpha$. We can thus integrate out the fermions degrees of freedom in order to explicit the spin structure embedded in $U^{\dagger}_{\boldsymbol{i}\alpha}U_{\boldsymbol{i}+\hat{\boldsymbol{e}}_j\alpha}$ and $U^{\dagger}_{\boldsymbol{i}\alpha}\partial_\tau U_{\boldsymbol{i}\alpha}$.

2.4. Final Remarks

In summary, we have presented an analytical approach suitable to investigate of the large-U Hubbard model on the honeycomb lattice. Our approach, based on field-theoretic and many-body techniques, has the advantage of allowing us to derive the Lagrangian density related to the charge (Grassmann fields) and spin [SU(2) gauge fields] degrees of freedom in a controllable scheme. As a result, we diagonalized exactly the Hamiltonian associated with the charge degrees of freedom only, in which case the electronic spectrum exhibits a charge Hubbard gap separating the Dirac cones. Moreover, we have shown that the two bands meet at the Dirac points in the non-interacting tight-binding case.

In the strong-coupling regime, by performing a perturbative expansion in the parameter t/U up to $\mathcal{O}\left(J=4t^2/U\right)$, we were able to derive a low-energy La-

grangian density appropriated to describe the (quantum) magnetic and superconducting phases of the large-U Hubbard model on the honeycomb lattice, as we shall demonstrate in Chapters 3 and 4.

3. Charge and Spin Quantum Fluctuations on the Honeycomb Lattice: Half-filled and Doped Regimes

In this chapter we shall investigate the effects of charge and spin quantum fluctuations in the breakdown of the AF order on the honeycomb lattice by means of the low-energy perturbative Lagrangian density [see Eq. (2.59)] derived in the Section 2.3. Section 3.1 is dedicated to the half-filling case, in which case the large-U Hubbard model is mapped onto the quantum Heisenberg model described by SU(2) gauge fields. In this context, we deal with the underlying spin degrees of freedom by employing a second-order spin-wave analysis, such that we have calculated the ground-state energy and staggered magnetization per site; the results are in very good agreement with previous studies [19–21, 23–26].

In Section 3.2, we focus on the challenging hole-doped regime. This topic is studied within a controllable perturbative scheme, so that our approach allows the derivation of a t-J Hamiltonian, and the analysis of the role played by charge and spin quantum fluctuations on the ground-state energy and, particularly, on the breakdown of the AF order at a critical hole doping; the results are benchmarked against recent Grassmann tensor product state [26]. Further, in Section 3.3, in the continuum limit, we map the effective large-U Lagrangian density [see Eq. (2.59)] onto the quantum nonlinear σ-model with a topological Hopf term [34–37], in which case its presence (Chern-Simons term) is crucial in the analysis of the AF-VBS competition. Lastly, final remarks are presented in Section 3.4.

3.1. Heisenberg Model and Quantum Spin Fluctuations

In the half-filled regime, the charge degrees of freedom are frozen ($\langle \alpha_{\boldsymbol{i}}^{\dagger} \partial_{\tau} \alpha_{\boldsymbol{i}} \rangle = 0$ and $\langle \alpha_{\boldsymbol{i}}^{\dagger} \alpha_{\boldsymbol{i}+\hat{\boldsymbol{e}}_j} \rangle = 0$), i.e., the lower-energy α band is completely filled by electrons: $n_{\alpha} \equiv \langle \alpha_{\boldsymbol{i}}^{\dagger} \alpha_{\boldsymbol{i}} \rangle = 1$. Accordingly, it turns out that only the spin degrees of freedom survive and are described by the SU(2) gauge fields in Eq.(2.59). Further, this localized electronic background allows the emergence of an AF phase [32, 33]. Indeed, by performing the following Legendre transform:

$$\mathcal{H}^{s} = -\sum_{\boldsymbol{i}\alpha\sigma} \frac{\partial \mathcal{L}}{\partial \left(\partial_{\tau} U_{\boldsymbol{i}\alpha}\right)_{\sigma\sigma}} \left(\partial_{\tau} U_{\boldsymbol{i}\alpha}\right)_{\sigma\sigma} + \mathcal{L}; \tag{3.1}$$

where

$$\frac{\partial \mathcal{L}}{\partial \left(\partial_\tau U_{i\alpha}\right)_{\sigma\sigma}} = \theta\left(\sigma\right)\left(U_{i\alpha}^{\dagger}\right)_{\sigma\sigma}, \tag{3.2}$$

we can map the large-U Hubbard model, in the half-filling limit of the effective Lagrangian density in Eq. (2.59), onto the following Heisenberg-like Hamiltonian written in terms of the SU(2) gauge fields:

$$\mathcal{H}^s = -\frac{J}{8}\sum_{ij\alpha\beta\sigma}\theta(\sigma)\left[\left|\left(U_{i\alpha}^{\dagger}U_{i+\hat{e}_j\beta}\right)_{\sigma\sigma}\right|^2 + \left|\left(U_{i\alpha}^{\dagger}U_{i-\hat{e}_j\beta}\right)_{\sigma\sigma}\right|^2\right]. \tag{3.3}$$

In fact, with the help of Eq. (2.18), we can write [55]:

$$\begin{aligned}\left|\left(U_{i\alpha}^{\dagger}U_{i+\hat{e}_j\beta}\right)_{\sigma\sigma}\right|^2 = {} & \left[1+\cos\left(\theta_{i\alpha}\right)\cos\left(\theta_{i+\hat{e}_j\beta}\right) + \sin\left(\theta_{i\alpha}\right)\sin\left(\theta_{i+\hat{e}_j\beta}\right)\right. \\ & \left.\times\cos\left(\phi_{i\alpha}-\phi_{i+\hat{e}_j\beta}\right)\right],\end{aligned} \tag{3.4}$$

or

$$\left|\left(U_{i\alpha}^{\dagger}U_{i+\hat{e}_j\beta}\right)_{\sigma\sigma}\right|^2 = \frac{1}{2}\left(1+\boldsymbol{n}_{i\alpha}\cdot\boldsymbol{n}_{i+\hat{e}_j\beta}\right), \tag{3.5}$$

where $\boldsymbol{n}_{i\alpha} = \sin\left(\theta_{i\alpha}\right)\left[\cos\left(\phi_{i\alpha}\right)\hat{\boldsymbol{x}} + \sin\left(\phi_{i\alpha}\right)\hat{\boldsymbol{y}}\right] + \cos\left(\theta_{i\alpha}\right)\hat{\boldsymbol{z}}$ is the unit vector. Accordingly, $\mathcal{H}^s$ can be brought to its standard form:

$$\mathcal{H}^s = -J\sum_{ij\alpha\beta}\boldsymbol{S}_{i\alpha}\cdot\boldsymbol{S}_{i+\hat{e}_j\beta} - h\sum_{i\alpha}\boldsymbol{S}_{i\alpha} + h\sum_{ij\beta}\boldsymbol{S}_{i+\hat{e}_j\beta} - \frac{zNJ}{8}, \tag{3.6}$$

where $\boldsymbol{S}_{i\alpha} = \boldsymbol{n}_{i\alpha}/2$, z is the coordination number ($z = 3$ for the honeycomb lattice) and the two additional Zeeman terms (h is the magnetic field) allow us to perform the calculation of the staggered magnetization.

The second-order spin-wave theory [21, 64] can offer an accurate description of the relevant physical quantities, such as the ground-state energy, E_0, and the staggered magnetization per site, m, which characterizes the AF order. In order to employ this method to the quantum AF Heisenberg model in Eq. (3.6) let us introduce the Holstein-Primakoff transformation:

$$\begin{aligned} S_{i\alpha}^z &= -a_i^{\dagger}a_i + S; \\ S_{i\alpha}^+ &= \sqrt{2S - a_i^{\dagger}a_i}\,a_i; \\ S_{i\alpha}^- &= a_i^{\dagger}\sqrt{2S - a_i^{\dagger}a_i}, \end{aligned} \tag{3.7}$$

for an up-spin on A site of sublattice A, and

$$\begin{aligned} S_{i+\hat{e}_j\beta}^z &= b_{i+\hat{e}_j}^{\dagger}b_{i+\hat{e}_j} - S; \\ S_{i+\hat{e}_j\beta}^+ &= \sqrt{2S - b_{i+\hat{e}_j}^{\dagger}b_{i+\hat{e}_j}}\,b_{i+\hat{e}_j}; \\ S_{i+\hat{e}_j\beta}^- &= b_{i+\hat{e}_j}^{\dagger}\sqrt{2S - b_{i+\hat{e}_j}^{\dagger}b_{i+\hat{e}_j}}, \end{aligned} \tag{3.8}$$

for a neighboring down-spin of sublattice B; the bosonic creation and annihilation operators $a_{\boldsymbol{i}}$ and $a_{\boldsymbol{i}}^{\dagger}$ obey the commutation relations: $[a_{\boldsymbol{i}},a_{\boldsymbol{i'}}^{\dagger}]=\delta_{\boldsymbol{ii'}}$ and $[b_{\boldsymbol{j}},b_{\boldsymbol{j'}}^{\dagger}]=\delta_{\boldsymbol{jj'}}$. Moreover, we apply the Fourier transform [see, e.g., Eq. (2.28)] together with the following Bogoliubov transformation:

$$\begin{aligned} a_{\boldsymbol{k}} &= \cosh\left(\theta_{\boldsymbol{k}}\right)\alpha_{\boldsymbol{k}} - \sinh\left(\theta_{\boldsymbol{k}}\right)\beta_{\boldsymbol{k}}^{\dagger}; \\ b_{\boldsymbol{k}} &= -\sinh\left(\theta_{\boldsymbol{k}}\right)\alpha_{\boldsymbol{k}}^{\dagger} - \cosh\left(\theta_{\boldsymbol{k}}\right)\beta_{\boldsymbol{k}}, \end{aligned} \tag{3.9}$$

where $\tanh\left(\theta_{\boldsymbol{k}}\right) = -\gamma_{\boldsymbol{k}}$ and the lattice structure factor $\gamma_{\boldsymbol{k}}$ reads:

$$\gamma_{\boldsymbol{k}} \equiv \frac{1}{z}\sum_{j} e^{i\boldsymbol{k}\cdot\boldsymbol{e}_j} = \frac{1}{3}\left[e^{ik_x} + 2e^{-i\frac{k_x}{2}}\cos\left(\frac{\sqrt{3}k_y}{2}\right)\right]. \tag{3.10}$$

The resulting diagonalized Hamiltonian up to $\mathcal{O}\left(1/S^2\right)$, in $\boldsymbol{k}$-space, takes the form:

$$\begin{aligned} \mathcal{H}^s \;=\; & -\frac{zS^2JN}{2} + hSN + zSJ\sum_{\boldsymbol{k}}\left[\left(\sqrt{1-\gamma_{\boldsymbol{k}}^2}-1\right) + \sqrt{1-\gamma_{\boldsymbol{k}}^2}\left(\alpha_{\boldsymbol{k}}^{\dagger}\alpha_{\boldsymbol{k}} + \beta_{\boldsymbol{k}}^{\dagger}\beta_{\boldsymbol{k}}\right)\right] \\ & -\frac{zJ}{2N}\left[\sum_{\boldsymbol{k}}\left(\sqrt{1-\gamma_{\boldsymbol{k}}^2}-1\right)\right]^2 - h\sum_{\boldsymbol{k}}\left[\left(\frac{1}{\sqrt{1-\gamma_{\boldsymbol{k}}^2}}-1\right) + \frac{\alpha_{\boldsymbol{k}}^{\dagger}\alpha_{\boldsymbol{k}} + \beta_{\boldsymbol{k}}^{\dagger}\beta_{\boldsymbol{k}}}{\sqrt{1-\gamma_{\boldsymbol{k}}^2}}\right] \\ & -\frac{zJN}{8} - \frac{2zJ}{N}\sum_{\boldsymbol{k},\boldsymbol{k'}}\alpha_{\boldsymbol{k}}^{\dagger}\alpha_{\boldsymbol{k}}\beta_{\boldsymbol{k'}}^{\dagger}\beta_{\boldsymbol{k'}}. \end{aligned} \tag{3.11}$$

Correspondingly, in the thermodynamic limit, the ground-state energy per site in the presence of a magnetic field becomes:

$$\begin{aligned} \frac{E_h}{N} = & -\frac{zS^2J}{2} + hS + \frac{zSJ}{4\pi^2}\int_{\mathrm{BZ}} d^2k\left(\sqrt{1-\gamma_{\boldsymbol{k}}^2}-1\right) \\ & -\frac{zJ}{32\pi^4}\left[\int_{\mathrm{BZ}} d^2k\left(\sqrt{1-\gamma_{\boldsymbol{k}}^2}-1\right)\right]^2 - \frac{h}{4\pi^2}\int_{\mathrm{BZ}} d^2k\left(\frac{1}{\sqrt{1-\gamma_{\boldsymbol{k}}^2}}-1\right) - \frac{zJ}{8}. \end{aligned} \tag{3.12}$$

In Appendix A, we present detailed calculations of the perturbative scheme used to derive Eqs. (3.11) and (3.12).

In the sequence, we take $S = 1/2$ and perform the integration over the first Brillouin zone (BZ): $\mid k_x \mid \leq 2\pi/3$ and $\mid k_y \mid \leq \pi/\sqrt{3}$. As a consequence, we have found that the ground-state energy per site at zero magnetic field is given by (we have subtracted the term $-zJ/8$ with the intention of comparing Eq. (3.12) at zero magnetic field to preceding results): $E_0/NJ \approx -0.5489$. Indeed, this result agrees very well with the preceding studies listed in Table 3.1

Table 3.1: Comparison of the results from several approaches for the ground-state energy per site E_0/NJ of the Heisenberg model at zero magnetic field.

Method	E_0/NJ
QMC [19, 20]	-0.5440
Spin Wave up to $\mathcal{O}(1/S^2)$ [21]	-0.5489
Our result [22]	-0.5489
Series Expansion [23]	-0.5443
TPS [24, 25]	-0.5445
GTPS [26]	-0.5441

On the other hand, with the help of Eq. (3.12), we can straightforwardly derive the staggered magnetization per site [65]:

$$m = \frac{1}{N}\frac{\partial E_h}{\partial h}|_{h=0}. \tag{3.13}$$

Thus, one finds:

$$m = S - \frac{1}{4\pi^2}\int_{\mathrm{BZ}} d^2k \left(\frac{1}{\sqrt{1-\gamma_{\boldsymbol{k}}^2}} - 1\right), \tag{3.14}$$

which stands for both first- and second-order spin-wave perturbation theory. Further, the integration over the first BZ yields for $S = 1/2$: $m \approx 0.2418$, which is in good agreement with preceding results summarized in Table 3.2.

We would like to mention that the evaluation of the staggered magnetization by the TPS and GTPS simulations is rather susceptible to the value of the virtual dimension D. For instance, as one can note in Table 3.2, GTPS studies have predicted slightly larger values for the staggered magnetization. Here, the "virtual dimension" D is a concept associated with the integer bond indices of classical tensor-networks on honeycomb lattices, and largely used in TPS and GTPS simulations [24–26].

Table 3.2: Comparison of the results from several approaches for the ground-state staggered magnetization per site m of the Heisenberg model at zero magnetic field.

Method	m
QMC [19]	0.22 ± 0.03
QMC [20]	0.2681(8)
Spin Wave up to $\mathcal{O}(1/S^2)$ [21]	0.2418
Our result [22]	0.2418
Series Expansion [23]	0.266(9)
TPS for $D = 8$ [24]	0.2142
TPS for $D \to \infty$ [25]	0.285
GTPS for $D = 10$ [26]	0.3257
GTPS for $D = 12$ [26]	0.3239

Furthermore, it has been indicated, through topological arguments, the possible occurrence of a VBS phase on the honeycomb lattice [36]. Thus, in Section 3.3, we map the effective large-U Lagrangian density in Eq. (2.59), in the continuum limit, onto the quantum nonlinear σ-model with a topological Hopf term, in which case its presence (Chern-Simons term) is crucial for the possible occurrence of a VBS order. However, despite that our results provide evidence for the existence of this topological term in the context of our approach, as mentioned in the Introduction, in the numerical studies of the Hubbard model at half-filling the VBS order did not appear as a stable phase [33].

3.2. t-J Model: Charge and Spin Quantum Fluctuations

In this section, we provide a systematic study of the interplay between quantum charge and spin fluctuations in the breakdown of the AF order in the doped regime. In order to obtain the corresponding t-J Hamiltonian, let us apply the Legendre transform in Eq. (2.59):

$$\begin{aligned}\mathcal{H}^{t\text{-}J} &= -\sum_{\boldsymbol{i}} \frac{\partial \mathcal{L}}{\partial\left(\partial_\tau \alpha_{\boldsymbol{i}}\right)} \partial_\tau \alpha_{\boldsymbol{i}} - \sum_{\boldsymbol{i}j\alpha\sigma} \frac{\partial \mathcal{L}}{\partial\left(\partial_\tau U_{\boldsymbol{i}\alpha}\right)_{\sigma\sigma}} \left(\partial_\tau U_{\boldsymbol{i}\alpha}\right)_{\sigma\sigma} \\ &\quad - \sum_{\boldsymbol{i}j\alpha\sigma} \frac{\partial \mathcal{L}}{\partial\left(\partial_\tau U_{\boldsymbol{i}\alpha}\right)_{\sigma,-\sigma}} \left(\partial_\tau U_{\boldsymbol{i}\alpha}\right)_{\sigma,-\sigma} + \mathcal{L}, \end{aligned} \tag{3.15}$$

where

$$\begin{aligned}
\frac{\partial \mathcal{L}}{\partial\left(\partial_\tau \alpha_{\boldsymbol{i}}\right)} &= \alpha_{\boldsymbol{i}}^{\dagger}; \\
\frac{\partial \mathcal{L}}{\partial\left(\partial_\tau U_{\boldsymbol{i}\alpha}\right)_{\sigma\sigma}} &= \theta(\sigma)\left(U_{\boldsymbol{i}\alpha}^{\dagger}\right)_{\sigma\sigma} \alpha_{\boldsymbol{i}}^{\dagger}\alpha_{\boldsymbol{i}}; \\
\frac{\partial \mathcal{L}}{\partial\left(\partial_\tau U_{\boldsymbol{i}\alpha}\right)_{\sigma,-\sigma}} &= \frac{J}{8t}\left(U_{\boldsymbol{i}\alpha}^{\dagger}\right)_{\sigma,-\sigma}\left[\theta(-\sigma)\,\alpha_{\boldsymbol{i}}^{\dagger}\left(\alpha_{\boldsymbol{i}+\hat{\boldsymbol{e}}_j} + \alpha_{\boldsymbol{i}-\hat{\boldsymbol{e}}_j}\right) + \text{H.c.}\right],
\end{aligned} \tag{3.16}$$

so that we indeed can map the large-U Hubbard model onto the following t-J Hamiltonian:

$$\begin{aligned}
\mathcal{H}^{t\text{-}J} &= -t\sum_{\boldsymbol{ij}\alpha\beta\sigma}\left[\theta(-\sigma)\left(U_{\boldsymbol{i}\alpha}^{\dagger}U_{\boldsymbol{i}+\hat{\boldsymbol{e}}_j\beta}\right)_{\sigma,-\sigma}\alpha_{\boldsymbol{i}}^{\dagger}\alpha_{\boldsymbol{i}+\hat{\boldsymbol{e}}_j} + \text{H.c.}\right] \\
&\quad -\frac{J}{8}\sum_{\boldsymbol{ij}\alpha\beta\sigma}\theta(\sigma)\left[\left|\left(U_{\boldsymbol{i}\alpha}^{\dagger}U_{\boldsymbol{i}+\hat{\boldsymbol{e}}_j\beta}\right)_{\sigma\sigma}\right|^2 + \left|\left(U_{\boldsymbol{i}\alpha}^{\dagger}U_{\boldsymbol{i}+\hat{\boldsymbol{e}}_j\beta}\right)_{\sigma\sigma}\right|^2\right]\alpha_{\boldsymbol{i}}^{\dagger}\alpha_{\boldsymbol{i}},
\end{aligned} \tag{3.17}$$

which describes the coupling between charge (Grassmann fields) and spin [SU(2) gauge fields] degrees of freedom in the regime where double occupancy is excluded [$\mathcal{O}(J)$].

In order to account for the effect of charge and spin quantum fluctuations on the ground-state energy and magnetization of the system under hole doping and in the presence of a magnetic field, we shall consider that, in the regime of interest (stable AF phase and U values not extremely high, such that the Nagaoka phenomenon is frozen; see discussion in the end of this section), these quantum fluctuations manifest independently, i.e., the charge and spin correlation functions can be decoupled and calculated separately. Below, we show that the consistent results which come out from this procedure are highly rewarding. The above reasoning amounts to consider that in Eq. (3.17) the charge correlation function is well described by the spinless tight-binding result [66, 67]:

$$\sum_j \langle \alpha_{\boldsymbol{i}}^{\dagger}\alpha_{\boldsymbol{i}+\hat{\boldsymbol{e}}_j}\rangle = \frac{1}{\pi^2}\left[\sqrt{2\pi\delta}\,\sin\left(\sqrt{2\pi\delta}\right) + \frac{8}{\sqrt{3}}\sin\left(\sqrt{\frac{\pi\delta}{2}}\right)\,\sin\left(\sqrt{\frac{3\pi\delta}{2}}\right)\right], \tag{3.18}$$

where $\delta = 1 - n_\alpha$ measures the hole doping away from half filling.

The above correlation function [Eq. (3.18)] can be derived by writting the lattice fermionic fields, in the $\boldsymbol{k}$-space, as:

$$\begin{aligned}
\alpha_{\boldsymbol{i}}^{\dagger} &= \frac{1}{\sqrt{N}}\sum_{\boldsymbol{k}} e^{-i\boldsymbol{k}\cdot\boldsymbol{i}}\alpha_{\boldsymbol{k}}; \\
\alpha_{\boldsymbol{i}+\boldsymbol{e}_j} &= \frac{1}{\sqrt{N}}\sum_{\boldsymbol{k},j} e^{i\boldsymbol{k}\cdot(\boldsymbol{i}+\boldsymbol{e}_j)}\alpha_{\boldsymbol{k}},
\end{aligned} \tag{3.19}$$

so that, after straightforward algebraic manipulations, in the thermodynamic limit $\left(\sum_k \longrightarrow \frac{N}{4\pi^2}\int d^2\boldsymbol{k}\right)$, the correlation function reads:

$$\sum_j \langle \alpha^\dagger_{\boldsymbol{i}} \alpha_{\boldsymbol{i}+\hat{\boldsymbol{e}}_j}\rangle = \frac{1}{4\pi^2}\sum_j \int e^{i\boldsymbol{k}\cdot\boldsymbol{e}_j} d^2\boldsymbol{k}. \tag{3.20}$$

In the sequence, one should take into account the three honeycomb lattice unit vectors

$$\boldsymbol{e}_1 = (1,0)\,; \quad \boldsymbol{e}_2 = \left(\frac{1}{2}, \frac{-\sqrt{3}}{2}\right); \quad \boldsymbol{e}_3 = \left(\frac{-1}{2}, \frac{-\sqrt{3}}{2}\right), \tag{3.21}$$

with the intention of writting the Eq. (3.20) in the form:

$$\sum_j \langle \alpha^\dagger_{\boldsymbol{i}} \alpha_{\boldsymbol{i}+\hat{\boldsymbol{e}}_j}\rangle = \frac{1}{4\pi^2}\int \left[e^{ik_x} + 2e^{-i\frac{k_x}{2}}\cos\left(\frac{\sqrt{3}k_y}{2}\right)\right] d^2\boldsymbol{k}. \tag{3.22}$$

Further, by performing the above integration over the first Brillouin zone:

$$\sum_j \langle \alpha^\dagger_{\boldsymbol{i}} \alpha_{\boldsymbol{i}+\hat{\boldsymbol{e}}_j}\rangle = \frac{1}{4\pi^2}\int_{-k_F}^{k_F} dk_x \int_{-k_F}^{k_F} dk_y \left[e^{ik_x} + 2e^{-i\frac{k_x}{2}}\cos\left(\frac{\sqrt{3}k_y}{2}\right)\right], \tag{3.23}$$

one ends in

$$\sum_j \langle \alpha^\dagger_{\boldsymbol{i}} \alpha_{\boldsymbol{i}+\hat{\boldsymbol{e}}_j}\rangle = \frac{1}{\pi^2}\left[k_F \sin(k_F) + \frac{8}{\sqrt{3}}\sin\left(\frac{k_F}{2}\right)\sin\left(\frac{\sqrt{3}k_F}{2}\right)\right]. \tag{3.24}$$

In two dimensions, the hole density, δ, is related to the Fermi momentum, k_F, in the following way: $k_F = \sqrt{2\pi\delta}$ [11]. Therefore, by inserting this mathematical expression into Eq. (3.24), we can rewrite the correlation function in terms of the hole doping as expressed in Eq. (3.18).

We now consider the spin sector in Eq. (3.17), which is described by the SU(2) gauge fields through the matrix elements: $\left(U^\dagger_{\boldsymbol{i}\alpha} U_{\boldsymbol{i}+\hat{\boldsymbol{e}}_j\beta}\right)_{\sigma,-\sigma}$ and $\left|\left(U^\dagger_{\boldsymbol{i}\alpha} U_{\boldsymbol{i}+\hat{\boldsymbol{e}}_j\beta}\right)_{\sigma\sigma}\right|^2$, in terms of the usual spin operators [55]. The latter is given in Eq. (3.5), whereas the former can be written as follows:

$$\begin{aligned}\left(U^\dagger_{\boldsymbol{i}\alpha} U_{\boldsymbol{i}+\hat{\boldsymbol{e}}_j\beta}\right)_{\sigma,-\sigma} &= \frac{1}{2}\Big\{\Big[1 + 2\left(S^z_{\boldsymbol{i}\alpha} + S^z_{\boldsymbol{i}+\hat{\boldsymbol{e}}_j\beta}\right) + 4S^z_{\boldsymbol{i}\alpha}S^z_{\boldsymbol{i}+\hat{\boldsymbol{e}}_j\beta}\Big]^{1/2} \\ &\quad + \Big[1 - 2\left(S^z_{\boldsymbol{i}\alpha} + S^z_{\boldsymbol{i}+\hat{\boldsymbol{e}}_j\beta}\right) + 4S^z_{\boldsymbol{i}\alpha}S^z_{\boldsymbol{i}+\hat{\boldsymbol{e}}_j\beta}\Big]^{1/2}\Big\}.\end{aligned} \tag{3.25}$$

At this point, it is worthwhile to introduce the vector potential, $\boldsymbol{A}$, by means of the Peierls substitution [68]:

$$t \longrightarrow t\exp\left(-i\int_{\boldsymbol{r}_i}^{\boldsymbol{r}_j} \boldsymbol{A}\cdot d\boldsymbol{r}\right), \tag{3.26}$$

which is the complex matrix element for tunneling between neighboring sites, in order to properly describes the effects of charge and spin quantum fluctuations on the ground-state properties of the AF order. Thus, inserting Eqs. (3.5), (3.18) and (3.25) into (3.17), we obtain the following effective t-J Hamiltonian:

$$\begin{aligned}\mathcal{H}^{t\text{-}J} &= \frac{-2te^{-i\int_{r_i}^{r_j}\boldsymbol{A}\cdot d\boldsymbol{r}}}{z\pi^2}\left[\sqrt{2\pi\delta}\sin\left(\sqrt{2\pi\delta}\right)+\frac{8}{\sqrt{3}}\sin\left(\sqrt{\frac{\pi\delta}{2}}\right)\sin\left(\sqrt{\frac{3\pi\delta}{2}}\right)\right]\\ &\times\sum_{ij\alpha\beta}\left[\sqrt{1-2S^z_{\boldsymbol{i}+\hat{\boldsymbol{e}}_j\beta}-2S^z_{\boldsymbol{i}\alpha}+4S^z_{\boldsymbol{i}\alpha}S^z_{\boldsymbol{i}+\hat{\boldsymbol{e}}_j\beta}}+\sqrt{1+2S^z_{\boldsymbol{i}+\hat{\boldsymbol{e}}_j\beta}+2S^z_{\boldsymbol{i}\alpha}+4S^z_{\boldsymbol{i}\alpha}S^z_{\boldsymbol{i}+\hat{\boldsymbol{e}}_j\beta}}\right]\\ &-J\left(1-\delta\right)\sum_{ij\alpha\beta}\boldsymbol{S}_{\boldsymbol{i}\alpha}\cdot\boldsymbol{S}_{\boldsymbol{i}+\hat{\boldsymbol{e}}_j\beta}-\frac{JNz\left(1-\delta\right)}{8}-h\sum_{\boldsymbol{i}\alpha}\boldsymbol{S}_{\boldsymbol{i}\alpha}+h\sum_{ij\beta}\boldsymbol{S}_{\boldsymbol{i}+\hat{\boldsymbol{e}}_j\beta}.\end{aligned}\tag{3.27}$$

Notice that we also coupled the external homogeneous magnetic field, h, to the spins on sublattices A and B.

Let us now implement the second-order spin-wave analysis in the spin sector of Eq. (3.27), with the help of Eqs. (3.7)-(3.10). Further, it is convenient to choose the following Landau gauge:

$$\boldsymbol{A}=hx\hat{\boldsymbol{y}}.\tag{3.28}$$

As a result we arrive at the following diagonalized Hamiltonian up to $\mathcal{O}\left(1/S^2\right)$:

$$\mathcal{H}^{t\text{-}J}=\mathcal{H}_1^t+\mathcal{H}_2^J,\tag{3.29}$$

where the hopping Hamiltonian, $\mathcal{H}_1^t$, reads ($\boldsymbol{k}$-space):

$$\begin{aligned}\mathcal{H}_1^t &= -\frac{8tze^{h\sqrt{3}/4}}{\pi^2}\left[\frac{SN}{z}+\sum_{\boldsymbol{k}}\left(\frac{1}{\sqrt{1-\gamma_{\boldsymbol{k}}^2}}-1\right)+\frac{1}{2}\sum_{\boldsymbol{k}}\frac{\alpha_{\boldsymbol{k}}^\dagger\alpha_{\boldsymbol{k}}+\beta_{\boldsymbol{k}}^\dagger\beta_{\boldsymbol{k}}}{\sqrt{1-\gamma_{\boldsymbol{k}}^2}}\right]\\ &\times\left[\sqrt{2\pi\delta}\sin\left(\sqrt{2\pi\delta}\right)+\frac{8}{\sqrt{3}}\sin\left(\sqrt{\frac{\pi\delta}{2}}\right)\sin\left(\sqrt{\frac{3\pi\delta}{2}}\right)\right],\end{aligned}\tag{3.30}$$

and the exchange one, $\mathcal{H}_2^J$, becomes ($\boldsymbol{k}$-space):

$$\begin{aligned}\mathcal{H}_2^J &= -\frac{zS^2J\left(1-\delta\right)N}{2}+hSN+zSJ\left(1-\delta\right)\sum_{\boldsymbol{k}}\left[\left(\sqrt{1-\gamma_{\boldsymbol{k}}^2}-1\right)\right.\\ &\left.+\sqrt{1-\gamma_{\boldsymbol{k}}^2}\left(\alpha_{\boldsymbol{k}}^\dagger\alpha_{\boldsymbol{k}}+\beta_{\boldsymbol{k}}^\dagger\beta_{\boldsymbol{k}}\right)\right]-h\sum_{\boldsymbol{k}}\left[\left(\frac{1}{\sqrt{1-\gamma_{\boldsymbol{k}}^2}}-1\right)+\frac{\alpha_{\boldsymbol{k}}^\dagger\alpha_{\boldsymbol{k}}+\beta_{\boldsymbol{k}}^\dagger\beta_{\boldsymbol{k}}}{\sqrt{1-\gamma_{\boldsymbol{k}}^2}}\right]\\ &-\frac{zJ\left(1-\delta\right)}{2N}\left[\sum_{\boldsymbol{k}}\left(\sqrt{1-\gamma_{\boldsymbol{k}}^2}-1\right)\right]^2-\frac{zJ\left(1-\delta\right)N}{8}.\end{aligned}\tag{3.31}$$

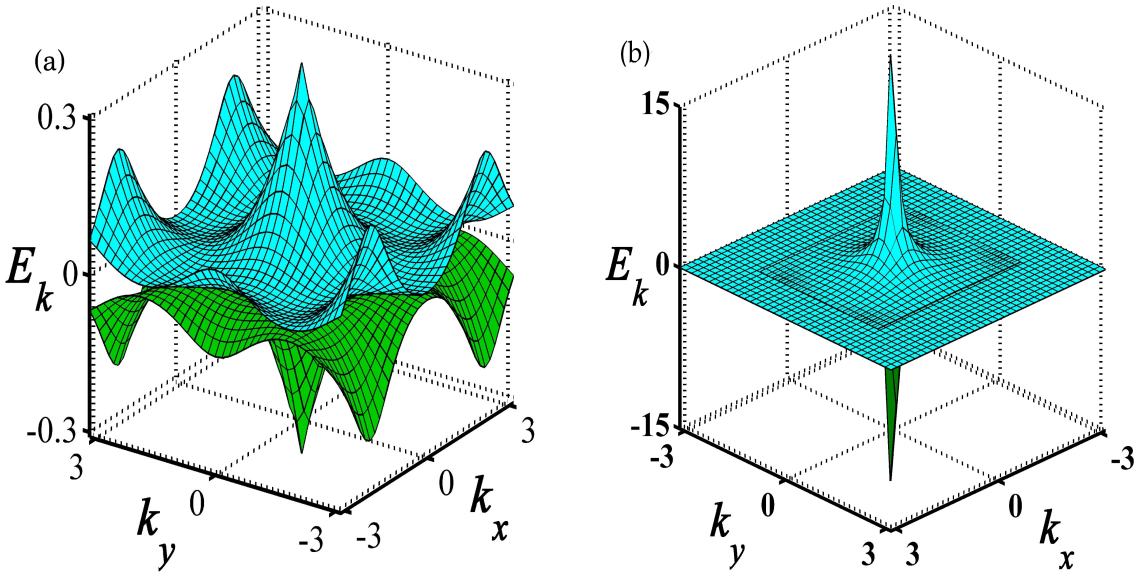

Figure 3.1: Energy spectrum of the doped AF phase at zero magnetic field and $t/J = 3$ for (a) $\delta = 0$, and (b) $\delta = 0.07$.

Therefore, the energy spectrum of $\mathcal{H}_1^t$ in the presence of a magnetic field takes the form:

$$E_1 = -\frac{8tze^{h\frac{\sqrt{3}}{4}}}{\pi^2}\left[\frac{SN}{z}+\sum_{\boldsymbol{k}}\left(\frac{1}{\sqrt{1-\gamma_{\boldsymbol{k}}^2}}-1\right)\right]\left[\sqrt{2\pi\delta}\,\sin\left(\sqrt{2\pi\delta}\right)\right.$$
$$\left.+\frac{8}{\sqrt{3}}\sin\left(\sqrt{\frac{\pi\delta}{2}}\right)\sin\left(\sqrt{\frac{3\pi\delta}{2}}\right)\right], \tag{3.32}$$

whereas the one of $\mathcal{H}_2^J$ reads:

$$E_2 = -\frac{zS^2J\,(1-\delta)\,N}{2}+hSN+zSJ\,(1-\delta)\sum_{\boldsymbol{k}}\left[\left(\sqrt{1-\gamma_{\boldsymbol{k}}^2}-1\right)\right]$$
$$-h\sum_{\boldsymbol{k}}\left[\left(\frac{1}{\sqrt{1-\gamma_{\boldsymbol{k}}^2}}-1\right)\right]-\frac{zJ\,(1-\delta)}{2N}\left[\sum_{\boldsymbol{k}}\left(\sqrt{1-\gamma_{\boldsymbol{k}}^2}-1\right)\right]^2$$
$$-\frac{zJ\,(1-\delta)\,N}{8}. \tag{3.33}$$

Lastly, by adding Eqs. (3.32) and (3.33) and taking the thermodynamic limit,

we find that the ground-state energy per site in the presence of a magnetic field:

$$\begin{aligned}\frac{E_h}{N} &= -\frac{zS^2J\left(1-\delta\right)}{2}+hS+zSJ\left(1-\delta\right)\frac{1}{4\pi^2}\int_{\mathrm{BZ}}d^2k\left[\left(\sqrt{1-\gamma_{\boldsymbol{k}}^2}-1\right)\right]\\ &-\frac{8tze^{h\frac{\sqrt{3}}{4}}}{\pi^2}\left[\frac{S}{z}+\frac{1}{4\pi^2}\int_{\mathrm{BZ}}d^2k\left(\frac{1}{\sqrt{1-\gamma_{\boldsymbol{k}}^2}}-1\right)\right]\left[\sqrt{2\pi\delta}\sin\left(\sqrt{2\pi\delta}\right)\right.\\ &\left.+\frac{8}{\sqrt{3}}\sin\left(\sqrt{\frac{\pi\delta}{2}}\right)\sin\left(\sqrt{\frac{3\pi\delta}{2}}\right)\right]-h\frac{1}{4\pi^2}\int_{\mathrm{BZ}}d^2k\left[\left(\frac{1}{\sqrt{1-\gamma_{\boldsymbol{k}}^2}}-1\right)\right]\\ &-\frac{zJ\left(1-\delta\right)}{32\pi^4}\left[\int_{\mathrm{BZ}}d^2k\left(\sqrt{1-\gamma_{\boldsymbol{k}}^2}-1\right)\right]^2-\frac{zJ\left(1-\delta\right)}{8}. \qquad (3.34)\end{aligned}$$

With the aim of corroborating the above analytical results with those obtained by GTPS simulations [26], let us choose $t/J=3$, $S=1/2$, and $z=3$. Initially, we analyze the destruction of the AF order through the evolution of the electronic structure by increasing hole doping. Indeed, in Figs. 3.1 (a) and (b) we show the evolution of the electronic structure from half-filled band ($\delta=0$), at which the system displays a fully staggered AF order, to the doped regime at $\delta=0.07$ which is quite close to the region of destruction of the AF phase. Moreover, after performing the integration over the first BZ zone in Eq. (3.34), we find that the doping-dependent ground-state energy per site at zero magnetic field can be written as follows:

$$\begin{aligned}\frac{E_0\left(\delta\right)}{NJ} &= -0.3444\left[\sqrt{2\pi\delta}\sin\left(\sqrt{2\pi\delta}\right)+\frac{8}{\sqrt{3}}\sin\left(\sqrt{\frac{\pi\delta}{2}}\right)\right.\\ &\left.\sin\left(\sqrt{\frac{3\pi\delta}{2}}\right)\right]-0.9239\left(1-\delta\right), \qquad (3.35)\end{aligned}$$

where one should notice that, here, for the sake of comparison with GTPS data, we have added the term $-z\left(1-\delta\right)/8$ to the exchange contribution [second term in Eq. (3.35)], not considered in our estimate of E_0/NJ at half filling in Section 3.1.

As shown in Fig 3.2 (a), we compare the analytical result from Eq. (3.35) with the recent GTPS [26] calculations, and QMC simulations [20] at $\delta=0$. Remarkably, our result for the doping-dependent ground-state energy agrees very well with the GTPS one up to hole doping $\delta\lesssim 0.1$. This critical value marks a region of strong magnetic instability, i.e., the breakdown of the AF order. We further indicate in the insets, Figs. 3.2 (b) and (c), the effect of hole doping in the energetic contributions of the hopping and exchange Hamiltonians, respectively. Based on physics ground, one can realize that the energetic contribution due to the hopping term decreases far below zero at $\delta=0$, as we tune up the hole doping

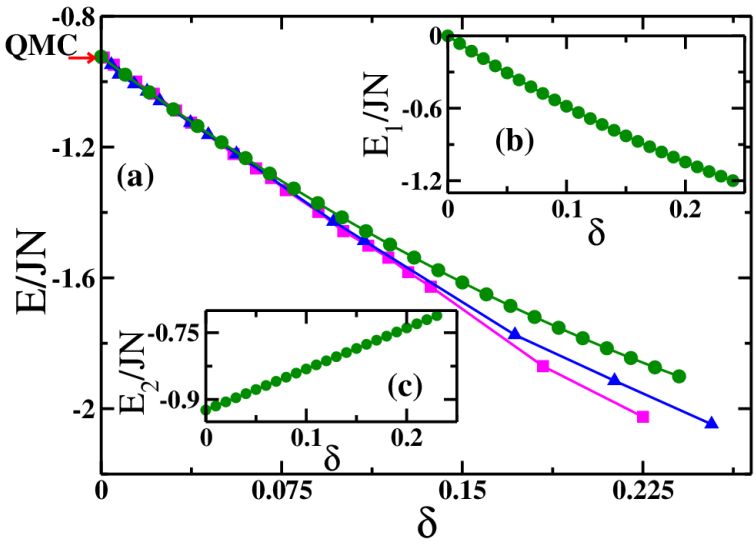

Figure 3.2: (a) Ground-state energy per site as a function of doping for $t/J = 3$. We also compare with GTPS numerical results for the virtual dimensions $D = 8$ (blue color) and $D = 12$ (magenta color). Insets: Energetic contributions of the (b) hopping and (c) exchange terms [see Eqs. (3.32) and (3.33), or first and second term in Eq. (3.35), respectively].

away from half filling, while a linear increase in the exchange energy for increasing hole doping is observed.

In order to better understand the effect of charge and spin quantum fluctuations on the AF order; we also examine the behavior of the staggered magnetization as a function of doping. In doing so, we obtain by means of Eq. (3.34) that the staggered magnetization per site, $m = \frac{1}{N}\frac{\partial E_h}{\partial h}|_{h=0}$, can be written as (for $S = 1/2$):

$$m(\delta) = 0.2418 - 0.1491\left[\sqrt{2\pi\delta}\,\sin\left(\sqrt{2\pi\delta}\right) + \frac{8}{\sqrt{3}}\sin\left(\sqrt{\frac{\pi\delta}{2}}\right)\sin\left(\sqrt{\frac{3\pi\delta}{2}}\right)\right]. \quad (3.36)$$

It is very important to stress the origin of the two contributions in Eq. (3.36): the first term stands for the Zeeman contribution to m (value of m at half filling), while the second term is the orbital contribution to m calculated by means of the Peierls substitution. Indeed, as seen in Fig. 4.10, the analytical result in Eq. (3.36) indicates that both charge and spin quantum fluctuations conspire for the breakdown of the AF order at $\delta \approx 0.1$. As a benchmark, we also display the GTPS simulations for the virtual dimension $D = 12$ [26]. Indeed, these findings are in good agreement for the critical hole concentration $\delta_c \approx 0.1$ beyond which the

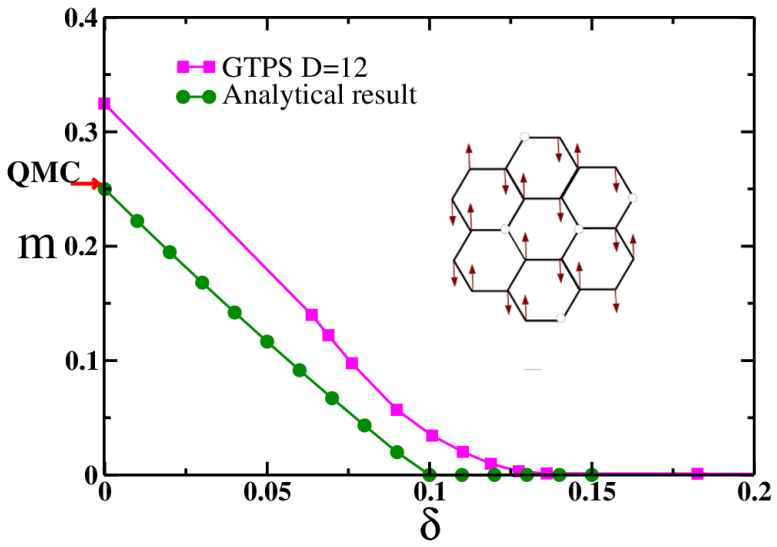

Figure 3.3: Staggered magnetization per site as a function of doping. We also benchmark against GTPS simulations for the virtual dimension $D = 12$. Inset: Illustration of the low hole doped AF phase.

AF phase disappears. However, at half filling ($\delta = 0$), the GTPS calculation has suggested a higher value for $m = 0.3239$ ($D = 12$), while QMC simulations [20] have found $m \approx 0.2681(8)$, closer to our value $m \approx 0.2418$. Notwithstanding, taking into account that the results for the ground-state energy and magnetization from quite distinct techniques (numerical and analytical) are compatible, we are confident that our analytical approach is indeed highly rewarding and claims for further development on this challenging topic.

We close this section by mentioning that the physical framework described by Eqs. (3.18) and (3.25) is in agreement with density-matrix renormalization-group results (DMRG) for hole-doped AB_2 t-J chains [69] with similar J values, in which case the holes exhibit charge-density order in anti-phase with the corresponding spin-density order. Accordingly, a similar behavior of m versus δ has also been observed in the low-doped regime of AB_2 t-J chains.

3.3. Nonlinear σ-Model with a Topological Hopf Term

The purpose of this section is to analyze the Néel-VBS competition [34–37] in the context of the nonlinear σ-model in the presence of a topological Hopf term. Actually, we shall explicit the spin fluctuations by integrating out the fermions degrees of freedom of the low-lying Lagrangian density in Eq. (2.59).

Before proceeding to more technical aspects of the mapping of the large-U model onto the nonlinear σ-model with a topological Hopf term, let us define the

order parameter used to describe the competition between the Néel state and the VBS order. Here, we shall use a five-component unit vector to describe the entire system:

$$\boldsymbol{\phi_{i\alpha}} = (n^1_{\boldsymbol{i\alpha}}, n^2_{\boldsymbol{i\alpha}}, n^3_{\boldsymbol{i\alpha}}, \rho^4_{\boldsymbol{i\alpha}}, \rho^5_{\boldsymbol{i\alpha}}), \tag{3.37}$$

which is composed of the Néel vector, $\boldsymbol{n_{i\alpha}} = \left(n^1_{\boldsymbol{i\alpha}}, n^2_{\boldsymbol{i\alpha}}, n^3_{\boldsymbol{i\alpha}}\right)$ [the Néel order parameter lies on the surface of a sphere S^2], and in competition with the VBS order parameter, $\boldsymbol{\rho_{i\alpha}} = \left(\rho^4_{\boldsymbol{i\alpha}}, \rho^5_{\boldsymbol{i\alpha}}\right)$ [the VBS order parameter lies on the circle S^1]. It should be noted that the field $\boldsymbol{\phi_{i\alpha}}$ defines a map from S^3 to S^4 [70].

Moreover, in order to establish a firm connection with the low-lying Lagrangian density in Eq. (2.59), we introduce the following representation of the SU(4) group [71]:

$$U_{\boldsymbol{i\alpha}} = \cos(\lambda) - i\sin(\lambda)\,\boldsymbol{\phi_{i\alpha}}\cdot\boldsymbol{\Gamma}, \tag{3.38}$$

where λ is a group parameter and $\boldsymbol{\Gamma}$ are the usual Dirac gamma matrices. Here, we need a set of five $\boldsymbol{\Gamma}$ matrices and among the possible choices [71], we use

$$\Gamma_{1,2,3} = \sigma_{x,y,z}\otimes\sigma_y, \quad \Gamma_4 = \sigma_0\otimes\sigma_x \quad \text{and} \quad \Gamma_5 = \sigma_0\otimes\sigma_z. \tag{3.39}$$

Also, notice that these matrices satisfy the anticommuting relations:

$$\{\Gamma_\mu, \Gamma_\nu\} = 2\delta_{\mu\nu} \quad \text{and} \quad \Gamma_5 = -\Gamma_1\Gamma_2\Gamma_3\Gamma_4. \tag{3.40}$$

Next, by considering the above SU(4) representation of $U_{\boldsymbol{i\alpha}}$ in Eq. (3.38), along with the approximation:

$$\partial_\tau\boldsymbol{\phi_{i\alpha}}\times\boldsymbol{\phi_{i\alpha}} \approx \partial_\tau\boldsymbol{\phi_{i\alpha}}, \tag{3.41}$$

we can turn the effective Lagrangian density, $\mathcal{L}$, in Eq. (2.59) into the ϕ representation:

$$\mathcal{L} \approx \sum_{\boldsymbol{i}}\alpha^\dagger_{\boldsymbol{i}}\partial_\tau\alpha_{\boldsymbol{i}} + \frac{J}{8t}\sum_{\boldsymbol{ij}\alpha}(1+i\boldsymbol{\phi_{i\alpha}}\cdot\boldsymbol{\Gamma})\left[\alpha^\dagger_{\boldsymbol{i}}\left(\alpha_{\boldsymbol{i}+\hat{\boldsymbol{e}}_j} + \alpha_{\boldsymbol{i}-\hat{\boldsymbol{e}}_j}\right) + \text{H.c.}\right]. \tag{3.42}$$

We would like to mention that terms which depend on the total time derivative and an irrelevant additive constant were excluded (such terms do not contribute to the effective action).

We proceed further to taking the continuum limit in Eq. (3.42); as a result, the partition function takes the form:

$$Z \approx \int D\bar{\alpha}D\alpha e^{-S_{\text{eff}}} = \int D\bar{\alpha}D\alpha\exp\left\{\int d^3x\bar{\alpha}\left[i\tau_\mu\partial_\mu + ig\tilde{\phi}\right]\alpha\right\}, \tag{3.43}$$

where $\boldsymbol{\tau}$ are the Pauli matrices; besides, we have defined

$$\bar{\alpha} \equiv i\tau_z\alpha^\dagger, \quad g \equiv J/4t \quad \text{and} \quad \tilde{\phi} \equiv \boldsymbol{\phi}\cdot\boldsymbol{\Gamma}. \tag{3.44}$$

Correspondingly, by means of the standard procedures [56, 57], we can write down the effective action as

$$S_{\text{eff}} = \ln \det \left(i\tau_\mu \partial_\mu + ig\tilde{\phi} \right). \tag{3.45}$$

At this stage, we follow Abanov and Wiegmann [72, 73], and write the Dirac operator in the form

$$\mathcal{D} = i\tau_\mu \partial_\mu + ig\tilde{\phi}, \tag{3.46}$$

which allow us to rewrite the fermionic determinant in Eq. (3.45) in a suitable form to evaluate a perturbative expansion. Hence, by calculating the variation of the effective action, S_{eff}, with respect to $\boldsymbol{\phi}$, we get

$$\delta S_{\text{eff}} = -\text{Tr} \left(\frac{\delta D D^\dagger}{-\partial^2 + g^2 - g\tau_\mu \partial_\mu \tilde{\phi}} \right). \tag{3.47}$$

Now, by applying the perturbative expansion up to first order in $g\tau_\mu \partial_\mu \tilde{\phi}$, we find that the effective action can be written as

$$\delta S_{\text{eff}} = \delta S_1 + \delta S_2, \tag{3.48}$$

where the first and second terms are given by

$$\delta S_1 = ig^2 \int d^3x \left[\int \frac{d^3p}{(2\pi)^3} \frac{1}{(p^2+g^2)^2} \right] \text{tr}\delta \left(\partial_\mu \tilde{\phi} \right) \partial_\mu \tilde{\phi}; \tag{3.49}$$

$$\delta S_2 = g^3 \int d^3x \left[\int \frac{d^3p}{(2\pi)^3} \frac{g^2}{(p^2+g^2)^4} \right] \text{tr}\tilde{\phi} \partial_\mu \tilde{\phi} \delta \tilde{\phi}, \tag{3.50}$$

respectively.

At this point, it is important to use the following auxiliary result [74]:

$$\int \frac{d^dp}{(2\pi)^d} \frac{1}{(p^2+m^2)^n} = \frac{i}{(4\pi)^{\frac{d}{2}}} \frac{\Gamma\left(n-\frac{d}{2}\right)}{\Gamma(n)} \left(\frac{1}{m^2} \right)^{n-\frac{d}{2}}, \tag{3.51}$$

with the purpose of solving the integral inside the brackets in Eqs. (3.49) and (3.50). By doing so, we obtain that the Eq. (3.49) yields a real contribution:

$$S_{\text{Re}} = \frac{g}{4\pi} \int d^3x \left(\partial_\mu \boldsymbol{\phi} \right)^2, \tag{3.52}$$

which is the nonlinear σ-model [72, 73, 75].

Less trivial is the evaluation of δS_2 in Eq. (3.50). Let us anticipate that this term gives rise to an imaginary contribution to the effective action that generates the topological Hopf term. With the purpose of making its derivation explicit, we must add a parameter ξ such that the field $\tilde{\phi}(x, \xi)$ continuously interpolates between the constant value $\tilde{\phi}(x, \xi = 0) = (0, 0, 0, 0, 1)$ and the physical value $\tilde{\phi}(x, \xi = 1) = \tilde{\boldsymbol{\phi}}(x)$. This leads to

$$S_{\text{Im}} = -i \frac{\epsilon_{abcde}}{12\pi} \int_0^1 d\xi \int d^3x \phi^a \partial_\tau \phi^b \partial_x \phi^c \partial_y \phi^d \partial_\xi \phi^e. \tag{3.53}$$

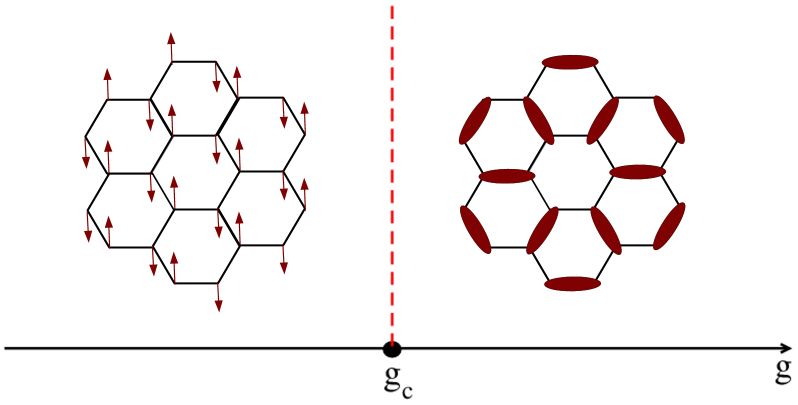

Figure 3.4: The schematic phase diagram of Eq. (3.58). The coupling g controls the strength of quantum spin fluctuations about the magnetically ordered Néel state. Left: There is broken spin rotation symmetry in the Néel state. Right: The valence bond solid (VBS) state spontaneously breaks lattice (e.g., translational) symmetry.

It is also worthwhile to introduce, without loss of generality, the four-component unit vector $\boldsymbol{\pi}$ according to the following parametrization:

$$\begin{aligned} &\phi^a = \sin(\xi\varphi)\,\pi^a,\ \phi^b = \sin(\xi\varphi)\,\pi^b,\ \phi^c = \sin(\xi\varphi)\,\pi^c,\ \phi^d = \sin(\xi\varphi)\,\pi^d, \\ &\text{and } \phi^e = \cos(\xi\varphi)\,. \end{aligned} \tag{3.54}$$

Thus, integrating over the auxiliary variable ξ, we find that

$$S_{\text{Im}} = -i\frac{\epsilon^{\mu\nu\lambda}\epsilon_{abcd}}{12\pi}\int d^3x\left[1-\frac{9}{8}\cos(\varphi)+\frac{1}{8}\cos(3\varphi)\right]\pi^a\partial_\mu\pi^b\partial_\nu\pi^c\partial_\lambda\pi^d, \tag{3.55}$$

where we can readily identify the topological Hopf term [36, 72, 73, 75]:

$$H = \frac{\epsilon_{abcd}}{12\pi^2}\int d^3x\pi^a\partial_\tau\pi^b\partial_x\pi^c\partial_y\pi^d, \tag{3.56}$$

and the θ-term:

$$\theta = \pi\left[1-\frac{9}{8}\cos(\varphi)+\frac{1}{8}\cos(3\varphi)\right]. \tag{3.57}$$

Lastly, by summing up Eqs. (3.52) and (3.55), we obtain the action of the nonlinear σ-model supplemented with a topological Hopf term:

$$S = \frac{g\sin^2\varphi}{4\pi}\int d^3x\,(\partial_\mu\boldsymbol{\pi})^2 - i\theta H. \tag{3.58}$$

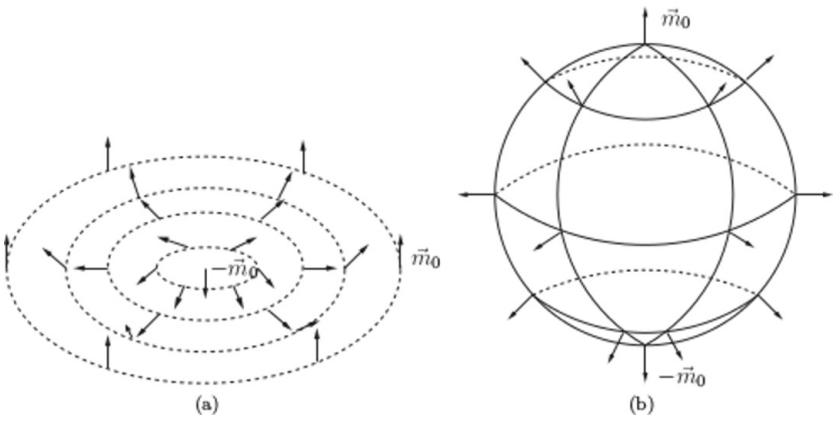

Figure 3.5: (a) Illustration of an instanton configuration in 2D Euclidean space-time, with topological charge $Q = 1$. In $(2 + 1)$ dimensions this configuration is known as a skyrmion or hedgehog. (b) An instanton on S^2 has the same topology as a monopole, that of a "hairy ball." Figure and caption taken form Ref. [56].

We would like to mention that by introducing a CP^{n-1} formulation this action can be mapped onto a bosonic representation with the well-known Chern-Simons term [36, 56, 72].

This nonlinear σ-model with the extra topological term describes the AF-VBS competition [34–37]. It is expected that, as the Coulombian interaction U varies, which means to tune the coupling constant g, so that the two insulating phases become accessible in distinct regimes, as illustrated in Fig. 3.4 (quite possibly in generalized Heisenberg models). The key point in the analysis of these two distinct ground states is to make explicit the hedgehog topological defect in the Néel order parameter (see Fig. 3.5). In order to realize this monopole configuration we parametrize the components of the four-component unit $\boldsymbol{\pi}$ in terms of the Néel vector as follows:

$$\pi^a = \sin(\upsilon)\, n^a; \quad \pi^b = \sin(\upsilon)\, n^b; \quad \pi^c = \sin(\upsilon)\, n^c \quad \text{and} \quad \pi^d = \cos(\upsilon), \tag{3.59}$$

such that we can write down the Lagrangian density, $\mathcal{L}_{BP}$, associated with the Berry phase term in Eq. (3.55) as

$$\mathcal{L}_{BP} = \frac{i}{3}(2\upsilon - \sin 2\upsilon)\left[1 - \frac{9}{8}\cos(\varphi) + \frac{1}{8}\cos(3\varphi)\right]\rho_m, \tag{3.60}$$

where

$$\rho_m = \frac{\epsilon_{abc}}{4\pi}\partial_\tau\left(n^a \partial_x n^b \partial_y n^c\right) \tag{3.61}$$

is the monopole charge density. Thus, when the monopole charge density ρ_m is integrated over the spacetime configuration of $\boldsymbol{n}$ there exists a change in the Skyrmion number:

$$\Delta Q_{xy} = \int d\tau dx dy \rho_m. \tag{3.62}$$

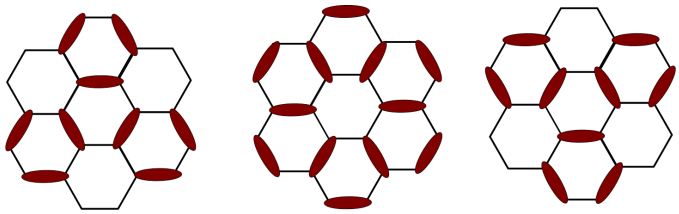

Figure 3.6: VBS order on the honeycomb lattice.

These monopoles proliferate at the deconfined AF-VBS critical point. Indeed, it has been shown that the presence of such monopole events correctly describes the quantum paramagnet VBS order [75–77], which spontaneously breaks lattice (e.g., translational) symmetry [see Fig. 3.4]. We may also identify the Berry phase, which leads to the VBS order by setting $\varphi = \pi/2$ together with the following set of $\upsilon = \{0, \pi, 2\pi\}$ in Eq. (3.60), in which case we find

$$S_{BP} = 1, \quad S_{BP} = e^{2i\pi/3\Delta Q_{xy}} \quad \text{and} \quad S_{BP} = e^{4i\pi/3\Delta Q_{xy}}, \tag{3.63}$$

respectively, which correspond to Berry phase shift equal to $2i\pi/3\Delta Q_{xy}$ [77]; in fact, by applying the symmetry operation in the honeycomb lattice we can construct the VBS order with distinct patterns [36], as shown in Fig. 3.6 .

3.4. Final Remarks

In fact, we have shown that the perturvative low-energy theory established in the previous Chapter is suitable to describe the magnetic properties of the large-U Hubbard model at half-filling band and in the doped regime.

At half-filling, in the context of the quantum Heisenberg model, we have used second-order spin-wave perturbation theory [$\mathcal{O}\left(1/S^2\right)$] to study the effect of quantum spin fluctuations on the ground-state energy and staggered magnetization of the AF order. The results are in very good agreement with previous numerical and analytical investigations.

We stress that the most challenging aspect of our analysis was the mapping of the hole-doped large-U Hubbard model onto a t-J Hamiltonian, and the formulation of a controllable perturbative scheme to analyze the role played by charge and spin quantum fluctuations on the breakdown of the hole-doped AF phase. Remarkably, our findings for the doping-dependent ground-state energy and staggered magnetization are quite consistent with recent GTPS numerical studies.

Lastly, in the continuum limit, we derived a nonlinear σ-model supplemented with a topological Hopf term that describes the AF-VBS competition, although numerical studies of the one band Hubbard model with on-site Coulombian interactions indicate a continuous quantum phase transition from a semi-metal (weak-coupling regime) to an AF phase (strong-coupling regime). As discussed in the

Introduction, the VBS order appears only in the context of the Heisenberg model with competing interactions.

4. Superconductivity and Competing Magnetic Phases

In this chapter we shall present a systematic study of the competition between superconducting and magnetic phases, using the strong-coupling low-energy effective Lagrangian density derived in the Section 2.3 [Eq. 2.59].

In order to investigate both low and high (particularly, near the Van Hove singularity) hole doping regimes, it is important to perform two changes in the referred Lagrangian density. Firstly, let us introduce the spinless hole field, $h_{\boldsymbol{i}}^{\dagger} \equiv \alpha_{\boldsymbol{i}}$ [54, 55], such that we can formally write the relation:

$$\alpha_{\boldsymbol{i}}^{\dagger}\alpha_{\boldsymbol{i}} = 1 - h_{\boldsymbol{i}}^{\dagger}h_{\boldsymbol{i}}. \tag{4.1}$$

Secondly, it is necessary to introduce the chemical potential μ, which regulates the doping levels. As a result, the large-U effective low-energy perturbative Lagrangian density in Eq. (2.59), in the hole representation, takes the form:

$$\begin{aligned}
\mathcal{L} \;=\; & \sum_{\boldsymbol{i}} h_{\boldsymbol{i}}^{\dagger}\left(\partial_{\tau}-\mu\right)h_{\boldsymbol{i}} + \sum_{\boldsymbol{i}\alpha\sigma}\theta(\sigma)\left(U_{\boldsymbol{i}\alpha}^{\dagger}\partial_{\tau}U_{\boldsymbol{i}\alpha}\right)_{\sigma\sigma}\left(1-h_{\boldsymbol{i}}^{\dagger}h_{\boldsymbol{i}}\right) \\
& -t\sum_{\boldsymbol{i}j\alpha\beta\sigma}\left[\theta(\sigma)\left(U_{\boldsymbol{i}\alpha}^{\dagger}U_{\boldsymbol{i}+\hat{\boldsymbol{e}}_j\beta}\right)_{\sigma,-\sigma}h_{\boldsymbol{i}}^{\dagger}h_{\boldsymbol{i}+\hat{\boldsymbol{e}}_j} + \text{H.c.}\right] \\
& +\frac{J}{8t}\sum_{\boldsymbol{i}j\alpha\sigma}\left(U_{\boldsymbol{i}\alpha}^{\dagger}\partial_{\tau}U_{\boldsymbol{i}\alpha}\right)_{\sigma,-\sigma}\left[\theta(\sigma)h_{\boldsymbol{i}}^{\dagger}\left(h_{\boldsymbol{i}+\hat{\boldsymbol{e}}_j}+h_{\boldsymbol{i}-\hat{\boldsymbol{e}}_j}\right)+\text{H.c.}\right] \\
& -\frac{J}{8}\sum_{\boldsymbol{i}j\alpha\beta\sigma}\theta(\sigma)\left[\left|\left(U_{\boldsymbol{i}\alpha}^{\dagger}U_{\boldsymbol{i}+\hat{\boldsymbol{e}}_j\beta}\right)_{\sigma\sigma}\right|^2+\left|\left(U_{\boldsymbol{i}\alpha}^{\dagger}U_{\boldsymbol{i}-\hat{\boldsymbol{e}}_j\beta}\right)_{\sigma\sigma}\right|^2\right]\left(1-h_{\boldsymbol{i}}^{\dagger}h_{\boldsymbol{i}}\right).
\end{aligned} \tag{4.2}$$

The derivation of Eq. (4.2) is presented in Appendix B. Further, by performing the Legendre transform:

$$\mathcal{H} = -\sum_{\boldsymbol{i}}\frac{\partial\mathcal{L}}{\partial\left(\partial_{\tau}h_{\boldsymbol{i}}\right)}\partial_{\tau}h_{\boldsymbol{i}} + \mathcal{L}; \tag{4.3}$$

where

$$\frac{\partial\mathcal{L}}{\partial\left(\partial_{\tau}h_{\boldsymbol{i}}\right)} = h_{\boldsymbol{i}}^{\dagger}, \tag{4.4}$$

we can write down the corresponding Hamiltonian as:

$$\begin{aligned}\mathcal{H} &= -\mu\sum_{\boldsymbol{i}}\left(1-h_{\boldsymbol{i}}^{\dagger}h_{\boldsymbol{i}}\right)-\sum_{\boldsymbol{i}\alpha\sigma}\theta(\sigma)\left(U_{\boldsymbol{i}\alpha}^{\dagger}\partial_{\tau}U_{\boldsymbol{i}\alpha}\right)_{\sigma\sigma}\left(1-h_{\boldsymbol{i}}^{\dagger}h_{\boldsymbol{i}}\right)\\ &-t\sum_{\boldsymbol{i}j\alpha\beta\sigma}\left[\theta(\sigma)\left(U_{\boldsymbol{i}\alpha}^{\dagger}U_{\boldsymbol{i}+\hat{\boldsymbol{e}}_j\beta}\right)_{\sigma,-\sigma}h_{\boldsymbol{i}}^{\dagger}h_{\boldsymbol{i}+\hat{\boldsymbol{e}}_j}+\text{H.c.}\right]\\ &+\frac{J}{8t}\sum_{\boldsymbol{i}j\alpha\sigma}\left(U_{\boldsymbol{i}\alpha}^{\dagger}\,\partial_{\tau}U_{\boldsymbol{i}\alpha}\right)_{\sigma,-\sigma}\left[\theta(\sigma)h_{\boldsymbol{i}}^{\dagger}\left(h_{\boldsymbol{i}+\hat{\boldsymbol{e}}_j}+h_{\boldsymbol{i}-\hat{\boldsymbol{e}}_j}\right)+\text{H.c.}\right]\\ &-\frac{J}{8}\sum_{\boldsymbol{i}j\alpha\beta\sigma}\theta(\sigma)\left[\left|\left(U_{\boldsymbol{i}\alpha}^{\dagger}U_{\boldsymbol{i}+\hat{\boldsymbol{e}}_j\beta}\right)_{\sigma\sigma}\right|^2+\left|\left(U_{\boldsymbol{i}\alpha}^{\dagger}U_{\boldsymbol{i}-\hat{\boldsymbol{e}}_j\beta}\right)_{\sigma\sigma}\right|^2\right]\left(1-h_{\boldsymbol{i}}^{\dagger}h_{\boldsymbol{i}}\right).\end{aligned} \tag{4.5}$$

The above Hamiltonian has the advantage of describing the entire system, i.e., superconducting and magnetic competing orders.

This Chapter is organized as follows: in Section 4.1, we shall describe the superconducting phases (SC) by using SU(2) gauge fields associated with the (spin-singlet) pairing symmetries: $s-$, $d_{x^2-y^2}$ - or d_{xy}-wave. Furthermore, we also perform a thermodynamic analysis of the referred states. In particular, this thermodynamic analysis shows that the critical temperature for the superconducting states is directly related to the exchange constant $J = 4t^2/U$. In Section 4.2, we also use the same formalism [SU(2) gauge fields associated with symmetries exhibited by each phase] to describe antiferromagnetic (AF) and ferromagnetic (FM) phases. Moreover, we calculate the electronic structure of the system for each one of the competing orders: AF, FM, s-, $d_{x^2-y^2}$- or d_{xy}-wave SC. In this context, an energetic analysis of the ground state of these phases reveal that the AF order prevails for low hole doping, while a dominantly chiral $d_{x^2-y^2}+id_{xy}$ superconducting state was found in the vicinity of the Van Hove singularity (high hole doping). Remarkably, in Section 4.3, we report that the competition between the AF and the chiral $d_{x^2-y^2}+id_{xy}$-wave SC phases takes place by the occurrence of a first-order transition accompanied by a spatial phase separation of the referred phases. Lastly, in Section 4.4, we draw some final remarks.

4.1. Superconducting Phases on the Honeycomb Lattice

In this section, our aim is to analyze the possible unconventional superconducting states of the large-U Hubbard on the honeycomb lattice.

As our starting point, let us consider the symmetries exhibited by the superconducting orders. Here, we shall use SU(2) gauge fields [39, 55, 78] parametrized according to the symmetry displayed by each phase. Thus, we shall describe the possible superconducting phases on the honeycomb lattice, i.e., the pairing symmetries: s-, $d_{x^2-y^2}$- and d_{xy}-wave SC states [46, 47, 79–83], through the following

$SU(2)$ gauge field [39]:

$$U_{i\alpha}^{\mathrm{SC}} = \begin{bmatrix} \sum_j \chi_{\hat{\boldsymbol{e}}_j} & -\sum_j \Delta_{\hat{\boldsymbol{e}}_j} \\ \sum_j \Delta_{\hat{\boldsymbol{e}}_j} & \sum_j \chi_{\hat{\boldsymbol{e}}_j} \end{bmatrix}, \tag{4.6}$$

where $\Delta_{\hat{\boldsymbol{e}}_j}$ is the nearest-neighbor spin-singlet pairing correlation (notice that on-site pairing is forbidden due to the very strong on-site Hubbard repulsion), and $\chi_{\hat{\boldsymbol{e}}_j}$ is the nearest-neighbor single-particle hopping correlation [39, 40, 47].

With the SU(2) gauge fields defined in Eq. (4.6), we can now study the occurrence of the mentioned superconducting phases using the Hamiltonian in Eq. (4.5), with the help of Eqs. (2.28), (2.31), (2.32) and (2.35). For this purpose, it is convenient to use the Nambu spinor representation [36]:

$$\Psi_{\boldsymbol{k}} = \begin{pmatrix} \alpha_{\boldsymbol{k}} \\ \beta_{\boldsymbol{k}} \end{pmatrix}, \tag{4.7}$$

such that the resulting Hamiltonian reads:

$$\mathcal{H}^{SC} = \sum_{\boldsymbol{k}} \Psi_{\boldsymbol{k}}^{\dagger} \tilde{E}_{\boldsymbol{k}}^{SC} \Psi_{\boldsymbol{k}} + \frac{3JN_c\chi^2}{2} + \sum_j \frac{JN_c\Delta_{\hat{\boldsymbol{e}}_j}^2}{2} - N_c\mu, \tag{4.8}$$

where

$$\tilde{E}_{\boldsymbol{k}}^{SC} = \begin{pmatrix} -E_{\boldsymbol{k}}^{SC} & 0 \\ 0 & E_{\boldsymbol{k}}^{SC} \end{pmatrix}; \tag{4.9}$$

in Eq. (4.9) $E_{\boldsymbol{k}}^{SC}$ defines the band spectrum of the superconducting phases and is given by

$$E_{\boldsymbol{k}}^{SC} = \left\{ \left[\epsilon_{\boldsymbol{k}}\chi_{\boldsymbol{k}}\Delta_{\boldsymbol{k}} + \frac{J}{4t^2}\chi_{\boldsymbol{k}}^2\epsilon_{\boldsymbol{k}}^2 - \frac{\mu}{2} + \frac{J}{4t^2}\chi_{\boldsymbol{k}}\Delta_{\boldsymbol{k}}\epsilon_{\boldsymbol{k}}^2 \right]^2 + (\epsilon_{\boldsymbol{k}}\chi_{\boldsymbol{k}}\Delta_{\boldsymbol{k}})^2 \right\}^{1/2}, \tag{4.10}$$

with

$$\Delta_{\boldsymbol{k}} \equiv \sum_j \Delta_{\hat{\boldsymbol{e}}_j} \cos\left(\boldsymbol{k}\cdot\hat{\boldsymbol{e}}_j\right), \tag{4.11}$$

$$\chi_{\boldsymbol{k}} \equiv \sum_j \chi_{\hat{\boldsymbol{e}}_j} \cos\left(\boldsymbol{k}\cdot\hat{\boldsymbol{e}}_j\right). \tag{4.12}$$

The reader can find detailed calculations of the diagonalization of $\mathcal{H}$ in Appendix B. Some comments about Eq. (4.10) are in order. One major aspect of our strong-coupling approach is the fact that at half-filling, $\mu = 0$, and $\chi_{\boldsymbol{k}} = 0$ the electronic spectrum $E_{\boldsymbol{k}}^{SC}$ is zero.

We now proceed in analyzing the symmetries exhibited by the pairing component of the superconducting order parameter, Δ. At a general level, the symmetry analysis of the pairing component of the superconducting order parameter, Δ, on

the honeycomb lattice [79–81] gives rise to the following basis-vector representation (for convenience, the normalization factor of the basis vectors is absorbed by the corresponding Δ):

$$\Delta_{\hat{\boldsymbol{e}}_j} = \begin{cases} \Delta\,(1,1,1)\,; \\ \Delta\,(2,-1,-1)\,; \\ \Delta\,(0,1,-1)\,, \end{cases} \tag{4.13}$$

for the s-, $d_{x^2-y^2}$-, and d_{xy}-wave states, respectively. Notwithstanding these possibilities, the precise realization of a particular (ground state) superconducting order parameter must be determined by energetic calculations. However, as we shall demonstrate, in the next Section, in the low hole doping regime that the AF order is more stable than the superconducting ones, while the chiral $d_{x^2+y^2}+id_{xy}$-wave superconducting phase prevails around the Van Hove singularity (the M point).

Before going through the energetic analysis, let us perform a small-wave-vector expansion [80,81], $|\boldsymbol{q}|a \ll 1$, in the function $\Delta_{\boldsymbol{k}}$ around the K points with the goal of examining the above mentioned pairing symmetries [see Fig. 4.1].

In the case of a s-wave symmetry, the superconducting order parameter $\Delta_{\boldsymbol{k}}$ becomes:

$$\Delta_{\boldsymbol{k}} = \Delta\left[\cos\left(\boldsymbol{k}\cdot\hat{\boldsymbol{e}}_1\right)+\cos\left(\boldsymbol{k}\cdot\hat{\boldsymbol{e}}_2\right)+\cos\left(\boldsymbol{k}\cdot\hat{\boldsymbol{e}}_3\right)\right], \tag{4.14}$$

and keeping in mind that the K points and the lattice unit vectors are given by [11]

$$K_{\pm} = \left(\frac{2\pi}{3a}, \pm\frac{2\pi}{3\sqrt{3}\,a}\right); \tag{4.15}$$

$$\boldsymbol{e}_1 = a\,(1,0)\,, \quad \boldsymbol{e}_2 = a\left(\frac{-1}{2},\frac{\sqrt{3}}{2}\right) \quad \text{and} \quad \boldsymbol{e}_3 = a\left(\frac{-1}{2},\frac{-\sqrt{3}}{2}\right), \tag{4.16}$$

respectively, we obtain, by employing a small-wave-vector expansion ($\boldsymbol{q} = \boldsymbol{K}_{\pm}+\boldsymbol{k}$) [81]:

$$\Delta_{\boldsymbol{q}} \approx -\frac{3a\Delta|\boldsymbol{k}|}{2}. \tag{4.17}$$

In a equivalent manner, for the $d_{x^2-y^2}$-wave symmetry:

$$\Delta_{\boldsymbol{k}} = \Delta\left[2\cos\left(\boldsymbol{k}\cdot\hat{\boldsymbol{e}}_1\right)-\cos\left(\boldsymbol{k}\cdot\hat{\boldsymbol{e}}_2\right)-\cos\left(\boldsymbol{k}\cdot\hat{\boldsymbol{e}}_3\right)\right], \tag{4.18}$$

so that the small-momentum expansion around the K points gives rise to

$$\Delta_{\boldsymbol{q}} \approx -\frac{\Delta\left(k_x^2-k_y^2\right)}{|\boldsymbol{k}|^2}. \tag{4.19}$$

Similarly, for the d_{xy}-wave symmetry:

$$\Delta_{\boldsymbol{k}} = \Delta\left[\cos\left(\boldsymbol{k}\cdot\hat{\boldsymbol{e}}_2\right)-\cos\left(\boldsymbol{k}\cdot\hat{\boldsymbol{e}}_3\right)\right], \tag{4.20}$$

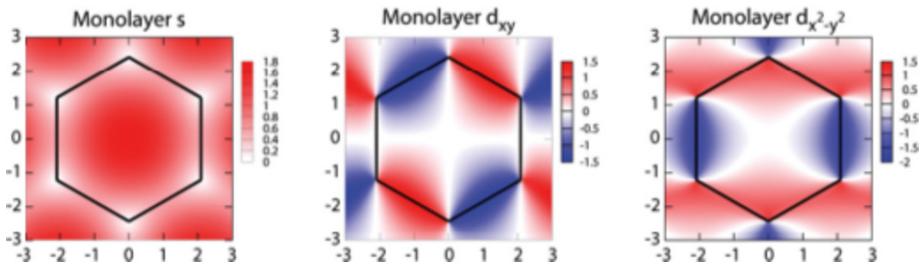

Figure 4.1: $\Delta_{\boldsymbol{k}}$ in the first Brillouin zone calculated for three possible symmetries on a (monolayer) honeycomb lattice. Figure and caption taken from Ref. [81].

we get

$$\Delta_{\boldsymbol{q}} \approx \pm \frac{\Delta\, k_x k_y}{\sqrt{3}\,|\boldsymbol{k}|^2}. \tag{4.21}$$

Eqs. (4.17), (4.19) and (4.21) above clearly indicate that near the K points the gap functions are nonzero and exhibit the corresponding symmetries, as shown in Fig. 4.1. [Although, these effective simple pictures do not emerge from a quick analysis of the electronic spectrum in Eq. (4.10); however, in Section 4.2, Figs. 4.7 these symmetries are clearly evidenced.]

In order to gain further information about distinct superconducting instabilities or ordering tendencies, we also carry out a thermodynamics analysis of the referred superconducting phases. By doing so, let us perform a Legendre transform:

$$\mathcal{H}^{SC} = -\sum_{\boldsymbol{k}} \frac{\partial \mathcal{L}_{SC}}{\partial\left(\partial_\tau \Psi_{\boldsymbol{k}}\right)} \partial_\tau \Psi_{\boldsymbol{k}} + \mathcal{L}_{SC}; \tag{4.22}$$

where

$$\frac{\partial \mathcal{L}_{SC}}{\partial\left(\partial_\tau \Psi_{\boldsymbol{k}}\right)} = \Psi^\dagger_{\boldsymbol{k}}, \tag{4.23}$$

in the diagonalized Hamiltonian in Eq. (4.8), such that the corresponding effective low-energy Lagrangian density can be written as

$$\mathcal{L}_{SC} = \sum_{\boldsymbol{k}} \Psi^\dagger_{\boldsymbol{k}} \left(\partial_\tau + \tilde{E}^{SC}_{\boldsymbol{k}}\right) \Psi_{\boldsymbol{k}} + \frac{JN_c}{2} \sum_j \Delta^2_{\hat{\boldsymbol{e}}_j} + \frac{3JN_c\chi^2}{2} - \mu N_c. \tag{4.24}$$

As a consequence, the effective action reads:

$$\mathcal{S}_{SC} = \int_0^\beta d\tau \left[\sum_{\boldsymbol{k}} \Psi^\dagger_{\boldsymbol{k}} \left(\partial_\tau + \tilde{E}^{SC}_{\boldsymbol{k}}\right) \Psi_{\boldsymbol{k}} + \frac{JN_c}{2} \sum_j \Delta^2_{\hat{\boldsymbol{e}}_j} + \frac{3JN_c\chi^2}{2} - \mu N_c\right]. \tag{4.25}$$

In the sequence, let us write the Nambu fields in Eq. (4.7) in terms of their Fourier components (from now on we shall use SI units; instead of the system of

natural units, with $\hbar = k_B = 1$):

$$\Psi_{\boldsymbol{k}} = \frac{1}{\sqrt{\hbar\beta}} \sum_n \Psi_{\boldsymbol{k}n} e^{-i\omega_n \tau}, \tag{4.26}$$

where $\omega_n = (2n+1)\,\pi k_B T/\hbar$ are the fermionic Matsubara frequencies [56–58, 84] and n is an integer. Thus, the partition function assumes the form:

$$\mathcal{Z} = \int d\Psi^{\dagger}_{\boldsymbol{k}n} d\Psi_{\boldsymbol{k}n} e^{-\mathcal{S}_{SC}\left[\Psi^{\dagger}_{\boldsymbol{k}n}, \Psi_{\boldsymbol{k}n}\right]/\hbar}, \tag{4.27}$$

with

$$\mathcal{S}_{SC} = \sum_{\boldsymbol{k}n} \Psi^{\dagger}_{\boldsymbol{k}n} \left(-i\hbar\omega_n + \tilde{E}^{SC}_{\boldsymbol{k}}\right) \Psi_{\boldsymbol{k}n} + \frac{JN_c\beta\hbar}{2} \sum_j \Delta^2_{\hat{\boldsymbol{e}}_j} + \frac{3JN_c\beta\hbar\chi^2}{2} - \beta\hbar\mu N_c. \tag{4.28}$$

Using now a saddle point procedure [56–58, 84], we can obtain the strong-coupling-BCS free energy ($\mathcal{F}_{SC} = -k_B T \ln \mathcal{Z}$):

$$\mathcal{F}_{SC} = -k_B T \sum_{\boldsymbol{k}n} \ln\left[(\hbar\omega_n)^2 + \left(E^{SC}_{\boldsymbol{k}}\right)^2\right] + \frac{JN_c}{2} \sum_j \Delta^2_{\hat{\boldsymbol{e}}_j} + \frac{3JN_c\chi^2}{2} - \mu N_c. \tag{4.29}$$

We then convert the Matsubara sum to a contour integral [84]:

$$\mathcal{F}_{SC} = -\sum_{\vec{k}} \oint \frac{dz}{2i\pi} f(z) \ln\left[z^2 - E^2_{\boldsymbol{k}}\right] + \frac{JN}{2} \sum_j \Delta^2_{\hat{\boldsymbol{e}}_j} + \frac{3JN\chi^2}{2} - N_c\mu, \tag{4.30}$$

and performing the contour integration method [85], where the integral runs anti-clockwise around the poles $\pm E^{SC}_{\boldsymbol{k}}$, as well as by realizing that the logarithm inside the integral can be split up into two terms:

$$\ln\left[z^2 - \left(E^{SC}_{\boldsymbol{k}}\right)^2\right] \longmapsto \ln\left[E^{SC}_{\boldsymbol{k}} - z\right] + \ln\left[-E^{SC}_{\boldsymbol{k}} - z\right], \tag{4.31}$$

we recognize that the strong-coupling-BCS free energy takes the form:

$$\begin{aligned} \mathcal{F}_{SC} &= -k_B T \sum_{\vec{k}} \left\{ \ln\left[1 + \exp\left(-\frac{E^{SC}_{\boldsymbol{k}}}{k_B T}\right)\right] + \ln\left[1 + \exp\left(\frac{E^{SC}_{\boldsymbol{k}}}{k_B T}\right)\right] \right\} \\ &\quad + \frac{JN_c}{2} \sum_j \Delta^2_{\hat{\boldsymbol{e}}_j} + \frac{3JN_c\chi^2}{2} - N_c\mu; \end{aligned} \tag{4.32}$$

and a simple rearrangement of the terms leads to

$$\mathcal{F}_{SC} = -2k_B T \sum_{\boldsymbol{k}} \ln\left[2\cosh\left(\frac{E^{SC}_{\boldsymbol{k}}}{2k_B T}\right)\right] + \frac{JN_c}{2} \sum_j \Delta^2_{\hat{\boldsymbol{e}}_j} + \frac{3JN_c\chi^2}{2} - N_c\mu. \tag{4.33}$$

With the purpose of finding the self-consistent equations for the s-wave and chiral $d_{x^2+y^2} + id_{xy}$-wave superconducting states [below, the reader can find the explanation for the choice of this ground state], we minimize $\mathcal{F}_{SC}$ in Eq. (4.33) with respect to Δ, χ and μ for the referred superconducting states. In the former case, the strong-coupling-BCS free energy in Eq. (4.33) takes the form:

$$\mathcal{F}_s = -2k_BT\sum_{\boldsymbol{k}} \ln\left[2\cosh\left(\frac{E_{\boldsymbol{k}}^{SC,s}}{2k_BT}\right)\right] + \frac{3JN_c}{2}\Delta^2 + \frac{3JN_c\chi^2}{2} - N_c\mu. \tag{4.34}$$

Accordingly, by minimizing $\mathcal{F}_s$ in Eq. (4.34) with respect to Δ and χ, i.e.,

$$\left(\frac{\partial\mathcal{F}_s}{\partial\Delta}\right)_{\chi,\mu} = 0 \quad \text{and} \quad \left(\frac{\partial\mathcal{F}_s}{\partial\chi}\right)_{\Delta,\mu} = 0, \tag{4.35}$$

respectively, we obtain that the strong-coupling-BCS self-consistent equations read:

$$\Delta_s = \frac{2}{3JN_c}\sum_{\boldsymbol{k}} \tanh\left(\frac{E_{\boldsymbol{k}}^{SC,s}}{2k_BT}\right)\frac{\partial E_{\boldsymbol{k}}^{SC,s}}{\partial\Delta_s}, \tag{4.36}$$

$$\chi_s = \frac{2}{3JN_c}\sum_{\boldsymbol{k}} \tanh\left(\frac{E_{\boldsymbol{k}}^{SC,s}}{2k_BT}\right)\frac{\partial E_{\boldsymbol{k}}^{SC,s}}{\partial\chi_s}. \tag{4.37}$$

It is important to note that as Δ_s and χ_s are elements of the SU(2) group, they must satisfy the constraint [$\det(U_{i\alpha}^{SC})$=1]:

$$3\left(\Delta_s\right)^2 + 3\left(\chi_s\right)^2 = 1. \tag{4.38}$$

Moreover, bear in mind that $N = -\partial F/\partial\mu$ [65], we can write down the electron density n as

$$n = \frac{N}{N_c} = -\frac{1}{N_c}\frac{\partial F}{\partial\mu}, \tag{4.39}$$

such that the above relation provides the equation for hole doping ($\delta = 1 - n$):

$$\delta_s = -\frac{1}{N_c}\sum_{\boldsymbol{k}} \tanh\left(\frac{E_{\boldsymbol{k}}^{SC,s}}{2k_BT}\right)\frac{\partial E_{\boldsymbol{k}}^{SC,s}}{\partial\mu}, \tag{4.40}$$

which connects δ_s with the components Δ_s and χ_s of the superconducting order parameter.

Now, by taking the limit $T \to 0$, we can rewrite the above set of self-consistent equations for the ground-state of the s-wave pairing in the form:

$$\begin{aligned}\Delta_s &= \frac{1}{24J\pi}\int_{BZ} d^2\boldsymbol{k}\frac{\partial E_{\boldsymbol{k}}^{SC,s}}{\partial\Delta_s};\\ \chi_s &= \frac{1}{24J\pi}\int_{BZ} d^2\boldsymbol{k}\frac{\partial E_{\boldsymbol{k}}^{SC,s}}{\partial\chi_s},\end{aligned} \tag{4.41}$$

and

$$\delta_s = -\frac{1}{8\pi}\int_{BZ} d^2\boldsymbol{k}\frac{\partial E^{SC,s}_{\boldsymbol{k}}}{\partial\mu}. \tag{4.42}$$

The above results, together with Eq. (4.10), allow us to determine the ground-state energy per site for the s-wave pairing:

$$\frac{E^s}{Nt} = \frac{1}{4\pi^2}\int_{BZ} d^2\boldsymbol{k}E^{SC,s}_{\boldsymbol{k}} + \frac{3J}{4t}\Delta^2 + \frac{3J\chi^2}{4t}. \tag{4.43}$$

In advance of the mathematical set up for the (chiral) $d_{x^2-y^2}+id_{xy}$ ($\equiv d_1+id_2$) pairing state, let us explain this choice for the honeycomb lattice. As elaborated in Refs. [46, 47, 79–83] on the grounds of lattice symmetry arguments, numerical calculations and functional renormalization group analysis, in both strong and weak coupling regimes, the dominant pairing term on the honeycomb lattice will be a mixture of $d_{x^2-y^2}-$ and $d_{xy}-$ wave [between nearest neighbor singlet pairing]:

$$\Delta_{\boldsymbol{k}} = \cos(\theta)\,\Delta_{x^2-y^2}(\boldsymbol{k}) \pm i\sin(\theta)\,\Delta_{xy}(\boldsymbol{k}), \tag{4.44}$$

in which, it was shown that: the minimum of the free energy happens for $\theta = \pi/3$; the $\pm$ signs are associated with the K and K' points, respectively, by means of the time-reversal symmetry, and the imaginary unit, i, is constrained to the free energy minimization (i.e., both $d_{x^2-y^2}$ and d_{xy} orders coexist).

Following the above prescription, let us apply the same mathematical routine performed for the s-wave pairing in order to establish the self-consistent equations for the chiral d-wave state. By doing so, for the d_1+id_2 pairing state, the strong-coupling-BCS free energy is given by

$$\mathcal{F}_{d_1+id_2} = -2k_BT\sum_{\boldsymbol{k}}\ln\left[2\cosh\left(\frac{E^{SC,d_1+id_2}_{\boldsymbol{k}}}{2k_BT}\right)\right] + 4JN_c\Delta^2 + \frac{3JN_c\chi^2}{2} - N_c\mu, \tag{4.45}$$

so that, at the stationary point of $\mathcal{F}_{d_1+id_2}$:

$$\left(\frac{\partial\mathcal{F}_{d_1+id_2}}{\partial\Delta}\right)_{\chi,\mu} = 0 \quad \text{and} \quad \left(\frac{\partial\mathcal{F}_{d_1+id_2}}{\partial\chi}\right)_{\Delta,\mu} = 0, \tag{4.46}$$

we obtain the following set of strong-coupling-BCS self-consistent equations:

$$\Delta_{d_1+id_2} = \frac{1}{4JN_c}\sum_{\boldsymbol{k}}\tanh\left(\frac{E^{SC,d_1+id_2}_{\boldsymbol{k}}}{2k_BT}\right)\frac{\partial E^{SC,d_1+id_2}_{\boldsymbol{k}}}{\partial\Delta_{d_1+id_2}}; \tag{4.47}$$

$$\chi_{d_1+id_2} = \frac{2}{3JN_c}\sum_{\boldsymbol{k}}\tanh\left(\frac{E^{SC,d_1+id_2}_{\boldsymbol{k}}}{2k_BT}\right)\frac{\partial E^{SC,d_1+id_2}_{\boldsymbol{k}}}{\partial\chi_{d_1+id_2}}, \tag{4.48}$$

and with the help of Eq. (4.39) we find:

$$\delta_{d_1+id_2} = -\frac{1}{N_c}\sum_{\boldsymbol{k}} \tanh\left(\frac{E_{\boldsymbol{k}}^{SC,d_1+id_2}}{2k_BT}\right)\frac{\partial E_{\boldsymbol{k}}^{SC,d_1+id_2}}{\partial\mu}. \tag{4.49}$$

Now, by taking the limit $T \to 0$, we obtain the following set of self-consistent equations for the ground state of the chiral $d_1 + id_2$-wave pairing:

$$\begin{aligned}\Delta_{d_1+id_2} &= \frac{1}{64J\pi}\int_{BZ} d^2\boldsymbol{k}\frac{\partial E_{\boldsymbol{k}}^{SC,d_1+id_2}}{\partial\Delta_{d_1+id_2}};\\ \chi_{d_1+id_2} &= \frac{1}{8J\pi}\int_{BZ} d^2\boldsymbol{k}\frac{\partial E_{\boldsymbol{k}}^{SC,d_1+id_2}}{\partial\chi_{d_1+id_2}},\end{aligned} \tag{4.50}$$

and

$$\delta = -\frac{1}{8\pi}\int_{BZ} d^2\boldsymbol{k}\frac{\partial E_{\boldsymbol{k}}^{SC,d_1+id_2}}{\partial\mu}. \tag{4.51}$$

Further, as $\Delta_{d_1+id_2}$ and $\chi_{d_1+id_2}$ are elements of the SU(2) group, they must satisfy the condition $[\det(U_{\boldsymbol{i}\alpha}^{SC}) = 1]$:

$$8\Delta^2 + 3\chi^2 = 1. \tag{4.52}$$

The above results, together with Eq. (4.10), allow us to determine the ground-state energy per site for the chiral $d_1 + id_2$-wave pairing:

$$\frac{E^{d_1+id_2}}{Nt} = \frac{1}{4\pi^2}\int_{BZ} d^2\boldsymbol{k}E_{\boldsymbol{k}}^{SC,d_1+id_2} + \frac{2J}{t}\Delta^2 + \frac{3J\chi^2}{4t}. \tag{4.53}$$

In Fig. 4.2(a) and (b), we show the pairing Δ and hopping χ components of the superconducting order parameter as a function of hole doping, δ, for the chiral $d_1 + id_2$-wave superconducting state. In Fig. 4.2(a), it is worth noting that the onset of the chiral $d_1 + id_2$-wave state occurs since nonzero doping values, with the optimal doping around $\delta \approx 0.15$. Further it should be noted that, beyond the critical hole doping $\delta_c \approx 0.39$, the chiral $d_1 + id_2$-wave superconducting phase disappears. Indeed, this finding is in good agreement with previous studies of the critical percolation density $\rho_c = 0.42 \pm 0.01$ for the honeycomb lattice [86]. In Fig. 4.2(b), notice that χ is nonzero everywhere. However, the system is an insulator at $\delta = 0$ (hopping is not allowed), which means that $\chi = 1/\sqrt{3}$ (open circle) is associated with the continuity condition in Eq. 4.52. It is interesting to remark that $\chi = 1/\sqrt{3}$ is in very good agreement with the maximum value (≈ 0.5760) of the tight-binding hopping correlation evaluated using Eq. (3.18), as shown in Fig. 4.3. Also, $\chi = 1/\sqrt{3}$ at $\delta = \delta_c$. This suggests that for the high-hole doped regime $\delta > \delta_c$ (open circle) the system is governed by the charge Hamiltonian $\mathcal{H}_0$ in Eq. 2.46, with the prediction of a sudden small decrease of the tight-binding hopping correlation at $\delta = \delta_c^+$.

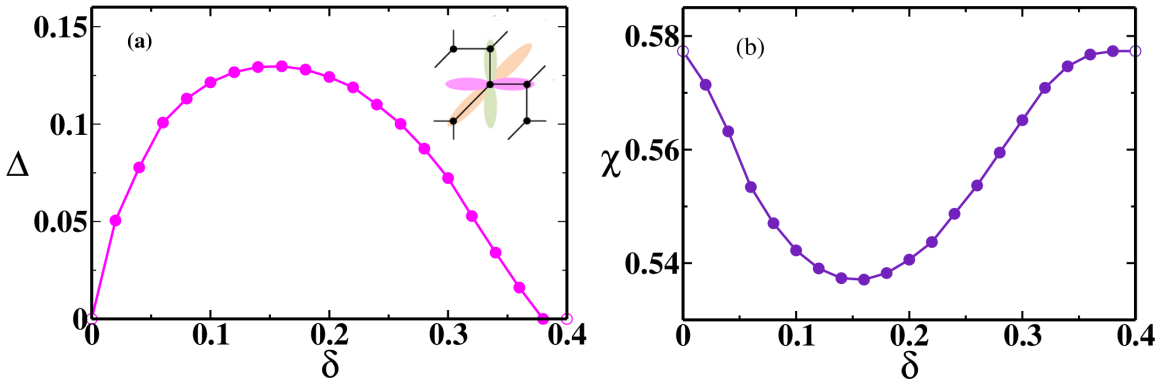

Figure 4.2: (a) Pairing Δ and (b) hopping χ components of the superconducting order parameter, at $T = 0$, as a function of doping δ for the chiral $d_1 + id_2$-wave state, with $J/t = 1/3$. Inset: Illustration of the chiral $d_1 + id_2$-wave state. Figure taken from [87].

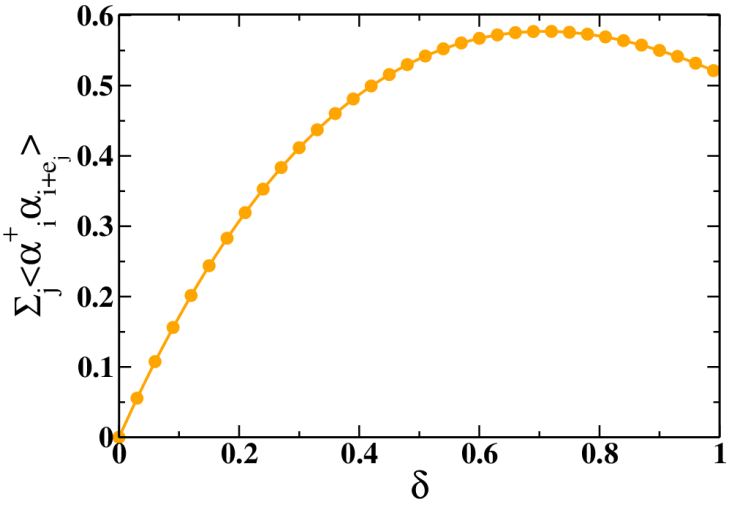

Figure 4.3: Tight-binding correlation as a function of hole doping.

Critical Temperature

Here, our aim is to examine the superconducting critical temperature for both the s-wave and the chiral $d_1 + id_2$-wave states. Thus, let us initially impose the

close gap condition [82]:

$$\frac{J}{4t^2}\chi_{\boldsymbol{k}}^2\epsilon_{\boldsymbol{k}}^2 - \frac{\mu}{2} = 0, \tag{4.54}$$

such that, in the vicinity of the Van Hove singularity $\mu \sim t$, we obtain:

$$\chi_{\boldsymbol{k}}\epsilon_{\boldsymbol{k}} = \sqrt{\frac{U}{2t}}. \tag{4.55}$$

In the sequence, by performing an expansion of the excitation spectrum in Eq. (4.10) for small Δ, we find that

$$E_{\boldsymbol{k}}^{SC} \approx \frac{3\epsilon_{\boldsymbol{k}}}{2}\chi_{\boldsymbol{k}}\Delta_{\boldsymbol{k}}. \tag{4.56}$$

Let us now estimate the superconducting critical temperature for the s-wave state. Thus, by rewriting Eq. (4.29) in the convenient form:

$$\mathcal{F}_{SC,s} = -k_BT\sum_{\boldsymbol{k}n}\ln\left[(\hbar\omega_n)^2 + \left(E_{\boldsymbol{k}}^{SC,s}\right)^2\right] + \frac{3JN_c}{2}\Delta^2 + \frac{3JN_c\chi^2}{2} - \mu N_c, \tag{4.57}$$

and minimizing with respect to Δ, i.e.,

$$\left(\frac{\partial\mathcal{F}_{SC,s}}{\partial\Delta}\right)_{\chi,\mu} = 0, \tag{4.58}$$

we obtain the following auxiliary result:

$$\Delta = \frac{2k_BT}{3JN_c}\sum_{\boldsymbol{k}n}\frac{1}{(\hbar\omega_n)^2 + (E_{\boldsymbol{k}}^{SC,s})^2}\frac{\partial E_{\boldsymbol{k}}^{SC}}{\partial\Delta}. \tag{4.59}$$

In the sequence, we replace the sum over momenta by an integral around the Van Hove singularity: $\frac{1}{N_c}\sum_{\boldsymbol{k}} \longrightarrow \frac{\rho(t)}{4\pi^2}\int d\varepsilon$, where $\rho(t) \approx 2/\pi^2 t$ (lower estimate) is the density of states close (above) to the Van Hove singularity (see pgs. 62 and 63). By doing so, as well as by substituting Eqs. (4.54)-(4.56) into Eq. (4.59), we find:

$$\frac{8\pi^2t^2}{9U^2} = 2\pi k_BT_c\sum_{n=0}^{\infty}\left[\frac{1}{\hbar\omega_n} - \frac{1}{\hbar\omega_n + \frac{J}{\Gamma^s}}\right], \tag{4.60}$$

where we have imposed the limit on $\hbar\omega_n$ by subtracting off an identical term, with $\hbar\omega_n \longrightarrow \hbar\omega_n + J/\Gamma^s$, $\Gamma^s = \sum_j \cos(\boldsymbol{k}\cdot\boldsymbol{e}_j)$ is the form factor evaluated at the M point. Keeping in mind that $\hbar\omega_n = (2n+1)\pi k_BT_c^s$, we can rewrite Eq. (4.60) in the form:

$$\frac{8\pi^2t^2}{9U^2} = \sum_{n=0}^{\infty}\left[\frac{1}{n+\frac{1}{2}} - \frac{1}{n+\frac{1}{2}+\frac{J}{2\pi k_BT_c^s\Gamma^s}}\right]. \tag{4.61}$$

At this point, we use the identity of the digamma function $\psi(z)$ [74]:

$$\psi(z) = -C - \sum_{n=0}^{\infty}\left(\frac{1}{z+n} - \frac{1}{1+n}\right), \tag{4.62}$$

where $C = 0.577$ is the Euler constant. Therefore, Eq. (4.61) can be written as

$$\frac{8\pi^2 t^2}{9U^2} = \psi\left(\frac{1}{2} + \frac{J}{2\pi k_B T_c^s \Gamma^s}\right) - \psi\left(\frac{1}{2}\right). \tag{4.63}$$

Further, by using the approximation $\psi(z) \approx \ln(z)$ [74], we obtain:

$$\frac{8\pi^2 t^2}{9U^2} = \ln\left[\frac{J e^{-\psi\left(\frac{1}{2}\right)}}{2\pi k_B T_c^s \Gamma^s}\right], \tag{4.64}$$

a simple rearrangement of the terms yields:

$$k_B T_c^s = \left[\frac{e^{-\psi\left(\frac{1}{2}\right)}}{2\pi}\right] \frac{J}{\Gamma^s} e^{-\frac{8\pi^2 t^2}{9U^2}}. \tag{4.65}$$

In an equivalent manner, the critical temperatures for the $d_1 + id_2$-wave states is given by

$$k_B T_c^d = \left[\frac{e^{-\psi\left(\frac{1}{2}\right)}}{2\pi}\right] \frac{J}{\Gamma^d} e^{-\frac{8\pi^2 t^2}{9U^2}}. \tag{4.66}$$

We remark that the above estimates of the critical temperatures in Eqs. (4.65) and (4.66) show a direct proportionality with the exchange constant $J = 4t^2/U$. Therefore, it suggests a scenario of superconductivity based on a purely electronic mechanism.

Let us also mention that in a two-dimensional system, the Mermin-Wagner theorem [88] asserts that there can be no real superconducting long-range order. However, a Kosterlitz-Thouless transition (T_{KT}) is allowed (a topological transition with power-law decay of the spin correlation function in the context of the XY model), with $k_B T_{\mathrm{KT}} = 2J/\pi$, where J denotes an exchange constant of the XY model on a square lattice [89]. It is interesting to note that using $U = 12t$ in Eq. (4.66) we find $k_B T_c^d \approx J/\Gamma^d$.

We would like to address a new theoretical analysis of the critical temperature for both superconducting phases right at the Van Hove singularity [this theoretical investigation was performed after the presentation of the above contents to the Thesis Committee].

In our first attempt in controlling the logarithmic divergence of the complete elliptic integral of the first kind, $\mathbb{F}(\theta; k = 1)$, as depicted in Fig. 4.4, we set a cutoff: J/t (energy scale) in the upper limit of the integration [see Eq. (4.92) and a detailed derivation of its analytical form in Appendix C]:

$$\mathbb{F}\left(\frac{J}{t}; k = 1\right) = \int_0^{\frac{J}{t}} \frac{d\phi}{\cos(\phi)}. \tag{4.67}$$

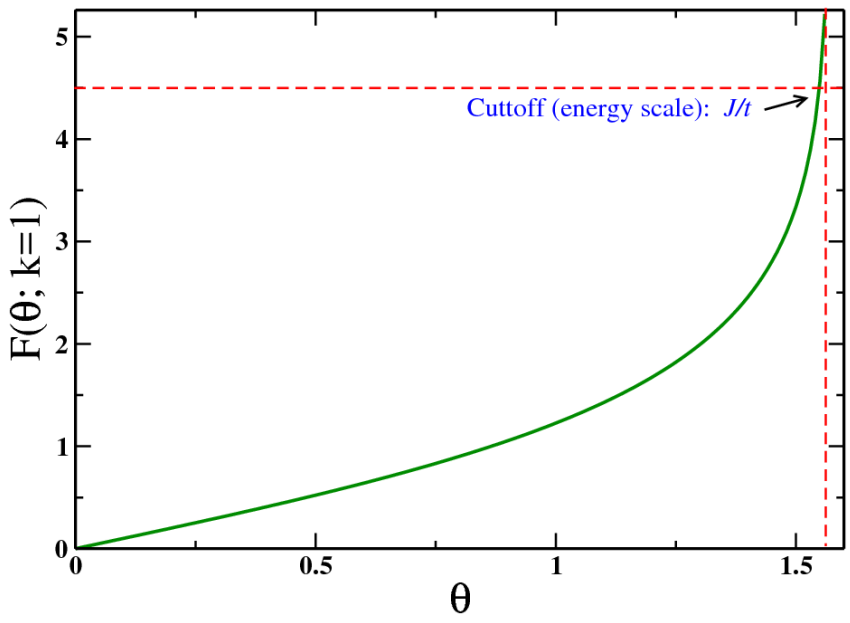

Figure 4.4: Behavior of $\mathbb{F}(\theta, k=1)$ over the interval of integration in θ [see Eq. (4.92)]. Inset: Schematic representation of the cutoff (energy scale), J/t, controlling the logarithmic divergence.

Evaluating this integral [74], one obtains:

$$\mathbb{F}\left(\frac{J}{t}; k=1\right) = \ln\left|\sec\left(\frac{J}{t}\right) + \tan\left(\frac{J}{t}\right)\right|. \tag{4.68}$$

At this point, it is important to keep in mind that in the strong-coupling regime: $J/t \ll 1$. This allows us to expand the two terms inside the bars, in Eq. (4.68), such that, after a straightforward series expansion up to $\mathcal{O}(J/t)$, we end up in the following compact form:

$$\mathbb{F}\left(\frac{J}{t}; k=1\right) = \ln\left(1+\frac{J}{t}\right). \tag{4.69}$$

Thereby, the density of states - at the Van Hove singularity - reads [see Appendix C]:

$$\rho(\varepsilon = t) = \frac{2}{\pi^2 t}\ln\left(1+\frac{J}{t}\right). \tag{4.70}$$

Now, we can readily derive an analytical expression for the critical temperature, T_c, right at the Van Hove singularity with the aid of the above density of states [Eq. (4.70)].

Next, we have used the same mathematical algorithm carried out from Eq. (4.59) to Eq. (4.64) in order to rewrite the mathematical expression of T_c, in

Eqs. (4.65) and (4.66) for the s-wave and $d_1 + id_2$-wave states (right at the Van Hove singularity), respectively. By doing so, we reached the following closed-form expressions:

$$k_B T_c^s = \left[\frac{e^{-\psi(\frac{1}{2})}}{2\pi}\right] \frac{J}{\Gamma^s} e^{-\frac{\pi^2 J}{6t}}, \tag{4.71}$$

for the s-wave superconducting order, and

$$k_B T_c^d = \left[\frac{e^{-\psi(\frac{1}{2})}}{2\pi}\right] \frac{J}{\Gamma^d} e^{-\frac{\pi^2 J}{6t}}, \tag{4.72}$$

related to the $d_1 + id_2$-wave superconducting state.

Finally, let us comment on two relevant aspects that rise up in this new theoretical analysis: (i) the above closed-form expressions also exhibit a direct link between T_c and the exchange constant $J = 4t^2/U$, which means that our previous conclusions remain valids; (ii) further, one should note that only the exponential behavior was affect by the logarithmic divergence of density of states in comparison with the preceding investigations [see Eqs. (4.65) and (4.66)]. Physically, these new theoretical findings keep up with the suggestion that the mechanism which governs the formation of the superconducting phases is purely of electronic origin.

4.2. Energetic Analysis of Superconducting and Magnetic Phases

In this section, we shall use the corresponding SU(2) gauge fields [55,78] to describe the antiferromagnetic (AF), $U_{\boldsymbol{i}\alpha}^{\mathrm{AF}}$, and ferromagnetic, $U_{\boldsymbol{i}\alpha}^{\mathrm{F}}$, phases:

$$U_{\boldsymbol{i}\alpha}^{\mathrm{M}} = \begin{bmatrix} \langle \boldsymbol{n}_{\boldsymbol{i}\alpha}\rangle \cos\left(\frac{\theta_{\boldsymbol{i}\alpha}}{2}\right) & -\langle \boldsymbol{n}_{\boldsymbol{i}\alpha}\rangle \sin\left(\frac{\theta_{\boldsymbol{i}\alpha}}{2}\right) e^{-i\phi_{\boldsymbol{i}\alpha}} \\ \langle \boldsymbol{n}_{\boldsymbol{i}\alpha}\rangle \sin\left(\frac{\theta_{\boldsymbol{i}\alpha}}{2}\right) e^{i\phi_{\boldsymbol{i}\alpha}} & \langle \boldsymbol{n}_{\boldsymbol{i}\alpha}\rangle \cos\left(\frac{\theta_{\boldsymbol{i}\alpha}}{2}\right) \end{bmatrix}, \tag{4.73}$$

where M=AF, F, $\phi_{\boldsymbol{i}\alpha}$ is an arbitrary azimuth angle due to the U(1) gauge freedom, $\theta_{\boldsymbol{i}\alpha}$ is the polar angle between the z-axis and $\langle \boldsymbol{n}_{\boldsymbol{i}\alpha}\rangle$ is the average occupation at the site $\boldsymbol{i}\alpha$ ($\boldsymbol{i}\alpha = A$ or $\boldsymbol{i}\alpha = B$) [90] . In the antiferromagnetic ground state (AF), the average occupancy at the sites the $\boldsymbol{i}A$ and $\boldsymbol{i}B$ read:

$$\langle \boldsymbol{n}_{\boldsymbol{i}A}\rangle = \frac{n}{2} + \frac{\langle m_{\boldsymbol{i}A}\rangle}{2}; \tag{4.74}$$

$$\langle \boldsymbol{n}_{\boldsymbol{i}B}\rangle = \frac{n}{2} - \frac{\langle m_{\boldsymbol{i}B}\rangle}{2}, \tag{4.75}$$

where n denotes the electron density, and $\langle m_{\boldsymbol{i}A}\rangle = -\langle m_{\boldsymbol{i}B}\rangle = m$ denotes the magnitude of the sublattice magnetization. For the ferromagnetic phase (F) the average occupation at the site $\boldsymbol{i}\alpha$ takes the form ($\langle m_{\boldsymbol{i}A}\rangle = \langle m_{\boldsymbol{i}B}\rangle = m$):

$$\langle \boldsymbol{n}_{\boldsymbol{i}A,B}\rangle = \frac{n}{2} + \frac{m}{2}. \tag{4.76}$$

We now apply the preceding formalism to the magnetic orders. Firstly, we plug Eq. (4.73) into Eq. (4.5), as well as with the help of Eqs. (2.28); (2.31); (2.32) and (2.35), we obtain, after the same pretty long calculations, that the electronic spectrum associated with the AF and F magnetic phases is given by (in the momentum space):

$$E_{\boldsymbol{k}}^{AF} = \left\{ \left[\epsilon_{\boldsymbol{k}}\left(1+m\right)\right]^2 + \left[\frac{J\left(1+m^2\right)}{8} + \frac{\mu}{2} - \frac{J\left(1-m^2\right)\epsilon_{\boldsymbol{k}}}{8t}\sum_j \cos\left(2\boldsymbol{k}\cdot\hat{\boldsymbol{e}}_j\right)\right]^2 \right\}^{1/2}; \tag{4.77}$$

$$E_{\boldsymbol{k}}^{F} = \left\{ \left[\epsilon_{\boldsymbol{k}}\left(1+m\right)\right]^2 + \left[\frac{J\left(1+m^2\right)}{8} + \frac{\mu}{2} - \frac{J\left(1+m^2\right)\epsilon_{\boldsymbol{k}}}{8t}\sum_j \cos\left(2\boldsymbol{k}\cdot\hat{\boldsymbol{e}}_j\right)\right]^2 \right\}^{1/2}, \tag{4.78}$$

respectively.

In addition, we also calculate the effective action for the AF and F phases:

$$\mathcal{S}_{AF} = \int_0^\beta d\tau \left[\sum_{\boldsymbol{k}} \Psi_{\boldsymbol{k}}^\dagger \left(\partial_\tau + \tilde{E}_{\boldsymbol{k}}^{AF}\right)\Psi_{\boldsymbol{k}} + \frac{JN_c}{4}\left(1+m^2\right) - N_c\mu \right]; \tag{4.79}$$

$$\mathcal{S}_{F} = \int_0^\beta d\tau \left[\sum_{\boldsymbol{k}} \Psi_{\boldsymbol{k}}^\dagger \left(\partial_\tau + \tilde{E}_{\boldsymbol{k}}^{F}\right)\Psi_{\boldsymbol{k}} + \frac{JN_c}{4}\left(1+m^2\right) - N_c\mu \right], \tag{4.80}$$

respectively.

In the sequence, we also evaluated the free energy related to the AF and F phases (we have performed the same calculations routine of the superconducting phases):

$$\mathcal{F}_{AF} = -2k_BT\sum_{\boldsymbol{k}} \ln\left[2\cosh\left(\frac{E_{\boldsymbol{k}}^{AF}}{2k_BT}\right)\right] + \frac{JN}{4}\left(1+m^2\right) - N_c\mu; \tag{4.81}$$

$$\mathcal{F}_{F} = -2k_BT\sum_{\boldsymbol{k}} \ln\left[2\cosh\left(\frac{E_{\boldsymbol{k}}^{F}}{2k_BT}\right)\right] + \frac{JN}{4}\left(1+m^2\right) - N_c\mu, \tag{4.82}$$

respectively.

By minimizing these free energies, we find, at $T = 0$, the following self-consistent equations for the magnetization of the AF and F orders:

$$m_{AF} = \frac{1}{8J\pi}\int d^2\boldsymbol{k}\frac{\partial E^{AF}_{\boldsymbol{k}}}{\partial m}; \tag{4.83}$$

$$\delta_{AF} = -\frac{1}{8\pi}\int d^2\boldsymbol{k}\frac{\partial E^{AF}_{\boldsymbol{k}}}{\partial \mu}, \tag{4.84}$$

and

$$m_{F} = \frac{1}{8J\pi}\int d^2\boldsymbol{k}\frac{\partial E^{F}_{\boldsymbol{k}}}{\partial m}; \tag{4.85}$$

$$\delta_{F} = -\frac{1}{8\pi}\int d^2\boldsymbol{k}\frac{\partial E^{F}_{\boldsymbol{k}}}{\partial \mu}, \tag{4.86}$$

respectively.

The above results, along with Eqs. (4.77) and (4.78), allow us to establish the ground-state energy per site for the AF and F phases:

$$\frac{E^{AF}}{Nt} = \frac{1}{4\pi^2}\int_{BZ} d^2\boldsymbol{k}E^{AF}_{\boldsymbol{k}} + \frac{J}{4t}\left(1+m^2\right); \tag{4.87}$$

$$\frac{E^{F}}{Nt} = \frac{1}{4\pi^2}\int_{BZ} d^2\boldsymbol{k}E^{F}_{\boldsymbol{k}} + \frac{J}{4t}\left(1+m^2\right), \tag{4.88}$$

respectively.

Before proceeding to the energetic analysis of the magnetic and superconducting phases in the low and high hole-doped regime, let us consider the electronic density of state in the non-interacting tight-binding case in order to build a physical picture of these doping levels. It is possible to derive an analytical expression for the density of states per unit cell from Eq. (2.34). In fact, after a pretty long calculation, we find that the density of states per unit cell for the non-interacting tight-binding case has the form [91]:

$$\rho\left(\varepsilon\right) = \frac{4\mid\varepsilon\mid}{\pi^2 t^2\sqrt{Z_0}}\mathbb{F}\left(\frac{\pi}{2},\sqrt{\frac{Z_0}{Z_1}}\right), \tag{4.89}$$

in which

$$Z_0 = \begin{cases} (1+\mid\varepsilon\mid)^2 - \frac{1}{4}\left(\mid\varepsilon\mid^2 - 1\right)^2, & \text{for} \quad \mid\varepsilon\mid\leq 1, \\ 4\mid\varepsilon\mid, & \text{for} \quad 1\leq\mid\varepsilon\mid\leq 3, \end{cases} \tag{4.90}$$

and

$$Z_1 = \begin{cases} 4\mid\varepsilon\mid, & \text{for} \quad \mid\varepsilon\mid\leq 1, \\ (1+\mid\varepsilon\mid)^2 - \frac{1}{4}\left(\mid\varepsilon\mid^2 - 1\right)^2, & \text{for} \quad 1\leq\mid\varepsilon\mid\leq 3, \end{cases} \tag{4.91}$$

where

$$\mathbb{F}\left(\frac{\pi}{2},k\right) = \int_0^{\frac{\pi}{2}}\frac{d\theta}{\sqrt{1-k^2\sin^2\left(\theta\right)}}, \tag{4.92}$$

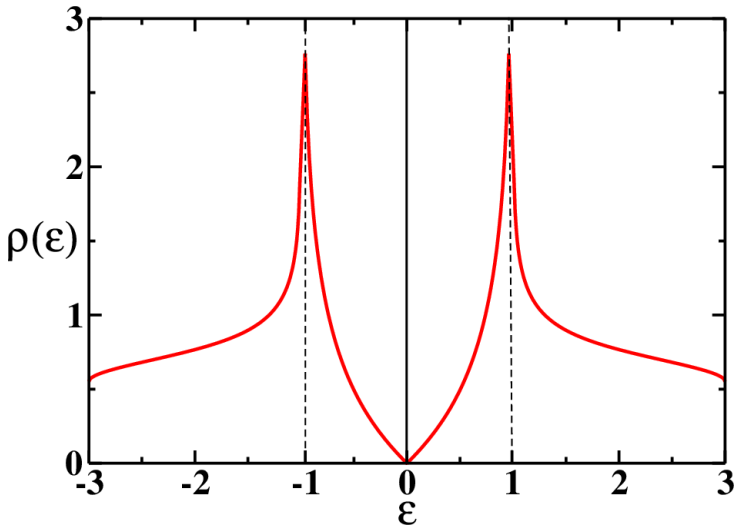

Figure 4.5: The density of states per unit cell as a function of energy ε (in units of t) for the non-interacting tight-binding case. The origin of energy has been chosen at the K points.

is the complete elliptic integral of the first kind. In Appendix C, we detailed the derivation of the above analytical expression for the density of states per unit cell. As shown in Fig. 4.3, the density of states close to the K points (the neutrality point $\varepsilon = 0$) vanishes linearly, i.e., when $\varepsilon \ll 1$ the density of states $\rho(\varepsilon) \approx 2|\varepsilon|/\left(\sqrt{3}\pi\right)$; whereas it presents a logarithmically divergent Van Hove singularity right at the M points ($\varepsilon = \pm t$).

From the above perspective, we can now study the competition between the superconducting and magnetic phases close to the K points (low hole doping) and around the Van Hove singularity (high hole doping). Technically speaking, one can realize that each self-consistent equation for a competing order is closely connected with its respective electronic spectrum. Thus, by solving numerically these self-consistent equations and performing a integration of the electronic structure in Eqs. (4.43), (4.53), (4.87) and (4.88) over the first Brillouin zone, we can obtain the ground-state energy for all competing phases.

Let us start the energetic analysis of the competing orders (at zero temperature) in the low hole doping regime. Thus, after performing the procedure explained above, we find that the doped AF prevails in the low hole doping regime, i.e., $\mu = -0.2t$, for the parameter range $0 \leq J/t \leq 1$, as shown in Fig. 4.6. We further indicate in the inset that the system is degenerated in the infinite-U limit, $J/t = 0$, as expected [61]. (We would like to mention that in the infinite-U limit there occurs the so-called Nagaoka phenomenon, which is dominated by the one-hole doped ferromagnetic ground state [66, 69].)

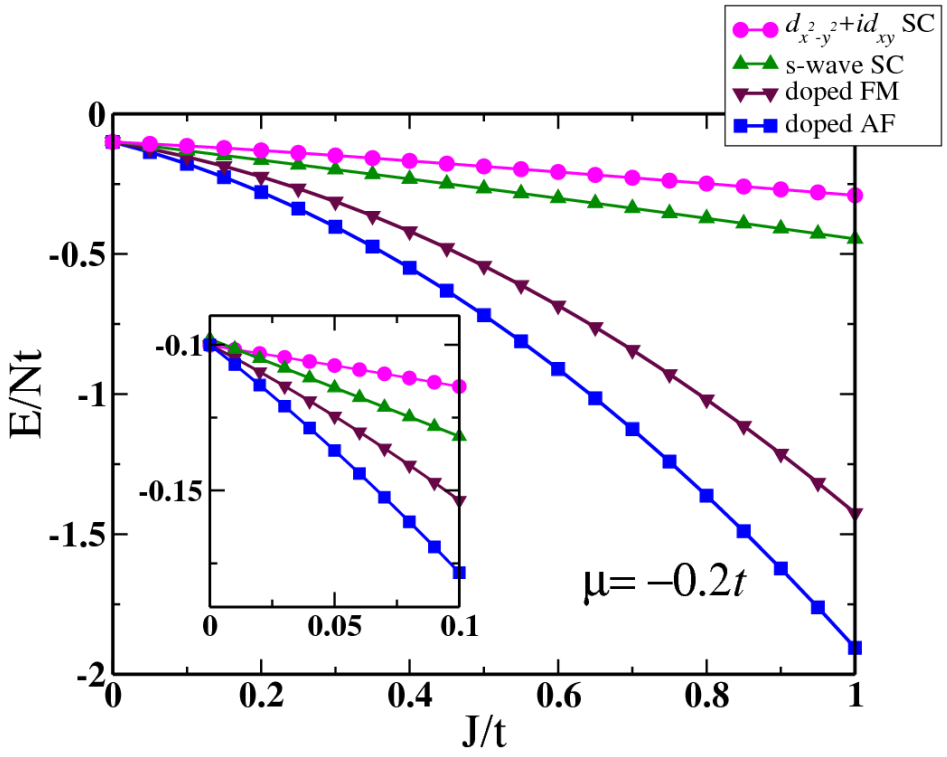

Figure 4.6: Ground-state energy per site as a function of J/t. Inset: Infinite-U limit.

Next, we investigate the system in the high hole-doped regime. As shown in Fig. 4.7, the energetic analysis displays a dominantly chiral $d-$wave superconducting order in the vicinity of the Van Hove singularity (VHS), i.e., $\mu = -t$, in the parameter range $0 \leq J/t \leq 1$. Indeed, this result is in agreement with previous theoretical studies in the weak-coupling [46] and strong-coupling [47, 79–83] regimes. We further indicate in the inset that the system is degenerated at $U = \infty$ (i.e, $J = 0$).

In Figs. 4.8(a) and 4.8(b), we plotted the electronic structure of the $d_{x^2-y^2}$-wave and d_{xy}-wave pairing symmetries, in which case one clearly sees the mentioned symmetries manifested. It is interesting to note that both lower and upper bands collapse in flat bands ($E_k = 0$) at $T = T_c^d$ for the respective symmetry. In fact, flat bands may emerge in fermionic systems with a diverging density of states [92].

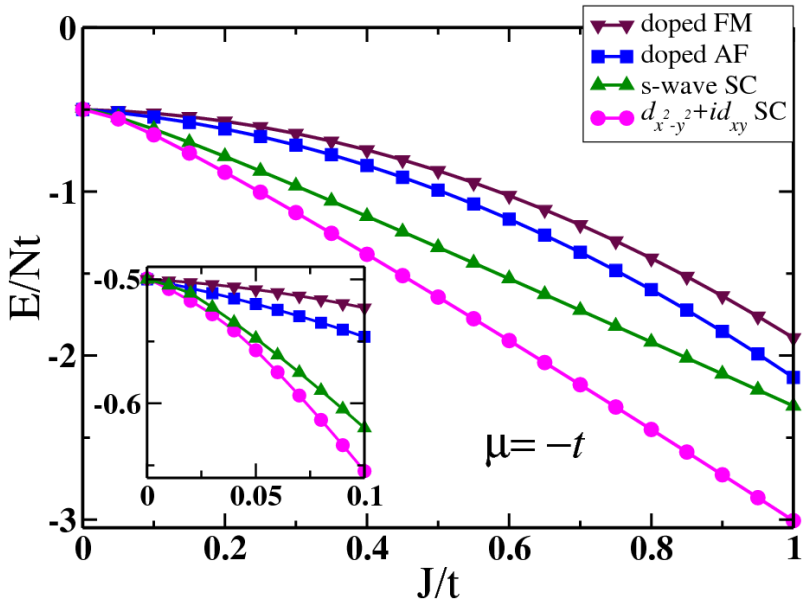

Figure 4.7: Ground-state energy per site as a function of J/t in the vicinity of the VHS. Inset: Infinite-U limit.

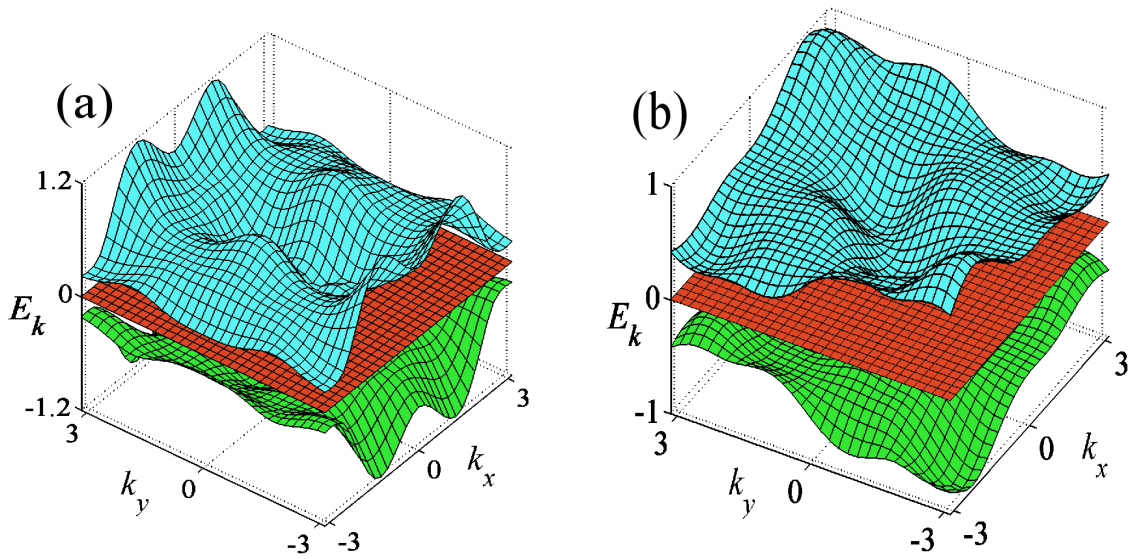

Figure 4.8: Energy spectrum of the (a) $d_{x^2-y^2}$-wave and (b) d_{xy}-wave superconducting phases with $J/t = 1/3$ and $\mu = -t$. We also present the flat band, $E_k = 0$, (red color) at $T = T_c^d$ for the respective symmetry.

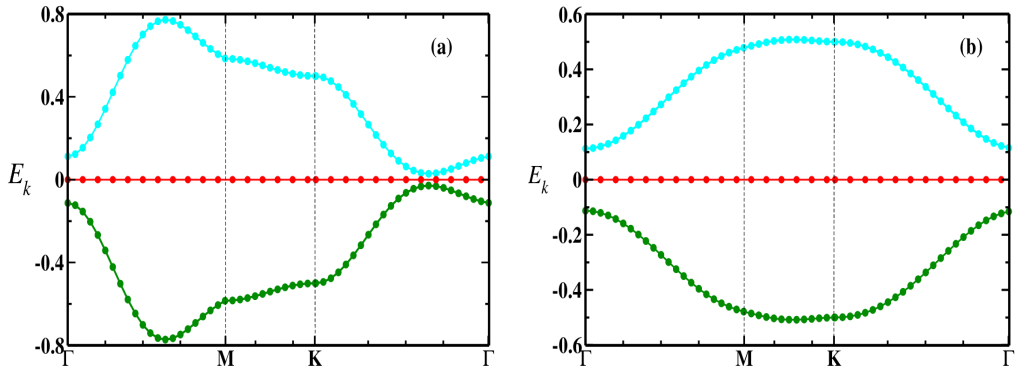

Figure 4.9: Energy spectrum along the lines connecting points of high symmetry: (a) $d_{x^2-y^2}$-wave and (b) d_{xy}-wave superconducting phases with $J/t = 1/3$ and $\mu = -t$. With the same color code of Fig. 4.8, we display the flat bands, $E_k = 0$, (red color) at $T = T_c^d$ for the respective symmetry.

In addition, in Figs. 4.9 (a) and (b), we show the projections of the energy spectrum along the lines connecting points of high symmetry of the honeycomb lattice. These projections provide a transparent link with the behavior of the d_{xy} and $d_{x^2-y^2}$ superconducting order parameters over the first Brillouin zone, depicted in Fig. 4.1. As expected, the strength of the superconducting order parameters [Eqs. (4.19) and (4.21)] ruled the behavior of the energy spectrum [Eq. (4.10)], i.e., in both symmetry cases the superconducting order parameters assume their maximum values (in modulus) in the surrounding of the M points [Figure 2.1 (b)], while they display their minimum values around the Γ and K points. Phenomenologically speaking, the spin-singlet pairing correlations acquire their maximum strength (in modulus) around the M points, so that, one can realize the formation of the superconducting state [this is a auxiliary perspective in relation to the robust energetic analysis employed in the high hole doping regime in Fig. 4.7]. Furthermore, the projections of the energy spectrum indicate that in the surrounding of the K points there exit hopping electrons in the lattice (in this region, the nearest-neighbor single particle hopping correlation governs the energy scale).

4.3. Néel-Chiral d-Wave Phase Separation

In this section, we provide evidence that a spatial phase separation takes place between the two competing ground states, i.e., the doped AF order (low hole doping) and the chiral $d_1 + id_2$-wave superconducting state (high hole doping) determined through an energetic analysis in the previous Section.

We now discuss the competition between the referred ground states through a sound thermodynamic analysis. Thus, with the help of Eqs. (4.83) and (4.84), we analyze the behavior of the magnetization, m, as a function of doping, δ, for the AF phase, in Fig. 4.10(a). At half-filling ($\delta = 0$), the magnetization has its maximum value, when we dope the AF phase away from half filling, the magnetization decreases rapidly and reaches zero at the critical hole concentration $\delta_c \approx 0.15$, which is in good agreement with preceding studies [22, 26] mentioned in Section 3.3. Further, in order to help the next explanation, we also present in the insets, Figs. 4.10(b) and 4.10(c), the pairing and hopping components of the superconducting order parameter, Δ and χ, as a function of doping, δ, (see Fig. 4.2). Hence, notice that the position of the optimal doping for the chiral $d_1 + id_2$-wave superconducting state is around $\delta \approx 0.16$, and the breakdown of the doped AF phase occurs for $\delta_c \approx 0.15$. Indeed, these findings suggest that the two ground states are in direct competition with each other; moreover, they also suggest that the AF-SC transition is not continuous for $U = 12t$, and the phases may coexist in some interval of hole concentration.

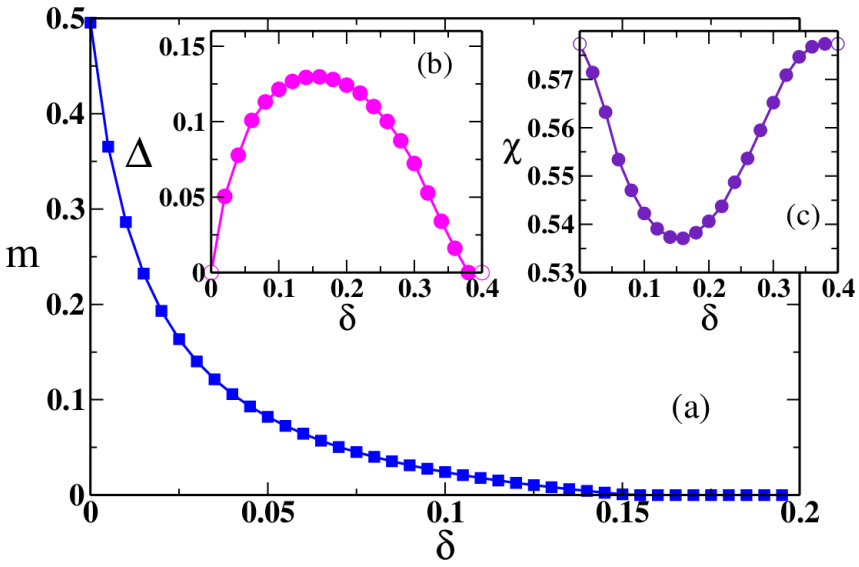

Figure 4.10: (a) Staggered magnetization as a function of doping at $t/J = 3$ in the self-consistent approach. Insets: (b) Pairing Δ and (c) hopping χ components of the superconducting order parameter as a function of doping.

In order to further understand the above-mentioned coexistence of phases, we also analyze the chemical potential as a function of doping [93], $\mu(\delta)$. Thus, with the help of Eqs. (4.50); (4.51); (4.83) and (4.84), we show chemical potential as a function of doping in Fig. 4.11 for the doped AF phase (blue line with square) and for the chiral $d_1 + id_2$-wave superconducting state (magenta line with circle) for $t/J = 3$. Further, we also compare the ground-state energies [see Eqs. (4.53) and (4.87)]:

$$\Delta E = \frac{E^{d_1+id_2}}{Nt} - \frac{E^{AF}}{Nt}, \tag{4.93}$$

since it determines the range of absolute stability of each phase. Indeed, as shown in the inset, the difference of energies ΔE becomes zero for $\mu/t \approx -0.58$, in which case the system jumps from the doped AF order to the chiral $d_1 + id_2$-wave superconducting state through a first-order phase transition, which indicates that there exists a window of forbidden doping, and, consequently, the necessity of a Maxwell construction [black line connecting the two $\mu-$curves] in the phase separation region (it can be shown in the canonical ensemble that this window of forbidden doping corresponds to the wrong convexity of the energy and a negative compressibility [62]). In fact, in this doped regime the energetic analysis [see Figs. 4.4 and 4.6] predicts unstable states (dashed blue line and dashed magenta line). Lastly, notice that while in the AF phase (see Chapter 3) χ is described by the tight-binding result shown in Fig. 4.3, in the superconducting phase χ is governed by the SU(2) condition in Eq. (4.52).

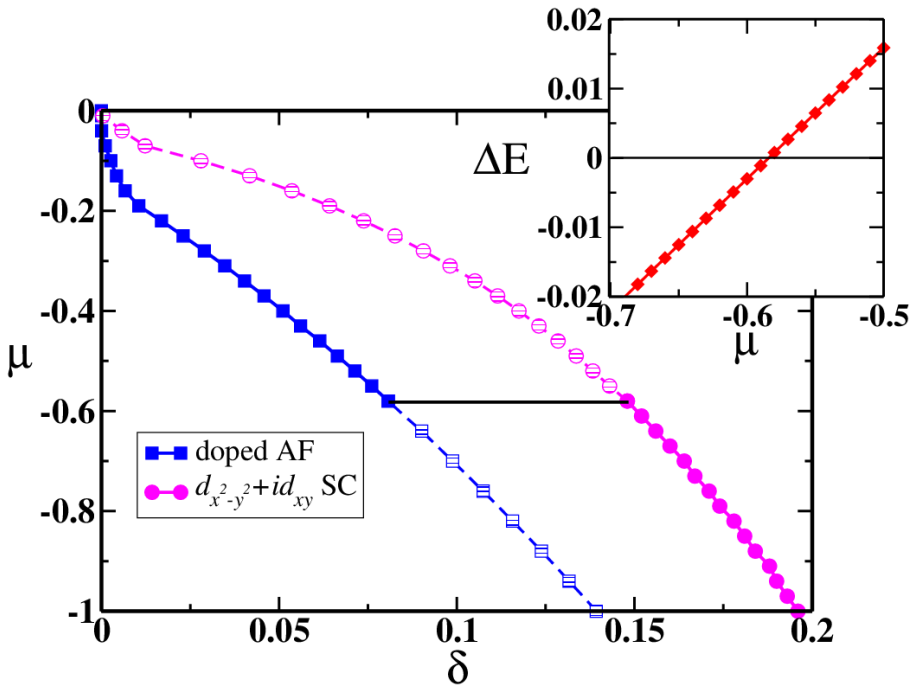

Figure 4.11: Chemical potential as a function of doping for $J/t = 1/3$. The black line indicates the phase separation regime (Maxwell construction). Inset: Difference between the ground-state energies of the doped AF phase and the chiral $d-$wave SC phases as a function of the chemical potential for $J/t = 1/3$.

By systematically employing the above careful examination of the chemical potential as a function of doping for other values of J/t, we have constructed the phase diagram of the doped strongly coupled Hubbard model on the honeycomb lattice, as depicted in Fig. 4.12.

In this phase diagram, besides the stunningly spatial phase separation between doped Néel phase (energetically stable in the low hole doping regime) and chiral $d_1 + id_2$-wave superconducting state (the dominant one in the high hole doping sector); it is interesting to notice that seemingly the two phase separation lines could meet at a quantum critical point by tunning the parameters t/U to high values [i.e., by decreasing the Coulombian interaction].

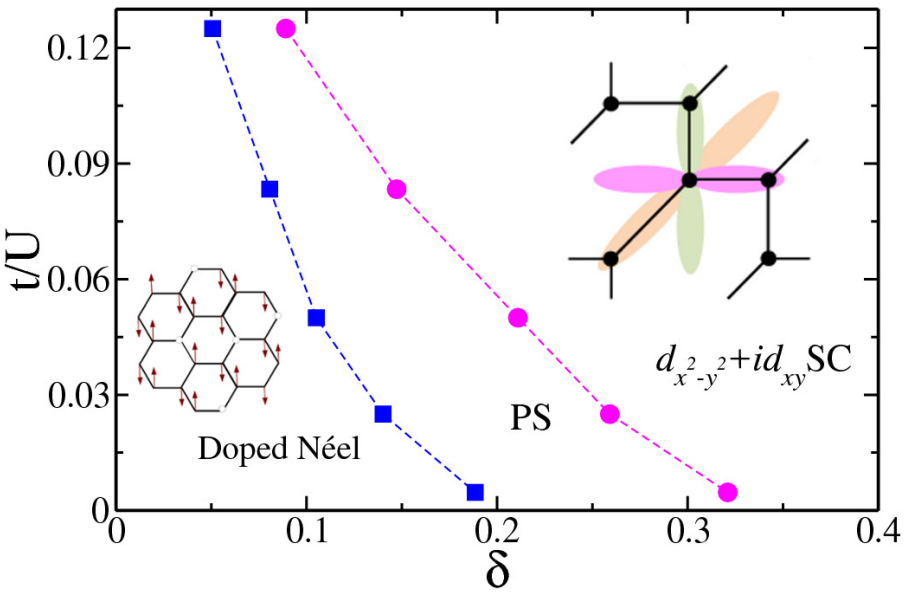

Figure 4.12: Phase diagram of the doped strongly coupled Hubbard model on the honeycomb lattice. (left) Doped Néel phase and (right) chiral $d_1 + id_2$-wave superconducting state are spatially separated (PS). Insets: (left) Doped Néel phase and (right) chiral d_1+id_2-wave superconducting state. The right cartoon was taken from Ref. [87].

4.4. Final Remarks

We have presented a extensive study of the unconventional superconducting phases on the honeycomb lattice, based on the effective low-energy Lagrangian density derived in Section 2.3. Indeed, our approach has proved very useful to describe both superconducting and magnetic orders in the low and high hole-doped regime. Further, through an energetic analysis, we have demonstrated that the AF order predominates in the low hole doping, while a dominantly chiral $d_1 + id_2$-wave superconducting state was found in the vicinity of the Van Hove singularity.

We would like to emphasize that our approach, based on SU(2) gauge fields, has proved fundamental in warranting that the long-range order associated with the chiral d-wave superconducting phase takes place only below the critical percolation concentration of the honeycomb lattice.

In addition, by means of a thermodynamic analysis, we have shown that the critical temperature for the superconducting states is directly related to the exchange constant $J = 4t^2/U$, which indicates a scenario of superconductivity rested on a purely electronic mechanism. Remarkably, we reported that the competition between the AF order and the chiral $d_1 + id_2$-wave superconducting phase takes

place by the occurrence of a first-order transition accompanied by a spatial phase separation of the mentioned phases.

In subsequent theoretical analysis of the role played by the Van Hove singularity on the critical temperature of the superconducting phase, we also have found that the exchange constant, J, is straightforward linked with the critical temperature, so that, it remains our conclusion about the purely electronic mechanism mediating the formation of the superconducting phases (the previous analysis was performed in the vicinity of the Van Hove singularity).

Additionally, we have built the phase diagram which clearly displays that the doped Néel and the chiral $d_1 + id_2$-wave superconducting phases are spatially separated. Moreover, these findings signal the tendency that the two phase separation lines could meet at a quantum critical point for small values of the Coulombian interaction. We would like to mention that the well-developed perturbative theory has provided robust results in the strong-coupling regime. But, the preceding comment about the possible existence of a quantum critical point in the phase diagram is worthy of a special analytical/simulational treatment starting in the weak-coupling limit, i.e., for small values of the Coulombian interaction, in order to establish further evidence about the occurrence of this quantum critical point.

5. Conclusions

In this work, we studied the magnetic and superconducting properties of the large-U Hubbard model on the honeycomb lattice at half-filling and in the hole-doped regime.

In Chapter 2, we reported in detail an analytical investigation of the large-U Hubbard model on the honeycomb lattice. Our approach, based on field-theoretic methods, has the advantage of allowing us to derive the Lagrangian density related to the charge and spin degrees of freedom in a controllable scheme. As a result, we diagonalized exactly the Hamiltonian associated with the charge degrees of freedom only, in which case the electronic spectrum exhibits a charge Hubbard gap separating the Dirac cones. In the strong-coupling regime, by performing a perturbative expansion in the parameter t/U up to $\mathcal{O}\left(J = 4t^2/U\right)$, we were able to derive a low-energy theory suitable to describe the (quantum) magnetic and superconducting phases at half-filling and in the hole-doped regime.

In Chapter 3, at half-filling (quantum Heisenberg model), we have used second-order spin-wave perturbation theory $[\mathcal{O}\left(1/S^2\right)]$ to study the effect of quantum spin fluctuations on the ground-state energy and staggered magnetization of the AF order. The results are in very good agreement with previous numerical and analytical investigations. Furthermore, in the continuum, we derived a nonlinear σ-model with a topological Hopf term that describes the AF-VBS competition, although numerical studies of the Hubbard model indicate a continuous quantum phase transition from a semi-metal (weak-coupling regime) to an AF phase (strong-coupling regime). Finally, we stress that the most challenging aspect of our analysis was the mapping of the hole-doped large-U Hubbard model onto a t-J Hamiltonian; and the formulation of a controllable perturbative scheme to analyze the role played by charge and spin quantum fluctuations on the breakdown of the hole-doped AF phase. In fact, our findings for the doping-dependent ground-state energy and staggered magnetization are quite consistent with recent GTPS numerical studies.

Finally, in Chapter 4, we extensively investigated the competition between the superconducting and magnetic phases in the low and high hole doping regimes. Through an energetic analysis based on a strong-coupling-BCS approach, we have demonstrated that the AF order prevails in the low hole doping, while a dominantly chiral $d_{x^2-y^2} + id_{xy}$ superconducting state was identified in the vicinity of the Van Hove singularity. We would like to emphasize that our approach, based on SU(2) gauge fields, has proved fundamental in warranting that the long-range

order associated with the chiral $d_{x^2-y^2} + id_{xy}$-wave superconducting phase takes place only below the critical percolation concentration of the honeycomb lattice. In addition, by means of a thermodynamic analysis, we have shown that the critical temperature for the superconducting states is directly related to the exchange constant $J = 4t^2/U$, which indicates a scenario of superconductivity rested on a purely electronic mechanism. Remarkably, we have found that the competition between the AF and the chiral $d_{x^2-y^2} + id_{xy}$ SC phases takes place by the occurrence of a first-order transition accompanied by a spatial phase separation of the mentioned phases.

In afterward theoretical examinations, we have also found that the exchange constant, J, is straightforward linked with the critical temperature, right at the Van Hove singularity, so that, our previous conclusion about the purely electronic mechanism mediating the formation of the superconducting phases hold. Moreover, we have also built the phase diagram which clearly exhibits a spatial phase separation between the doped Neel and the chiral $d_{x^2-y^2} + id_{xy}$-wave superconducting phases. Besides, these findings indicate the likelihood that the two phase separation lines could run into a quantum critical point for small values of the Coulombian interaction. Let us mention that the well-developed perturbative theory has yielded robust results in the strong-coupling regime. However, the previous conclusion about the possible existence of a quantum critical point in the phase diagram is worthy of a special analytical/simulational treatment beginning with the weak-coupling limit, i.e., for small values of the Coulombian interaction, with the purpose of providing further evidence about the occurrence of this quantum critical point.

6. References

[1] P. A. M. Dirac, Proc. R. Soc. A **123**, 714 (1929); see also A. Zangwill, *A half century of density functional theory*, Physics Today **68**, 34 (July, 2015).

[2] P. W. Anderson, Science **177**, 393 (1972); see also P. Coleman, *Many-Body Physics: Unfinished Revolution*, Ann. Henri Poincaré **4**, 1 (2003).

[3] J. Orenstein and A. J. Millis, Science **288**, 468 (2000).

[4] B. Keimer, S. A. Kivelson, M. R. Norman, S. Uchida, and J. Zaanen, Nature **518**, (180) (2015).

[5] J.G. Bednorz and K.A. Müller, Z. Phys. B **64**, 189 (1986).

[6] A. Montorsi, *The Hubbard Model* (World Scientific Publishing, Singapore, 1992).

[7] A. Damascelli, Z. Hussain, and Z. X. Shen, Rev. Mod. Phys. **75**, 473 (2003).

[8] J. Bardeen, L. N. Cooper, and J. R. Schrieffer, Phys. Rev. **108**, 1175 (1957); for a historical review of how this theory developed, see L. N. Cooper and D. Feldman, BCS: 50 Years, eds. World Scientific (2010).

[9] A. V. Chubukov and P. J. Hirschfeld, Physics Today **68**, 46 (June, 2015).

[10] S. Sachdev and B. Kreimer, Physics Today **64**, 29 (2011).

[11] A. H. Castro Neto, F. Guinea, N. M. R. Peres, K. S. Novoselov, and A. K. Geim, Rev. Mod. Phys. **81**, 109 (2009); V. N. Kotov, B. Uchoa, V. M. Pereira, F. Guinea, and A. H. Castro Neto, *ibid* **84**, 1067 (2012).

[12] V. Kataev, A. Möller, U. Löw, W. Jung, N. Schittner, M. Kriener, and A. Freimuth, J. Magn. Magn. Mater. **290-291**, 310 (2005).

[13] A. Moller, U. Löw, T. Taetz, M. Kriener, G. André, F. Damay, O. Heyer, M. Braden, and J. A. Mydosh, Phys. Rev. B **78**, 024420 (2008).

[14] Y. J. Yan, Z. Y. Li, T. Zhang, X. G. Luo, G. J. Ye, Z. J. Xiang, P. Cheng, L. J. Zou, and X. H. Chen, Phys. Rev. B **85**, 085102 (2012).

[15] Y. Miura, R. Hirai, Y. Kobayashi, and M. Sato, J. Phys. Soc. Jpn. **75**, 084707 (2006).

[16] S. A. J. Kimber, I. I. Mazin, J. S. Shen, H. O. Jeschke, S. V. Streltsov, D. N. Argyriou, R. Valentí, and D. Khomskii, Phys. Rev. B **89**, 081408(R) (2014).

[17] Y. Singh and P. Gegenwart, Phys. Rev. B **82**, 064412 (2010).

[18] B. D. Piazza, M. Mourigal, N. B. Christensen, G. J. Nilsen, P. Tregenna-Piggott, T. G. Perring, M. Enderle, D. F. McMorrow, D. A. Ivanov and H. M. Ronnow, Nature Physics **11**, 62 (2015).

[19] J. D. Reger, J. A. Riera, and A. P. Young, J. Phys.: Condens. Matter **1**, 1855 (1989).

[20] U. Löw, Condens. Matter Phys. **12**, 497 (2009).

[21] Z. Weihong, J. Oitmaa, and C. J. Hamer, Phys. Rev. B **44**, 11 869 (1991).

[22] F. G. Ribeiro and M. D. Coutinho-Filho, Phys. Rev. B **92**, 045105 (2015).

[23] J. Oitmaa, C. J. Hamer, and W. Zheng, Phys. Rev. B **45**, 9834 (1992).

[24] H. C. Jiang, Z. Y. Weng, and T. Xiang, Phys. Rev. Lett. **101**, 090603 (2008); Z. Y. Xie, H. C. Jiang, Q. N. Chen, Z. Y. Weng, and T. Xiang, *ibid.* **103**, 160601 (2009).

[25] H. H. Zhao, Z. Y. Xie, Q. N. Chen, Z. C. Wei, J. W. Cai, and T. Xiang, Phys. Rev. B **81**, 174411 (2010).

[26] Z. C. Gu, H. C. Jiang, D. N. Sheng, H. Yao, L. Balents, and X. G. Wen, Phys. Rev. B **88**, 155112 (2013).

[27] H. T. Diep, *Frustrated Spin Systems* (World Scientific, New Jersey, 2004); 2nd Edition (2013).

[28] H. Mosadeq, F. Shahbazi, and S. A. Jafari, J. Phys.: Condens. Matter **23**, 226006 (2011).

[29] A. F. Albuquerque, D. Schwandt, B. Hetényi, S. Capponi, M. Mambrini, and A. M. Läuchli, Phys. Rev. B **84** 024406 (2011).

[30] R. Ganesh, J. V. D. Brink, and S. Nishimoto, Phys. Rev. Lett. **110**, 127203 (2013).

[31] Z. Zhu, D. A. Huse, and S. R. White, Phys. Rev. Lett. **110**, 127205 (2013).

[32] Z. Y. Meng, T. C. Lang, S. Wessel, F. F. Assaad, and A. Muramatsu, Nature **464**, 847 (2010).

[33] S. Sorella, Y. Otsuka and S. Yunoki, Scientific Reports **2**, 992 (2012); see, also T. Paiva, R. T. Scalettar, W. Zheng, R. R. P. Singh, and J. Oitmaa, Phys. Rev. B **72**, 085123 (2005).

[34] O. I. Motrunich and A. Vishwanath, Phys. Rev. B **70**, 075104 (2004).

[35] T. Senthil, A. Vishwanath, L. Balents, S. Sachdev, and M. P. A. Fisher, Science **303**, 1490 (2004); T. Senthil, L. Balents, S. Sachdev, A. Vishwanath, and M. P. A. Fisher, Phys. Rev. B **70**, 144407 (2004).

[36] L. Fu, S. Sachdev, and C. Xu, Phys. Rev. B **83**, 165123 (2011).

[37] C. Xu, Int. J. Mod. Phys. B **26**, 1230007 (2012), and references therein.

[38] Y. Izyumov, Phys.-Usp. **40**, 445 (1997).

[39] P. A. Lee, N. Nagaosa, and X. G. Wen, Rev. Mod. Phys.**78**, 17 (2006).

[40] P. W. Anderson, P. A. Lee, M. Randeria, T. M. Rice, N. Trivedi, and F. C. Zhang, J. Phys.: Condens. Matter **16**, 755 (2004).

[41] M. Ogata and H. Fukuyama, Rep. Prog. Phys. **71**, 036501 (2008).

[42] J. L. McChesney, A. Bostwick, T. Ohta, T. Seyller, K. Horn, J. González, and Eli Rotenberg, Phys. Rev. Lett. **104**, 136803 (2010).

[43] http://www.nanoscience.de/HTML/research/graphene.html.

[44] S. J. Youn, M. H. Fischer, S. H. Rhim, M. Sigrist, and D. F. Agterberg, Phys. Rev. B **85**, 220505 (2012).

[45] P. K. Biswas, H. Luetkens, T. Neupert, T. Stürzer, C. Baines, G. Pascua, A. P. Schnyder, M. H. Fischer, J. Goryo, M. R. Lees, H. Maeter, F. Brückner, H. H. Klauss, M. Nicklas, P. J. Baker, A. D. Hillier, M. Sigrist, A. Amato, and D. Johrendt, Phys. Rev. B **87**, 180503(R) (2013).

[46] R. Nandkishore, L. S. Levitov and A. V. Chubukov, Nat. Phys. **8**, 158 (2012).

[47] W. Wu, M. M. Scherer, C. Honerkamp, and K. L. Hur, Phys. Rev. B **87**, 094521 (2013).

[48] R. L. Stratonovich, Dokl. Akad. Nauk SSSR **115**, 1094 (1957) [Sov. Phys. Dokl. **2**, 416 (1958)]; J. Hubbard, Phys. Rev. Lett. **3**, 77 (1959).

[49] C. A. Macêdo and M. D. Coutinho-Filho, Phys. Rev. B **25**, 5965 (1982); C. A. Macêdo and M. D. Coutinho-Filho, *ibid.* **43**, 13515 (1991).

[50] M. L. Lyra, M. D. Coutinho-Filho, and A. M. Nemirovsky, Phys. Rev. B **48**, 3755 (1993).

[51] H. J. Schulz, Phys. Rev. Lett. **65**, 2462 (1990).

[52] Z. Y. Weng, C. S. Ting, and T. K. Lee, Phys. Rev. B. **43**, 3790(R) (1991).

[53] Z. Y. Weng, Phys. Rev. Lett. **66**, 2156 (1991).

[54] Z. Y. Weng, D. N. Sheng, C. S. Ting, and Z. B. Su, Phys. Rev. Lett. **67**, 3318 (1991); Phys. Rev. B **45**, 7850 (1992).

[55] M. H. Oliveira, E. P. Raposo, and M. D. Coutinho-Filho, Phys. Rev. B **80**, 205119 (2009).

[56] E. Fradkin, *Field Theories of Condensed Matter Systems* (Cambrigde University Press, Cambrigde, 2013).

[57] H. Kleinert *Path Integral in Quantum Mechanics, Statistics and Polymer Physics* (World Scientific, New Jersey, 1995).

[58] X. G. Wen, *Quantum Field Theory of Many-Body Systems* (Oxford University Press, Oxford, 2010).

[59] W. K. Tung, *Group Theory in Physics* (World Scientific, New Jersey, 2010).

[60] A. Giuliani and V. Mastropietro, Commun. Math. Phys. **293**, 301 (2010).

[61] A. Auerbach, *Interacting Eletrons and Quantum Magnetism* (Springer-Verlag, New York, 1994).

[62] A. M. S. Macêdo, M. C. dos Santos, M. D. Coutinho-Filho, and C. A. Macêdo, Phys. Rev. Lett. **74**, 1851 (1995).

[63] M. H. Oliveira, *Masters Dissertation*, UFPE (2001).

[64] J. Oitmaa, C. Hamer, and W. Zheng, *Series Expansion Methods for Strongly Interacting Lattice Models* (Cambrigde University Press, Cambrigde, 2010).

[65] H. B. Callen, *Thermodynamics and an Introduction to Thermostatistics* (John Wiley Sons, New York, 1985).

[66] R. R. Montenegro-Filho and M. D. Coutinho-Filho, Phys. Rev. B **74**, 125117 (2006).

[67] C. Vitoriano and M. D. Coutinho-Filho, Phys. Rev. B **82**, 125126 (2010).

[68] F. H. L. Essler, H. Frahm, F. Göhmann, A. Klümper, and V. E. Korepin, *The One-Dimensional Hubbard Model* (Cambrigde University Press, Cambrigde, 2010).

[69] R. R. Montenegro-Filho and M. D. Coutinho-Filho, Phys. Rev. B **90**, 115123 (2014).

[70] M. Nakahara, *Geometry, Topology and Physics* (Taylor Francis Group, London, 2003).

[71] V. M. Redḱov, A. A. Bogush, and N. G. Tokarevskaya, Sigma **4**, 021 (2008).

[72] A. G. Abanov, Phys. Lett. B **492**, 321 (2000).

[73] A. G. Abanov and P. B. Wiegmann, Nucl. Phys. B **570**, 685 (2000).

[74] I. S. Gradstein, I. M. Ryshik, *Tables of Series, Products and Integrals* (Seventh Edition, Elsevier, 2007).

[75] A. Tanaka and X. Hu, Phys. Rev. Lett. **95**, 036402 (2005).

[76] F. D. M. Haldane, Phys. Rev. Lett. **61**, 1029 (1988).

[77] N. Read and S. Sachdev, Phys. Rev. Lett. **62**, 1694 (1989); Phys. Rev. B **42**, 4568 (1990).

[78] I. Affleck and F. D. M. Haldane, Phys. Rev. B **36**, 5291 (1987).

[79] A. M. Black-Schaffer and S. Doniach, Phys. Rev. B. **75**, 134512 (2007).

[80] J. Linder, A. M. Black-Schaffer, T. Yokoyama, S. Doniach and A. Sudbo, Phys. Rev. B **80**, 094522 (2009).

[81] J. Vucicevic, M. O. Goerbig and V. Milovanovic, Phys. Rev. B **86**, 215405 (2012).

[82] A. M. Black-Schaffer, Phys. Rev. Lett. **109**, 197001 (2012).

[83] A. M. Black-Schaffer, W. Wu, and K. L. Hur, Phys. Rev. B **90**, 054521 (2014).

[84] A. Altland and B. Simons, *Condensed Matter Field Theory* (Cambridge University Press, Cambridge, 2010).

[85] J. W. Brown and R. V. Churchill, *Complex Variables and Applications* (McGraw-Hill Higher Education, New York, 2009).

[86] H. Scher and R. Zallen, J. Chem. Phys. **53**, 3759 (1970); and references therein.

[87] T. Watanabe, and S. Ishihara, J. Phys. Soc. Jpn. **82**, 034704 (2013).

[88] N. D. Mermin and H. Wagner, Phys. Rev. Lett. **17**, 1133 (1966).

[89] D. R. Nelson, *Defects and Geometry in Condensed Matter Physics* (Cambridge University Press, Cambridge, 2002).

[90] N. M. R. Peres, M. A. N. Araújo, and D. Bozi, Phys. Rev. B **70**, 195122 (2004); M. A. N. Araújo and N. M. R. Peres, J. Phys. Condens. Matter **18**, 1769 (2006).

[91] J. P. Hobson and W. A. Nierenberg, Phys. Rev. **89**, 662 (1953).

[92] N. B. Kopnin, T. T. Heikkilä, and G. E. Volovik, Phys. Rev. B **83**, 220503(R) (2011); and references therein.

[93] M. Capone and G. Kotliar, Phys. Rev. B **74**, 054513 (2006).

[94] H. B. Rosenstock, J. Chem. Phys. **21**, 2064 (1953).

A.Derivation of Eq. (3.12)

We begin with the effective low-energy Lagrangian density of the honeycomb Hubbard model in the large-U regime, up to $\mathcal{O}(J)$:

$$\begin{aligned}\mathcal{L} &= \sum_{\boldsymbol{i}} \alpha_{\boldsymbol{i}}^{\dagger}\partial_{\tau}\alpha_{\boldsymbol{i}} + \sum_{\boldsymbol{i}\alpha\sigma}\theta(\sigma)\left(U_{\boldsymbol{i}\alpha}^{\dagger}\partial_{\tau}U_{\boldsymbol{i}\alpha}\right)_{\sigma\sigma}\alpha_{\boldsymbol{i}}^{\dagger}\alpha_{\boldsymbol{i}} - t\sum_{\boldsymbol{i}j\alpha\beta\sigma}\Big[\theta(-\sigma)\left(U_{\boldsymbol{i}\alpha}^{\dagger}U_{\boldsymbol{i}+\hat{\boldsymbol{e}}_j\beta}\right)_{\sigma,-\sigma} \\ &\times\alpha_{\boldsymbol{i}}^{\dagger}\alpha_{\boldsymbol{i}+\hat{\boldsymbol{e}}_j} + \text{H.c.}\Big] + \frac{J}{8t}\sum_{\boldsymbol{i}j\alpha\sigma}\left(U_{\boldsymbol{i}\alpha}^{\dagger}\ \partial_{\tau}U_{\boldsymbol{i}\alpha}\right)_{\sigma,-\sigma}\left[\theta(-\sigma)\alpha_{\boldsymbol{i}}^{\dagger}\left(\alpha_{\boldsymbol{i}+\hat{\boldsymbol{e}}_j}+\alpha_{\boldsymbol{i}-\hat{\boldsymbol{e}}_j}\right)+\text{H.c.}\right] \\ &-\frac{J}{8}\sum_{\boldsymbol{i}j\alpha\beta\sigma}\theta(\sigma)\left[\left|\left(U_{\boldsymbol{i}\alpha}^{\dagger}U_{\boldsymbol{i}+\hat{\boldsymbol{e}}_j\beta}\right)_{\sigma\sigma}\right|^2+\left|\left(U_{\boldsymbol{i}\alpha}^{\dagger}U_{\boldsymbol{i}-\hat{\boldsymbol{e}}_j\beta}\right)_{\sigma\sigma}\right|^2\right]\alpha_{\boldsymbol{i}}^{\dagger}\alpha_{\boldsymbol{i}}. \qquad (A.1)\end{aligned}$$

At half-filling, we have that $\langle\phi_0|\alpha_{\boldsymbol{i}}^{\dagger}\alpha_{\boldsymbol{i}}|\phi_0\rangle = 1$ ($n\equiv 1$), in which $|\ \phi_0\rangle$ is the unperturbed state, i.e., state with N electrons filling (totally) the lower-energy sector (α band). As a consequence, charge degrees of freedom are frozen:

$$\langle\phi_0|\alpha_{\boldsymbol{i}}^{\dagger}\partial_{\tau}\alpha_{\boldsymbol{i}}|\phi_0\rangle = 0;\ \langle\phi_0|\alpha_{\boldsymbol{i}}^{\dagger}\alpha_{\boldsymbol{i}+\hat{\boldsymbol{e}}_j}|\phi_0\rangle = 0. \qquad (A.2)$$

Hence, by using the projector operator

$$\mathcal{P}_0 = |\ \phi_0\rangle\langle\phi_0\ |, \qquad (A.3)$$

we can formally write the Lagrangian density, $\mathcal{L}_s$, in terms of the spin degrees of freedom as follows:

$$\mathcal{L}_s = \mathcal{P}_0\mathcal{L}\mathcal{P}_0 = |\ \phi_0\rangle\langle\phi_0|\mathcal{L}|\phi_0\rangle\langle\phi_0\ |, \qquad (A.4)$$

such that, by inserting Eqs. (A.1) and (A.2) into Eq. (A.4), we obtain

$$\mathcal{L}_s = \sum_{\boldsymbol{i}\alpha\sigma}\theta(\sigma)\left(U_{\boldsymbol{i}\alpha}^{\dagger}\partial_{\tau}U_{\boldsymbol{i}\alpha}\right)_{\sigma\sigma} - \frac{J}{8}\sum_{\boldsymbol{i}j\alpha\beta\sigma}\theta(\sigma)\left[\left|\left(U_{\boldsymbol{i}\alpha}^{\dagger}U_{\boldsymbol{i}+\hat{\boldsymbol{e}}_j\beta}\right)_{\sigma\sigma}\right|^2+\left|\left(U_{\boldsymbol{i}\alpha}^{\dagger}U_{\boldsymbol{i}-\hat{\boldsymbol{e}}_j\beta}\right)_{\sigma\sigma}\right|^2\right]. \qquad (A.5)$$

Let us now perform the Legendre transform:

$$\mathcal{H}^s = -\sum_{\boldsymbol{i}\alpha\sigma}\frac{\partial\mathcal{L}_s}{\partial\left(\partial_{\tau}U_{\boldsymbol{i}\alpha}\right)_{\sigma\sigma}}\left(\partial_{\tau}U_{\boldsymbol{i}\alpha}\right)_{\sigma\sigma} + \mathcal{L}_s; \qquad (A.6)$$

where

$$\frac{\partial\mathcal{L}_s}{\partial\left(\partial_{\tau}U_{\boldsymbol{i}\alpha}\right)_{\sigma\sigma}} = \theta(\sigma)\left(U_{\boldsymbol{i}\alpha}^{\dagger}\right)_{\sigma\sigma}. \qquad (A.7)$$

Substituting Eq. (A.5) into Eq. (A.6), we get the following Heisenberg-like Hamiltonian written in terms of the SU(2) gauge fields:

$$\mathcal{H}^s = -\frac{J}{8}\sum_{\boldsymbol{ij}\alpha\beta\sigma}\theta(\sigma)\left[\left|\left(U^{\dagger}_{\boldsymbol{i}\alpha}U_{\boldsymbol{i}+\hat{\boldsymbol{e}}_j\beta}\right)_{\sigma\sigma}\right|^2+\left|\left(U^{\dagger}_{\boldsymbol{i}\alpha}U_{\boldsymbol{i}-\hat{\boldsymbol{e}}_j\beta}\right)_{\sigma\sigma}\right|^2\right]. \quad \text{(A.8)}$$

In order to write the above Hamiltonian in its standard form (in the spin language); it is convenient to write the SU(2) gauge fields in the $\boldsymbol{n}$-representation. By doing so, let us use the following representation of SU(2) group: [59]:

$$U_{\boldsymbol{i}\alpha}=\begin{bmatrix}\cos\left(\frac{\theta_{\boldsymbol{i}\alpha}}{2}\right) & -\sin\left(\frac{\theta_{\boldsymbol{i}\alpha}}{2}\right)e^{-i\phi_{\boldsymbol{i}\alpha}}\\ \sin\left(\frac{\theta_{\boldsymbol{i}\alpha}}{2}\right)e^{i\phi_{\boldsymbol{i}\alpha}} & \cos\left(\frac{\theta_{\boldsymbol{i}\alpha}}{2}\right)\end{bmatrix}, \quad \text{(A.9)}$$

so that, after a straightforward calculation, one obtains the following diagonal matrix elements:

$$\begin{aligned}\left(U^{\dagger}_{\boldsymbol{i}\alpha}U_{\boldsymbol{i}+\hat{\boldsymbol{e}}_j\beta}\right)_{\sigma\sigma} &= \cos\left(\frac{\theta_{\boldsymbol{i}\alpha}}{2}\right)\cos\left(\frac{\theta_{\boldsymbol{i}+\hat{\boldsymbol{e}}_j\beta}}{2}\right)\\ &\quad \sin\left(\frac{\theta_{\boldsymbol{i}\alpha}}{2}\right)\sin\left(\frac{\theta_{\boldsymbol{i}+\hat{\boldsymbol{e}}_j\beta}}{2}\right)e^{i\left(\phi_{\boldsymbol{i}\alpha}-\phi_{\boldsymbol{i}+\hat{\boldsymbol{e}}_j\beta}\right)}. \quad \text{(A.10)}\end{aligned}$$

Correspondingly,

$$\begin{aligned}\left|\left(U^{\dagger}_{\boldsymbol{i}\alpha}U_{\boldsymbol{i}+\hat{\boldsymbol{e}}_j\beta}\right)_{\sigma\sigma}\right|^2 &= \frac{1}{2}\left[\cos\left(\theta_{\boldsymbol{i}\alpha}\right)\cos\left(\theta_{\boldsymbol{i}+\hat{\boldsymbol{e}}_j\beta}\right)\right.\\ &\quad \left.+\sin\left(\theta_{\boldsymbol{i}\alpha}\right)\sin\left(\theta_{\boldsymbol{i}+\hat{\boldsymbol{e}}_j\beta}\right)\cos\left(\phi_{\boldsymbol{i}\alpha}-\phi_{\boldsymbol{i}+\hat{\boldsymbol{e}}_j\beta}\right)\right]. \quad \text{(A.11)}\end{aligned}$$

At this stage, it is convenient to use the unit vector $\boldsymbol{n}_{\boldsymbol{i}\alpha}$ in the form:

$$\boldsymbol{n}_{\boldsymbol{i}\alpha}=\sin\left(\theta_{\boldsymbol{i}\alpha}\right)\left[\cos\left(\phi_{\boldsymbol{i}\alpha}\right)\hat{\boldsymbol{x}}+\sin\left(\phi_{\boldsymbol{i}\alpha}\right)\hat{\boldsymbol{y}}\right]+\cos\left(\theta_{\boldsymbol{i}\alpha}\right)\hat{\boldsymbol{z}}, \quad \text{(A.12)}$$

such that, the inner product reads:

$$\begin{aligned}\boldsymbol{n}_{\boldsymbol{i}\alpha}\cdot\boldsymbol{n}_{\boldsymbol{i}+\hat{\boldsymbol{e}}_j\beta} &= \cos\left(\theta_{\boldsymbol{i}\alpha}\right)\cos\left(\theta_{\boldsymbol{i}+\hat{\boldsymbol{e}}_j\beta}\right)\\ &\quad +\sin\left(\theta_{\boldsymbol{i}\alpha}\right)\sin\left(\theta_{\boldsymbol{i}+\hat{\boldsymbol{e}}_j\beta}\right)\cos\left(\phi_{\boldsymbol{i}\alpha}-\phi_{\boldsymbol{i}+\hat{\boldsymbol{e}}_j\beta}\right). \quad \text{(A.13)}\end{aligned}$$

Substituting Eq. (A.13) into Eq. (A.11) gives rise to

$$\left|\left(U^{\dagger}_{\boldsymbol{i}\alpha}U_{\boldsymbol{i}+\hat{\boldsymbol{e}}_j\beta}\right)_{\sigma\sigma}\right|^2=\frac{1}{2}\left(1+\boldsymbol{n}_{\boldsymbol{i}\alpha}\cdot\boldsymbol{n}_{\boldsymbol{i}+\hat{\boldsymbol{e}}_j\beta}\right). \quad \text{(A.14)}$$

Next, we plug Eq. (A.14) into Eq. (A.8), such that we find

$$\mathcal{H}^s=-\frac{J}{8}\sum_{\boldsymbol{ij}\alpha\beta}\boldsymbol{n}_{\boldsymbol{i}\alpha}\cdot\left(\boldsymbol{n}_{\boldsymbol{i}+\hat{\boldsymbol{e}}_j\beta}-\boldsymbol{n}_{\hat{\boldsymbol{e}}_j\beta}\right)-\frac{JNz}{8}, \quad \text{(A.15)}$$

where z is the coordination number ($z = 3$ for the honeycomb lattice). With the purpose of bringing $\mathcal{H}^s$ to its standard form, we now use the auxiliary result: $\boldsymbol{S}_{\boldsymbol{i}\alpha} = \boldsymbol{n}_{\boldsymbol{i}\alpha}/2$, so that, $\mathcal{H}^s$ becomes

$$\mathcal{H}^s = -J\sum_{\boldsymbol{ij}\alpha\beta}\boldsymbol{S}_{\boldsymbol{i}\alpha}\cdot\boldsymbol{S}_{\boldsymbol{i}+\hat{\boldsymbol{e}}_j\beta} - h\sum_{\boldsymbol{i}\alpha}\boldsymbol{S}_{\boldsymbol{i}\alpha} + h\sum_{\boldsymbol{ij}\beta}\boldsymbol{S}_{\boldsymbol{i}+\hat{\boldsymbol{e}}_j\beta} - \frac{zNJ}{8}. \quad \text{(A.16)}$$

It also should be noted the two additional Zeeman terms (h is the magnetic field) which allow us to perform the calculation of the staggered magnetization.

In order to explicit the AF order, it is necessary to perform the following transformation [61]:

$$\boldsymbol{S}_{\boldsymbol{i}\alpha} = \begin{cases} S^x_{\boldsymbol{i}\alpha}; \\ S^y_{\boldsymbol{i}\alpha}; \\ S^z_{\boldsymbol{i}\alpha}, \end{cases} \qquad \boldsymbol{S}_{\boldsymbol{i}+\hat{\boldsymbol{e}}_j\beta} = \begin{cases} S^x_{\boldsymbol{i}+\hat{\boldsymbol{e}}_j\beta}; \\ -S^y_{\boldsymbol{i}+\hat{\boldsymbol{e}}_j\beta}; \\ -S^z_{\boldsymbol{i}+\hat{\boldsymbol{e}}_j\beta}, \end{cases} \quad \text{(A.17)}$$

such that, $\mathcal{H}^s$ in Eq. (A.16) can be written as

$$\begin{aligned}\mathcal{H}^s = & -J\sum_{\boldsymbol{ij}\alpha\beta}\left[\left(S^x_{\boldsymbol{i}\alpha}S^x_{\boldsymbol{i}+\hat{\boldsymbol{e}}_j\beta} - S^y_{\boldsymbol{i}\alpha}S^y_{\boldsymbol{i}+\hat{\boldsymbol{e}}_j\beta}\right) - S^z_{\boldsymbol{i}\alpha}S^z_{\boldsymbol{i}+\hat{\boldsymbol{e}}_j\beta}\right] \\ & -h\sum_{\boldsymbol{i}\alpha}S^z_{\boldsymbol{i}\alpha} + h\sum_{\boldsymbol{ij}\beta}S^z_{\boldsymbol{i}+\hat{\boldsymbol{e}}_j\beta} - \frac{zNJ}{8}. \end{aligned} \quad \text{(A.18)}$$

Next, we introduce the ladder operators [61]

$$S^{\pm} = S^x \pm iS^y, \quad \text{(A.19)}$$

such that

$$S^x_{\boldsymbol{i}\alpha}S^x_{\boldsymbol{i}+\hat{\boldsymbol{e}}_j\beta} = \frac{1}{4}\left(S^+_{\boldsymbol{i}\alpha}S^+_{\boldsymbol{i}+\hat{\boldsymbol{e}}_j\beta} + S^+_{\boldsymbol{i}\alpha}S^-_{\boldsymbol{i}+\hat{\boldsymbol{e}}_j\beta} + S^-_{\boldsymbol{i}\alpha}S^+_{\boldsymbol{i}+\hat{\boldsymbol{e}}_j\beta} + S^-_{\boldsymbol{i}\alpha}S^-_{\boldsymbol{i}+\hat{\boldsymbol{e}}_j\beta}\right); \quad \text{(A.20)}$$

and

$$S^y_{\boldsymbol{i}\alpha}S^y_{\boldsymbol{i}+\hat{\boldsymbol{e}}_j\beta} = -\frac{1}{4}\left(S^-_{\boldsymbol{i}\alpha}S^-_{\boldsymbol{i}+\hat{\boldsymbol{e}}_j\beta} - S^-_{\boldsymbol{i}\alpha}S^+_{\boldsymbol{i}+\hat{\boldsymbol{e}}_j\beta} - S^+_{\boldsymbol{i}\alpha}S^-_{\boldsymbol{i}+\hat{\boldsymbol{e}}_j\beta} + S^+_{\boldsymbol{i}\alpha}S^+_{\boldsymbol{i}+\hat{\boldsymbol{e}}_j\beta}\right); \quad \text{(A.21)}$$

Substituting Eqs. (A.20) and (A.21) into Eq. (A.18) leads to

$$\begin{aligned}\mathcal{H}^s = & -J\sum_{\boldsymbol{ij}\alpha\beta}\left[\frac{1}{2}\left(S^+_{\boldsymbol{i}\alpha}S^+_{\boldsymbol{i}+\hat{\boldsymbol{e}}_j\beta} + S^-_{\boldsymbol{i}\alpha}S^-_{\boldsymbol{i}+\hat{\boldsymbol{e}}_j\beta}\right) - S^z_{\boldsymbol{i}\alpha}S^z_{\boldsymbol{i}+\hat{\boldsymbol{e}}_j\beta}\right] \\ & -h\sum_{\boldsymbol{i}\alpha}S^z_{\boldsymbol{i}\alpha} + h\sum_{\boldsymbol{ij}\beta}S^z_{\boldsymbol{i}+\hat{\boldsymbol{e}}_j\beta} - \frac{zNJ}{8}. \end{aligned} \quad \text{(A.22)}$$

At this point, we apply the Holstein-Primakoff transformation [61]:

$$\begin{aligned} S^z_{\boldsymbol{i}\alpha} &= -a^\dagger_{\boldsymbol{i}}a_{\boldsymbol{i}} + S; \\ S^+_{\boldsymbol{i}\alpha} &= \sqrt{2S - a^\dagger_{\boldsymbol{i}}a_{\boldsymbol{i}}}\,a_{\boldsymbol{i}}; \\ S^-_{\boldsymbol{i}\alpha} &= a^\dagger_{\boldsymbol{i}}\sqrt{2S - a^\dagger_{\boldsymbol{i}}a_{\boldsymbol{i}}}, \end{aligned} \quad \text{(A.23)}$$

for an up-spin on A site of sublattice A, and

$$\begin{aligned} S^{z}_{\boldsymbol{i}+\hat{\boldsymbol{e}}_j\beta} &= b^{\dagger}_{\boldsymbol{i}+\hat{\boldsymbol{e}}_j} b_{\boldsymbol{i}+\hat{\boldsymbol{e}}_j} - S; \\ S^{+}_{\boldsymbol{i}+\hat{\boldsymbol{e}}_j\beta} &= \sqrt{2S - b^{\dagger}_{\boldsymbol{i}+\hat{\boldsymbol{e}}_j} b_{\boldsymbol{i}+\hat{\boldsymbol{e}}_j}}\, b_{\boldsymbol{i}+\hat{\boldsymbol{e}}_j}; \\ S^{-}_{\boldsymbol{i}+\hat{\boldsymbol{e}}_j\beta} &= b^{\dagger}_{\boldsymbol{i}+\hat{\boldsymbol{e}}_j} \sqrt{2S - b^{\dagger}_{\boldsymbol{i}+\hat{\boldsymbol{e}}_j} b_{\boldsymbol{i}+\hat{\boldsymbol{e}}_j}}\,, \end{aligned} \tag{A.24}$$

for a neighboring down-spin of sublattice B; the bosonic creation and annihilation operators $a_{\boldsymbol{i}}$ and $a^{\dagger}_{\boldsymbol{i}}$ obey the commutation relations: $[a_{\boldsymbol{i}},a^{\dagger}_{\boldsymbol{i}'}]=\delta_{\boldsymbol{i}\boldsymbol{i}'}$ and $[b_{\boldsymbol{j}},b^{\dagger}_{\boldsymbol{j}'}]=\delta_{\boldsymbol{j}\boldsymbol{j}'}$.

With the purpose of performing a second-order spin-wave analysis [64], it is important to evaluate the following terms:

$$\begin{aligned} S^{+}_{\boldsymbol{i}\alpha} S^{+}_{\boldsymbol{i}+\hat{\boldsymbol{e}}_j\beta} &= 2S \left(a_{\boldsymbol{i}} b_{\boldsymbol{i}+\hat{\boldsymbol{e}}_j} - \frac{a_{\boldsymbol{i}} b_{\boldsymbol{i}+\hat{\boldsymbol{e}}_j} b^{\dagger}_{\boldsymbol{i}+\hat{\boldsymbol{e}}_j} b_{\boldsymbol{i}+\hat{\boldsymbol{e}}_j}}{4S} \right. \\ &\quad \left. - \frac{a^{\dagger}_{\boldsymbol{i}} a_{\boldsymbol{i}} a_{\boldsymbol{i}} b_{\boldsymbol{i}+\hat{\boldsymbol{e}}_j}}{4S} + \frac{a^{\dagger}_{\boldsymbol{i}} a_{\boldsymbol{i}} a_{\boldsymbol{i}} b_{\boldsymbol{i}+\hat{\boldsymbol{e}}_j} b^{\dagger}_{\boldsymbol{i}+\hat{\boldsymbol{e}}_j} b_{\boldsymbol{i}+\hat{\boldsymbol{e}}_j}}{16S^2} \right), \end{aligned} \tag{A.25}$$

and

$$\begin{aligned} S^{-}_{\boldsymbol{i}\alpha} S^{-}_{\boldsymbol{i}+\hat{\boldsymbol{e}}_j\beta} &= 2S \left(a^{\dagger}_{\boldsymbol{i}} b^{\dagger}_{\boldsymbol{i}+\hat{\boldsymbol{e}}_j} - \frac{a^{\dagger}_{\boldsymbol{i}} b^{\dagger}_{\boldsymbol{i}+\hat{\boldsymbol{e}}_j} b_{\boldsymbol{i}+\hat{\boldsymbol{e}}_j} b^{\dagger}_{\boldsymbol{i}+\hat{\boldsymbol{e}}_j}}{4S} \right. \\ &\quad \left. - \frac{a^{\dagger}_{\boldsymbol{i}} a^{\dagger}_{\boldsymbol{i}} a_{\boldsymbol{i}} b^{\dagger}_{\boldsymbol{i}+\hat{\boldsymbol{e}}_j}}{4S} + \frac{a^{\dagger}_{\boldsymbol{i}} a^{\dagger}_{\boldsymbol{i}} a_{\boldsymbol{i}} b^{\dagger}_{\boldsymbol{i}+\hat{\boldsymbol{e}}_j} b_{\boldsymbol{i}+\hat{\boldsymbol{e}}_j} b^{\dagger}_{\boldsymbol{i}+\hat{\boldsymbol{e}}_j}}{16S^2} \right). \end{aligned} \tag{A.26}$$

By inserting Eqs. (A.25) and (A.26) into Eq. (A.22), $\mathcal{H}^s$ takes the form:

$$\begin{aligned} \mathcal{H}^s &= -J \sum_{\boldsymbol{i}\boldsymbol{j}} \left\{ \left[S^2 - S \left(a^{\dagger}_{\boldsymbol{i}} a_{\boldsymbol{i}} + b^{\dagger}_{\boldsymbol{i}+\hat{\boldsymbol{e}}_j} b_{\boldsymbol{i}+\hat{\boldsymbol{e}}_j} \right) + a^{\dagger}_{\boldsymbol{i}} a_{\boldsymbol{i}} b^{\dagger}_{\boldsymbol{i}+\hat{\boldsymbol{e}}_j} b_{\boldsymbol{i}+\hat{\boldsymbol{e}}_j} \right] + S \left(a_{\boldsymbol{i}} b_{\boldsymbol{i}+\hat{\boldsymbol{e}}_j} + a^{\dagger}_{\boldsymbol{i}} b^{\dagger}_{\boldsymbol{i}+\hat{\boldsymbol{e}}_j} \right) \right. \\ &\quad - \frac{1}{4} \left(a_{\boldsymbol{i}} b_{\boldsymbol{i}+\hat{\boldsymbol{e}}_j} b^{\dagger}_{\boldsymbol{i}+\hat{\boldsymbol{e}}_j} b_{\boldsymbol{i}+\hat{\boldsymbol{e}}_j} + a^{\dagger}_{\boldsymbol{i}} b^{\dagger}_{\boldsymbol{i}+\hat{\boldsymbol{e}}_j} b_{\boldsymbol{i}+\hat{\boldsymbol{e}}_j} b^{\dagger}_{\boldsymbol{i}+\hat{\boldsymbol{e}}_j} + a^{\dagger}_{\boldsymbol{i}} a_{\boldsymbol{i}} a_{\boldsymbol{i}} b_{\boldsymbol{i}+\hat{\boldsymbol{e}}_j} + a^{\dagger}_{\boldsymbol{i}} a^{\dagger}_{\boldsymbol{i}} a_{\boldsymbol{i}} b^{\dagger}_{\boldsymbol{i}+\hat{\boldsymbol{e}}_j} \right) \\ &\quad + \frac{1}{16S} \left(a^{\dagger}_{\boldsymbol{i}} a_{\boldsymbol{i}} a_{\boldsymbol{i}} b_{\boldsymbol{i}+\hat{\boldsymbol{e}}_j} b^{\dagger}_{\boldsymbol{i}+\hat{\boldsymbol{e}}_j} b_{\boldsymbol{i}+\hat{\boldsymbol{e}}_j} + a^{\dagger}_{\boldsymbol{i}} a^{\dagger}_{\boldsymbol{i}} a_{\boldsymbol{i}} b^{\dagger}_{\boldsymbol{i}+\hat{\boldsymbol{e}}_j} b_{\boldsymbol{i}+\hat{\boldsymbol{e}}_j} b^{\dagger}_{\boldsymbol{i}+\hat{\boldsymbol{e}}_j} \right) \\ &\quad \left. - h \sum_{\boldsymbol{i}} a^{\dagger}_{\boldsymbol{i}} a_{\boldsymbol{i}} + h \sum_{\boldsymbol{i}\boldsymbol{j}} b^{\dagger}_{\boldsymbol{i}+\hat{\boldsymbol{e}}_j} b_{\boldsymbol{i}+\hat{\boldsymbol{e}}_j} + hSN - \frac{JNz}{8} \right\}. \end{aligned} \tag{A.27}$$

Clearly, one recognizes that due to the form of $\mathcal{H}^s$ in Eq. (A.27) the steps to turn $\mathcal{H}^s$ into the $\boldsymbol{k}$-space are pretty long! Then, it is appropriated to write $\mathcal{H}^s$ as:

$$\mathcal{H}^s = \mathcal{H}_0 + \mathcal{H}_1 + \mathcal{H}_2, \tag{A.28}$$

in which

$$\mathcal{H}_0 = -\frac{zJS^2}{8} + hSN - \frac{JNz}{8}, \quad \text{(it contains only constants terms)} \tag{A.29}$$

$$\begin{aligned}\mathcal{H}_1 &= -\frac{J}{8}\sum_{\boldsymbol{ij}}\left[-S\left(a_{\boldsymbol{i}}^{\dagger}a_{\boldsymbol{i}} + b_{\boldsymbol{i}+\hat{\boldsymbol{e}}_j}^{\dagger}b_{\boldsymbol{i}+\hat{\boldsymbol{e}}_j}\right) + S\left(a_{\boldsymbol{i}}b_{\boldsymbol{i}+\hat{\boldsymbol{e}}_j} + a_{\boldsymbol{i}}^{\dagger}b_{\boldsymbol{i}+\hat{\boldsymbol{e}}_j}^{\dagger}\right)\right] - h\sum_{\boldsymbol{i}} a_{\boldsymbol{i}}^{\dagger}a_{\boldsymbol{i}} \\ &\quad + h\sum_{\boldsymbol{ij}} b_{\boldsymbol{i}+\hat{\boldsymbol{e}}_j}^{\dagger}b_{\boldsymbol{i}+\hat{\boldsymbol{e}}_j},\end{aligned} \tag{A.30}$$

with just quadratic terms (notice that there are anomalous terms), and

$$\begin{aligned}\mathcal{H}_2 &= -\frac{J}{8}\sum_{\boldsymbol{ij}}\left[-\frac{1}{4}\left(a_{\boldsymbol{i}}b_{\boldsymbol{i}+\hat{\boldsymbol{e}}_j}b_{\boldsymbol{i}+\hat{\boldsymbol{e}}_j}^{\dagger}b_{\boldsymbol{i}+\hat{\boldsymbol{e}}_j} + a_{\boldsymbol{i}}^{\dagger}b_{\boldsymbol{i}+\hat{\boldsymbol{e}}_j}^{\dagger}b_{\boldsymbol{i}+\hat{\boldsymbol{e}}_j}b_{\boldsymbol{i}+\hat{\boldsymbol{e}}_j}^{\dagger} + a_{\boldsymbol{i}}^{\dagger}a_{\boldsymbol{i}}a_{\boldsymbol{i}}b_{\boldsymbol{i}+\hat{\boldsymbol{e}}_j} + a_{\boldsymbol{i}}^{\dagger}a_{\boldsymbol{i}}^{\dagger}a_{\boldsymbol{i}}b_{\boldsymbol{i}+\hat{\boldsymbol{e}}_j}^{\dagger}\right)\right. \\ &\quad \left. a_{\boldsymbol{i}}^{\dagger}a_{\boldsymbol{i}}b_{\boldsymbol{i}+\hat{\boldsymbol{e}}_j}^{\dagger}b_{\boldsymbol{i}+\hat{\boldsymbol{e}}_j} + \frac{1}{16S}\left(a_{\boldsymbol{i}}^{\dagger}a_{\boldsymbol{i}}a_{\boldsymbol{i}}b_{\boldsymbol{i}+\hat{\boldsymbol{e}}_j}b_{\boldsymbol{i}+\hat{\boldsymbol{e}}_j}^{\dagger}b_{\boldsymbol{i}+\hat{\boldsymbol{e}}_j} + a_{\boldsymbol{i}}^{\dagger}a_{\boldsymbol{i}}^{\dagger}a_{\boldsymbol{i}}b_{\boldsymbol{i}+\hat{\boldsymbol{e}}_j}^{\dagger}b_{\boldsymbol{i}+\hat{\boldsymbol{e}}_j}b_{\boldsymbol{i}+\hat{\boldsymbol{e}}_j}^{\dagger}\right)\right],\end{aligned} \tag{A.31}$$

where it includes both quartic and sextic terms.

In the sequence, we focus on $\mathcal{H}_1$ in Eq. (A.30). Thus, by introducing the Fourier transformation:

$$\begin{aligned}a_{\boldsymbol{k}\sigma} &= \frac{1}{\sqrt{N_c}}\sum_{\boldsymbol{i}} e^{i\boldsymbol{k}\cdot\boldsymbol{i}}a_{\boldsymbol{i}\sigma}; \\ b_{\boldsymbol{k}\sigma} &= \frac{1}{\sqrt{N_c}}\sum_{\boldsymbol{j}} e^{-i\boldsymbol{k}\cdot\boldsymbol{j}}b_{\boldsymbol{j}\sigma},\end{aligned} \tag{A.32}$$

we find that $\mathcal{H}_1$ in $\boldsymbol{k}$-space takes the form:

$$\begin{aligned}\mathcal{H}_1 &= \frac{J}{2}\sum_{\boldsymbol{k}}\left[zS\left(a_{\boldsymbol{k}}^{\dagger}a_{\boldsymbol{k}} + b_{\boldsymbol{k}}^{\dagger}b_{\boldsymbol{k}}\right) + zS\gamma_{\boldsymbol{k}}\left(a_{-\boldsymbol{k}}^{\dagger}b_{\boldsymbol{k}}^{\dagger} + a_{-\boldsymbol{k}}b_{\boldsymbol{k}}\right)\right] \\ &\quad -h\sum_{\boldsymbol{k}}\left(a_{\boldsymbol{k}}^{\dagger}a_{\boldsymbol{k}} - b_{\boldsymbol{k}}^{\dagger}b_{\boldsymbol{k}}\right),\end{aligned} \tag{A.33}$$

in which the lattice structure factor $\gamma_{\boldsymbol{k}}$ reads:

$$\gamma_{\boldsymbol{k}} \equiv \frac{1}{z}\sum_{j} e^{i\boldsymbol{k}\cdot\boldsymbol{e}_j} = \frac{1}{3}\left[e^{ik_x} + 2e^{-i\frac{k_x}{2}}\cos\left(\frac{\sqrt{3}k_y}{2}\right)\right]. \tag{A.34}$$

It should be noted that the anomalous terms, $a_{-\boldsymbol{k}}^{\dagger}b_{\boldsymbol{k}}^{\dagger}$and $a_{-\boldsymbol{k}}b_{\boldsymbol{k}}$, persist. So, we perform a Bogoliubov transformation:

$$\begin{aligned}a_{\boldsymbol{k}} &= \cosh\left(\theta_{\boldsymbol{k}}\right)\alpha_{\boldsymbol{k}} - \sinh\left(\theta_{\boldsymbol{k}}\right)\beta_{\boldsymbol{k}}^{\dagger}; \\ b_{\boldsymbol{k}} &= -\sinh\left(\theta_{\boldsymbol{k}}\right)\alpha_{\boldsymbol{k}}^{\dagger} - \cosh\left(\theta_{\boldsymbol{k}}\right)\beta_{\boldsymbol{k}},\end{aligned} \tag{A.35}$$

Inserting Eq. (A.35) into Eq. (A.33), after a pretty long calculation, $\mathcal{H}_1$ can be expressed in terms of the Bogoliubov quasiparticles:

$$\begin{aligned}\mathcal{H}_1 &= \frac{J}{2}\sum_{\boldsymbol{k}}\Big\{zS\Big[\cosh^2(\theta_{\boldsymbol{k}})\left(\alpha^\dagger_{\boldsymbol{k}}\alpha_{\boldsymbol{k}}+\beta^\dagger_{\boldsymbol{k}}\beta_{\boldsymbol{k}}\right)+\sinh(\theta_{\boldsymbol{k}})\cosh(\theta_{\boldsymbol{k}})\left(\alpha^\dagger_{\boldsymbol{k}}\alpha^\dagger_{-\boldsymbol{k}}+\alpha_{-\boldsymbol{k}}\alpha_{\boldsymbol{k}}\right.\\ &\left.-\beta^\dagger_{\boldsymbol{k}}\beta^\dagger_{-\boldsymbol{k}}-\beta_{-\boldsymbol{k}}\beta_{\boldsymbol{k}}\right)+\sinh^2(\theta_{\boldsymbol{k}})\left(\alpha_{-\boldsymbol{k}}\alpha^\dagger_{-\boldsymbol{k}}+\beta_{-\boldsymbol{k}}\beta^\dagger_{-\boldsymbol{k}}\right)\Big]+\frac{zS\gamma_{\boldsymbol{k}}}{2}\left[\cosh^2(\theta_{\boldsymbol{k}})\times\right.\\ &\left(\alpha^\dagger_{-\boldsymbol{k}}\alpha^\dagger_{\boldsymbol{k}}+\alpha_{-\boldsymbol{k}}\alpha_{\boldsymbol{k}}-\beta^\dagger_{-\boldsymbol{k}}\beta^\dagger_{\boldsymbol{k}}-\beta_{-\boldsymbol{k}}\beta_{\boldsymbol{k}}\right)+\cosh(\theta_{\boldsymbol{k}})\sinh(\theta_{\boldsymbol{k}})\left(\alpha^\dagger_{-\boldsymbol{k}}\alpha_{\boldsymbol{k}}+\alpha_{-\boldsymbol{k}}\alpha^\dagger_{-\boldsymbol{k}}\right.\\ &+\alpha^\dagger_{-\boldsymbol{k}}\beta_{\boldsymbol{k}}+\alpha_{-\boldsymbol{k}}\beta^\dagger_{-\boldsymbol{k}}+\alpha_{\boldsymbol{k}}\alpha^\dagger_{\boldsymbol{k}}+\alpha^\dagger_{\boldsymbol{k}}\alpha_{\boldsymbol{k}}-\alpha_{\boldsymbol{k}}\beta^\dagger_{\boldsymbol{k}}+\alpha^\dagger_{\boldsymbol{k}}\beta^\dagger_{\boldsymbol{k}}+\beta^\dagger_{-\boldsymbol{k}}\alpha_{-\boldsymbol{k}}+\beta_{-\boldsymbol{k}}\alpha^\dagger_{-\boldsymbol{k}}+\\ &\left.\beta^\dagger_{-\boldsymbol{k}}\beta^\dagger_{-\boldsymbol{k}}+\beta_{-\boldsymbol{k}}\beta^\dagger_{-\boldsymbol{k}}-\beta_{\boldsymbol{k}}\alpha^\dagger_{\boldsymbol{k}}+\beta^\dagger_{\boldsymbol{k}}\alpha_{\boldsymbol{k}}+\beta_{\boldsymbol{k}}\beta^\dagger_{\boldsymbol{k}}+\beta^\dagger_{\boldsymbol{k}}\beta_{\boldsymbol{k}}\right)-\cosh^2(\theta_{\boldsymbol{k}})\left(\alpha^\dagger_{-\boldsymbol{k}}\beta^\dagger_{\boldsymbol{k}}+\alpha_{-\boldsymbol{k}}\beta_{\boldsymbol{k}}\right.\\ &\left.-\beta^\dagger_{-\boldsymbol{k}}\alpha^\dagger_{\boldsymbol{k}}-\beta_{-\boldsymbol{k}}\alpha_{\boldsymbol{k}}\right)+\sinh^2(\theta_{\boldsymbol{k}})\left(\alpha_{\boldsymbol{k}}\alpha^\dagger_{-\boldsymbol{k}}+\alpha^\dagger_{\boldsymbol{k}}\alpha^\dagger_{-\boldsymbol{k}}-\beta_{\boldsymbol{k}}\beta_{-\boldsymbol{k}}+\beta^\dagger_{\boldsymbol{k}}\beta^\dagger_{-\boldsymbol{k}}\right)+\sinh^2(\theta_{\boldsymbol{k}})\\ &\left.\times\left(\alpha_{\boldsymbol{k}}\beta_{-\boldsymbol{k}}+\alpha^\dagger_{\boldsymbol{k}}\beta^\dagger_{-\boldsymbol{k}}-\beta_{\boldsymbol{k}}\alpha_{-\boldsymbol{k}}+\beta^\dagger_{\boldsymbol{k}}\alpha^\dagger_{-\boldsymbol{k}}\right)\right]\Big\}-h\sum_{\boldsymbol{k}}\Big[\cosh^2(\theta_{\boldsymbol{k}})\left(\alpha^\dagger_{\boldsymbol{k}}\alpha_{\boldsymbol{k}}+\beta^\dagger_{\boldsymbol{k}}\beta_{\boldsymbol{k}}\right)\\ &+\sinh^2(\theta_{\boldsymbol{k}})\left(\alpha_{-\boldsymbol{k}}\alpha^\dagger_{-\boldsymbol{k}}+\beta_{-\boldsymbol{k}}\beta^\dagger_{-\boldsymbol{k}}\right)+\sinh(\theta_{\boldsymbol{k}})\ \cosh(\theta_{\boldsymbol{k}})\left(\alpha^\dagger_{\boldsymbol{k}}\alpha^\dagger_{-\boldsymbol{k}}+\alpha_{-\boldsymbol{k}}\alpha_{\boldsymbol{k}}-\beta^\dagger_{\boldsymbol{k}}\beta^\dagger_{-\boldsymbol{k}}\right.\\ &\left.-\beta_{-\boldsymbol{k}}\beta_{\boldsymbol{k}})\right].\end{aligned}\tag{A.36}$$

In order to diagonalized the above Hamiltonian we now choose $\theta_{\boldsymbol{k}}$ so that terms like $\alpha^\dagger_{\boldsymbol{k}}\alpha_{\boldsymbol{k}}$ and $\beta^\dagger_{\boldsymbol{k}}\beta_{\boldsymbol{k}}$ do not vanish. These lead to the following conditions:

$$\sinh(2\theta_{\boldsymbol{k}})+\gamma_{\boldsymbol{k}}\cosh(2\theta_{\boldsymbol{k}})=0;\tag{A.37}$$

and

$$\sinh^2(\theta_{\boldsymbol{k}})+\cosh^2(\theta_{\boldsymbol{k}})=\sinh(\theta_{\boldsymbol{k}})\cosh(\theta_{\boldsymbol{k}})=0.\tag{A.38}$$

Substituting Eqs. (A.37) and (A.38) into Eq. (A.36), we obtain the following clean expression

$$\begin{aligned}\mathcal{H}_1 &= \frac{zSJ}{2}\sum_{\boldsymbol{k}}\Big\{\left[\cosh(2\theta_{\boldsymbol{k}})+\gamma_{\boldsymbol{k}}\sinh(2\theta_{\boldsymbol{k}})\right]\left(\alpha^\dagger_{\boldsymbol{k}}\alpha_{\boldsymbol{k}}+\beta^\dagger_{\boldsymbol{k}}\beta_{\boldsymbol{k}}\right)+2\sinh^2(\theta_{\boldsymbol{k}})\\ &+\gamma_{\boldsymbol{k}}\sinh(2\theta_{\boldsymbol{k}})\Big\}-h\sum_{\boldsymbol{k}}\left[\cosh(2\theta_{\boldsymbol{k}})\left(\alpha^\dagger_{\boldsymbol{k}}\alpha_{\boldsymbol{k}}+\beta^\dagger_{\boldsymbol{k}}\beta_{\boldsymbol{k}}\right)+2\sinh^2(\theta_{\boldsymbol{k}})\right].\end{aligned}\tag{A.39}$$

Next, it convenient to write

$$\cosh(2\theta_{\boldsymbol{k}})+\gamma_{\boldsymbol{k}}\sinh(2\theta_{\boldsymbol{k}})=\omega_{\boldsymbol{k}},\tag{A.40}$$

as well as Eq. (A.37) in a slightly different form:

$$\tanh(\theta_{\boldsymbol{k}})=-\gamma_{\boldsymbol{k}}.\tag{A.41}$$

such that after a straightforward algebra, one finds

$$\omega_{\boldsymbol{k}} = \sqrt{1-\gamma_{\boldsymbol{k}}^2}\,, \tag{A.42}$$

with

$$\gamma_{\boldsymbol{k}}^2 = \frac{1}{9}\left[1 + 4\cos\left(\frac{3k_x}{2}\right)\cos\left(\frac{\sqrt{3}\,k_y}{2}\right) + 4\cos^2\left(\frac{\sqrt{3}\,k_y}{2}\right)\right]. \tag{A.43}$$

Then, a slightly rearrangement of the terms yields the resulting diagonalized Hamiltonian $\mathcal{H}_1$:

$$\begin{aligned}\mathcal{H}_1 &= \frac{zSJ}{2}\sum_{\boldsymbol{k}}\left[\left(\sqrt{1-\gamma_{\boldsymbol{k}}^2}\right)\alpha_{\boldsymbol{k}}^{\dagger}\alpha_{\boldsymbol{k}} + \left(\sqrt{1-\gamma_{\boldsymbol{k}}^2}\right)\beta_{\boldsymbol{k}}^{\dagger}\beta_{\boldsymbol{k}} + \sqrt{1-\gamma_{\boldsymbol{k}}^2} - 1\right] \\ &\quad -h\sum_{\boldsymbol{k}}\left[\frac{\alpha_{\boldsymbol{k}}^{\dagger}\alpha_{\boldsymbol{k}}}{\sqrt{1-\gamma_{\boldsymbol{k}}^2}} + \frac{\beta_{\boldsymbol{k}}^{\dagger}\beta_{\boldsymbol{k}}}{\sqrt{1-\gamma_{\boldsymbol{k}}^2}} + \frac{1}{\sqrt{1-\gamma_{\boldsymbol{k}}^2}} - 1\right].\end{aligned} \tag{A.44}$$

Its contribution for the ground-state energy is given by

$$\epsilon_{1\boldsymbol{k}} = \frac{zSJ}{2}\left(\sqrt{1-\gamma_{\boldsymbol{k}}^2} - 1\right) - h\left(\frac{1}{\sqrt{1-\gamma_{\boldsymbol{k}}^2}} - 1\right). \tag{A.45}$$

We now proceed to analyze the quartic terms of $\mathcal{H}_2$:

$$\begin{aligned}\mathcal{H}_2 &= -\frac{J}{8}\sum_{ij}\left[-\frac{1}{4}\left(a_{\boldsymbol{i}}b_{\boldsymbol{i}+\hat{\boldsymbol{e}}_j}b_{\boldsymbol{i}+\hat{\boldsymbol{e}}_j}^{\dagger}b_{\boldsymbol{i}+\hat{\boldsymbol{e}}_j} + a_{\boldsymbol{i}}^{\dagger}b_{\boldsymbol{i}+\hat{\boldsymbol{e}}_j}^{\dagger}b_{\boldsymbol{i}+\hat{\boldsymbol{e}}_j}b_{\boldsymbol{i}+\hat{\boldsymbol{e}}_j}^{\dagger} + a_{\boldsymbol{i}}^{\dagger}a_{\boldsymbol{i}}a_{\boldsymbol{i}}b_{\boldsymbol{i}+\hat{\boldsymbol{e}}_j} + a_{\boldsymbol{i}}^{\dagger}a_{\boldsymbol{i}}^{\dagger}a_{\boldsymbol{i}}b_{\boldsymbol{i}+\hat{\boldsymbol{e}}_j}^{\dagger}\right)\right. \\ &\quad \left.a_{\boldsymbol{i}}^{\dagger}a_{\boldsymbol{i}}b_{\boldsymbol{i}+\hat{\boldsymbol{e}}_j}^{\dagger}b_{\boldsymbol{i}+\hat{\boldsymbol{e}}_j}\right],\end{aligned} \tag{A.46}$$

in which case we shall find for terms that are diagonal in the $\boldsymbol{k}$-space. By doing so, let us apply the Fourier transform to the above equation, such that

$$\begin{aligned}\mathcal{H}_2 &= -\frac{zJ}{8N}\sum_{\boldsymbol{k},\boldsymbol{k}'}\left[a_{\boldsymbol{k}}^{\dagger}a_{\boldsymbol{k}}b_{\boldsymbol{k}'}^{\dagger}b_{\boldsymbol{k}'} - \frac{1}{4}\left(\gamma_{\boldsymbol{k}}^{*}a_{\boldsymbol{k}}b_{\boldsymbol{k}}b_{\boldsymbol{k}'}^{\dagger}b_{\boldsymbol{k}'} + \gamma_k a_{\boldsymbol{k}}^{\dagger}b_{\boldsymbol{k}}^{\dagger}b_{\boldsymbol{k}'}b_{\boldsymbol{k}'}^{\dagger}\right.\right. \\ &\quad \left.\left.\gamma_{\boldsymbol{k}'}^{*}a_{\boldsymbol{k}}^{\dagger}a_{\boldsymbol{k}}a_{\boldsymbol{k}'}^{\dagger}b_{\boldsymbol{k}'} + \gamma_{\boldsymbol{k}'}a_{\boldsymbol{k}}^{\dagger}a_{\boldsymbol{k}}^{\dagger}a_{\boldsymbol{k}'}b_{\boldsymbol{k}'}\right)\right].\end{aligned} \tag{A.47}$$

Let us pursue by employing the Bogoliubov transformation in Eq. (A.35) to each term of the above Hamiltonian. Hence, each reads:

$$\begin{aligned}a_{\boldsymbol{k}}^{\dagger}a_{\boldsymbol{k}}b_{\boldsymbol{k}'}^{\dagger}b_{\boldsymbol{k}'} &= \left[\cosh^2(\theta_{\boldsymbol{k}})\,\alpha_{\boldsymbol{k}}^{\dagger}\alpha_{\boldsymbol{k}} + \cosh(\theta_{\boldsymbol{k}})\sinh(\theta_{\boldsymbol{k}})\,\alpha_{\boldsymbol{k}}^{\dagger}\beta_{\boldsymbol{k}}^{\dagger} + \sinh(\theta_{\boldsymbol{k}})\cosh(\theta_{\boldsymbol{k}})\,\beta_{\boldsymbol{k}}\alpha_{\boldsymbol{k}}\right. \\ &\quad \left.+\sinh^2(\theta_{\boldsymbol{k}})\,\beta_{\boldsymbol{k}}\beta_{\boldsymbol{k}}^{\dagger}\right]\left[\sinh^2(\theta_{\boldsymbol{k}'})\,\alpha_{\boldsymbol{k}'}\alpha_{\boldsymbol{k}'}^{\dagger} - \sinh(\theta_{\boldsymbol{k}'})\cosh(\theta_{\boldsymbol{k}'})\,\alpha_{\boldsymbol{k}'}\beta_{\boldsymbol{k}'}\right. \\ &\quad \left.-\sinh(\theta_{\boldsymbol{k}'})\cosh(\theta_{\boldsymbol{k}'})\,\beta_{\boldsymbol{k}'}^{\dagger}\alpha_{\boldsymbol{k}'}^{\dagger} + \cosh^2(\theta_{\boldsymbol{k}'})\,\beta_{\boldsymbol{k}'}^{\dagger}\beta_{\boldsymbol{k}'}\right];\end{aligned} \tag{A.48}$$

$$a_{\boldsymbol{k}}b_{\boldsymbol{k}}b^{\dagger}_{\boldsymbol{k}'}b_{\boldsymbol{k}'} = \Big[-\cosh(\theta_{\boldsymbol{k}})\sinh(\theta_{\boldsymbol{k}})\,\alpha_{\boldsymbol{k}}\alpha^{\dagger}_{\boldsymbol{k}} + \cosh^2(\theta_{\boldsymbol{k}})\,\alpha_{\boldsymbol{k}}\beta_{\boldsymbol{k}} - \sinh^2(\theta_{\boldsymbol{k}})\,\beta_{\boldsymbol{k}}\alpha^{\dagger}_{\boldsymbol{k}} + \sinh(\theta_{\boldsymbol{k}})\cosh(\theta_{\boldsymbol{k}})\,\beta^{\dagger}_{\boldsymbol{k}}\beta_{\boldsymbol{k}}\Big]\Big[\sinh^2(\theta_{\boldsymbol{k}'})\,\alpha_{\boldsymbol{k}'}\alpha^{\dagger}_{\boldsymbol{k}'} - \sinh(\theta_{\boldsymbol{k}'})\cosh(\theta_{\boldsymbol{k}'})\,\alpha_{\boldsymbol{k}'}\beta_{\boldsymbol{k}'} - \cosh(\theta_{\boldsymbol{k}'})\sinh(\theta_{\boldsymbol{k}'})\,\beta^{\dagger}_{\boldsymbol{k}'}\alpha^{\dagger}_{\boldsymbol{k}'} + \cosh^2(\theta_{\boldsymbol{k}'})\,\beta^{\dagger}_{\boldsymbol{k}'}\beta_{\boldsymbol{k}'}\Big]; \tag{A.49}$$

$$a^{\dagger}_{\boldsymbol{k}}b^{\dagger}_{\boldsymbol{k}}b_{\boldsymbol{k}'}b^{\dagger}_{\boldsymbol{k}'} = \Big[-\cosh(\theta_{\boldsymbol{k}})\sinh(\theta_{\boldsymbol{k}})\,\alpha^{\dagger}_{\boldsymbol{k}}\alpha_{\boldsymbol{k}} + \cosh^2(\theta_{\boldsymbol{k}})\,\alpha^{\dagger}_{\boldsymbol{k}}\beta^{\dagger}_{\boldsymbol{k}} - \sinh^2(\theta_{\boldsymbol{k}})\,\beta_{\boldsymbol{k}}\alpha_{\boldsymbol{k}} + \sinh(\theta_{\boldsymbol{k}})\cosh(\theta_{\boldsymbol{k}})\,\beta_{\boldsymbol{k}}\beta^{\dagger}_{\boldsymbol{k}}\Big]\Big[\sinh^2(\theta_{\boldsymbol{k}'})\,\alpha^{\dagger}_{\boldsymbol{k}'}\alpha_{\boldsymbol{k}'} - \sinh(\theta_{\boldsymbol{k}'})\cosh(\theta_{\boldsymbol{k}'})\,\alpha^{\dagger}_{\boldsymbol{k}'}\beta^{\dagger}_{\boldsymbol{k}'} - \cosh(\theta_{\boldsymbol{k}'})\sinh(\theta_{\boldsymbol{k}'})\,\beta_{\boldsymbol{k}'}\alpha_{\boldsymbol{k}'} + \cosh^2(\theta_{\boldsymbol{k}'})\,\beta_{\boldsymbol{k}'}\beta^{\dagger}_{\boldsymbol{k}'}\Big]; \tag{A.50}$$

$$a^{\dagger}_{\boldsymbol{k}}a_{\boldsymbol{k}}a^{\dagger}_{\boldsymbol{k}'}b_{\boldsymbol{k}'} = \Big[\cosh^2(\theta_{\boldsymbol{k}})\,\alpha^{\dagger}_{\boldsymbol{k}}\alpha_{\boldsymbol{k}} + \cosh(\theta_{\boldsymbol{k}})\sinh(\theta_{\boldsymbol{k}})\,\alpha^{\dagger}_{\boldsymbol{k}}\beta^{\dagger}_{\boldsymbol{k}} + \sinh(\theta_{\boldsymbol{k}})\cosh(\theta_{\boldsymbol{k}})\,\beta_{\boldsymbol{k}}\alpha_{\boldsymbol{k}} \sinh^2(\theta_{\boldsymbol{k}})\,\beta_{\boldsymbol{k}}\beta^{\dagger}_{\boldsymbol{k}}\Big]\Big[-\cosh(\theta_{\boldsymbol{k}'})\sinh(\theta_{\boldsymbol{k}'})\,\alpha_{\boldsymbol{k}'}\alpha^{\dagger}_{\boldsymbol{k}'} + \cosh(\theta_{\boldsymbol{k}'})\cosh(\theta_{\boldsymbol{k}'})\,\alpha_{\boldsymbol{k}'}\beta_{\boldsymbol{k}'} - \sinh(\theta_{\boldsymbol{k}'})\sinh(\theta_{\boldsymbol{k}'})\,\beta^{\dagger}_{\boldsymbol{k}'}\alpha_{\boldsymbol{k}'} + \sinh(\theta_{\boldsymbol{k}'})\cosh(\theta_{\boldsymbol{k}'})\,\beta^{\dagger}_{\boldsymbol{k}'}\beta_{\boldsymbol{k}'}\Big], \tag{A.51}$$

finally,

$$a^{\dagger}_{\boldsymbol{k}}a^{\dagger}_{\boldsymbol{k}}a_{\boldsymbol{k}'}b_{\boldsymbol{k}'} = \Big[\cosh^2(\theta_{\boldsymbol{k}})\,\alpha^{\dagger}_{\boldsymbol{k}}\alpha^{\dagger}_{\boldsymbol{k}} + \cosh(\theta_{\boldsymbol{k}})\sinh(\theta_{\boldsymbol{k}})\,\alpha^{\dagger}_{\boldsymbol{k}}\beta_{\boldsymbol{k}} + \sinh(\theta_{\boldsymbol{k}})\cosh(\theta_{\boldsymbol{k}})\,\beta_{\boldsymbol{k}}\alpha^{\dagger}_{\boldsymbol{k}} \sinh^2(\theta_{\boldsymbol{k}})\,\beta_{\boldsymbol{k}}\beta_{\boldsymbol{k}}\Big]\Big[-\cosh(\theta_{\boldsymbol{k}'})\sinh(\theta_{\boldsymbol{k}'})\,\alpha_{\boldsymbol{k}'}\alpha^{\dagger}_{\boldsymbol{k}'} + \cosh(\theta_{\boldsymbol{k}'})\cosh(\theta_{\boldsymbol{k}'})\,\alpha_{\boldsymbol{k}'}\beta_{\boldsymbol{k}'} - \sinh(\theta_{\boldsymbol{k}'})\sinh(\theta_{\boldsymbol{k}'})\,\beta^{\dagger}_{\boldsymbol{k}'}\alpha_{\boldsymbol{k}'} + \sinh(\theta_{\boldsymbol{k}'})\cosh(\theta_{\boldsymbol{k}'})\,\beta^{\dagger}_{\boldsymbol{k}'}\beta_{\boldsymbol{k}'}\Big]. \tag{A.52}$$

We now substitute Eqs. (A.48), (A.49), (A.50), (A.51) and (A.52) into Eq. (A.47); after a pretty long calculation together with a careful analysis, the relevant terms of $\mathcal{H}_2$ which contribute to the ground-state energy are

$$\mathcal{H}_2 = -\frac{zJ}{4N}\sum_{\boldsymbol{k},\boldsymbol{k}'}\Big\{\sinh^2(\theta_{\boldsymbol{k}})\sinh^2(\theta_{\boldsymbol{k}'}) - \frac{|\,\gamma_{\boldsymbol{k}}\,|}{2}\left[-2\sinh^2(\theta_{\boldsymbol{k}'})\sinh(\theta_{\boldsymbol{k}})\cosh(\theta_{\boldsymbol{k}})\right. \left.-2\sinh^2(\theta_{\boldsymbol{k}})\cosh(\theta_{\boldsymbol{k}'})\sinh(\theta_{\boldsymbol{k}'})\right] - |\,\gamma_{\boldsymbol{k}}\,|^2\left[-\cosh(\theta_{\boldsymbol{k}'})\sinh(\theta_{\boldsymbol{k}'})\cosh(\theta_{\boldsymbol{k}'})\right. \left.\times\sinh(\theta_{\boldsymbol{k}'}) - \sinh(\theta_{\boldsymbol{k}})\cosh(\theta_{\boldsymbol{k}})\sinh(\theta_{\boldsymbol{k}'})\cosh(\theta_{\boldsymbol{k}'})\right]\Big\} - \frac{2zJ}{N}\sum_{\boldsymbol{k},\boldsymbol{k}'}\alpha^{\dagger}_{\boldsymbol{k}}\alpha_{\boldsymbol{k}}\beta^{\dagger}_{\boldsymbol{k}'}\beta_{\boldsymbol{k}'}. \tag{A.53}$$

A slightly rearrangement of the terms yields:

$$\mathcal{H}_2 = -\frac{zJ}{4N}\left\{\sum_{\boldsymbol{k}}\left[\sinh^2(\theta_{\boldsymbol{k}}) + \frac{|\,\gamma_{\boldsymbol{k}}\,|}{2}\sinh(2\theta_{\boldsymbol{k}})\right]\right\}^2 - \frac{2zJ}{N}\sum_{\boldsymbol{k},\boldsymbol{k}'}\alpha^{\dagger}_{\boldsymbol{k}}\alpha_{\boldsymbol{k}}\beta^{\dagger}_{\boldsymbol{k}'}\beta_{\boldsymbol{k}'}. \tag{A.54}$$

With the help of Eq. (A.41), we find that the energetic contribution of $\mathcal{H}_2$ reads:

$$\epsilon_{2\boldsymbol{k}} = -\frac{zJ}{4N}\left[\sum_{\boldsymbol{k}}\left(\sqrt{1-\gamma_{\boldsymbol{k}}}-1\right)\right]^2. \tag{A.55}$$

Therefore, by adding Eqs. (A.29), (A.44) and (A.54), the resulting diagonalized Hamiltonian up to $\mathcal{O}\left(1/S^2\right)$, in $\boldsymbol{k}$-space, takes the form:

$$\begin{aligned}\mathcal{H}^s_{\boldsymbol{k}} = &-\frac{zS^2JN}{2} + hSN + zSJ\sum_{\boldsymbol{k}}\left[\left(\sqrt{1-\gamma^2_{\boldsymbol{k}}}-1\right)\right.\\ &\left.+\sqrt{1-\gamma^2_{\boldsymbol{k}}}\left(\alpha^\dagger_{\boldsymbol{k}}\alpha_{\boldsymbol{k}}+\beta^\dagger_{\boldsymbol{k}}\beta_{\boldsymbol{k}}\right)\right] - \frac{zJ}{2N}\left[\sum_{\boldsymbol{k}}\left(\sqrt{1-\gamma^2_{\boldsymbol{k}}}-1\right)\right]^2\\ &-h\sum_{\boldsymbol{k}}\left[\left(\frac{1}{\sqrt{1-\gamma^2_{\boldsymbol{k}}}}-1\right)+\frac{\alpha^\dagger_{\boldsymbol{k}}\alpha_{\boldsymbol{k}}+\beta^\dagger_{\boldsymbol{k}}\beta_{\boldsymbol{k}}}{\sqrt{1-\gamma^2_{\boldsymbol{k}}}}\right] - \frac{zJN}{8}\\ &-\frac{2zJ}{N}\sum_{\boldsymbol{k},\boldsymbol{k'}}\alpha^\dagger_{\boldsymbol{k}}\alpha_{\boldsymbol{k}}\beta^\dagger_{\boldsymbol{k'}}\beta_{\boldsymbol{k'}}.\end{aligned} \tag{A.56}$$

Finally, by adding Eqs. (A.29), (A.45) and (A.55), the ground-state energy per site in the presence of a magnetic field, in the thermodynamic limit, becomes:

$$\begin{aligned}\frac{E_h}{N} = &-\frac{zS^2J}{2} + hS + \frac{zSJ}{4\pi^2}\int_{\mathrm{BZ}} d^2k\left(\sqrt{1-\gamma^2_{\boldsymbol{k}}}-1\right)\\ &-\frac{zJ}{32\pi^4}\left[\int_{\mathrm{BZ}} d^2k\left(\sqrt{1-\gamma^2_{\boldsymbol{k}}}-1\right)\right]^2 - \frac{h}{4\pi^2}\int_{\mathrm{BZ}} d^2k\left(\frac{1}{\sqrt{1-\gamma^2_{\boldsymbol{k}}}}-1\right) - \frac{zJ}{8}.\end{aligned} \tag{A.57}$$

B.Derivation of Eq. (4.10)

We begin by writing the Hamiltonian of the Hubbard model on the honeycomb lattice, with the chemical potential μ, in the form:

$$\mathcal{H} = -t \sum_{\boldsymbol{ij}\alpha\beta\sigma} \left(\hat{c}^{\dagger}_{\boldsymbol{i}\alpha\sigma} \hat{c}_{\boldsymbol{j}\beta\sigma} + \hat{c}^{\dagger}_{\boldsymbol{j}\beta\sigma} \hat{c}_{\boldsymbol{i}\alpha\sigma} \right) + U \sum_{\boldsymbol{i}\alpha} \hat{n}_{\boldsymbol{i}\alpha\uparrow} \hat{n}_{\boldsymbol{i}\alpha\downarrow} - \mu \sum_{\boldsymbol{i}\alpha} \left(\hat{n}_{\boldsymbol{i}\alpha\uparrow} + \hat{n}_{\boldsymbol{i}\alpha\downarrow} \right). \quad \text{(B.1)}$$

Now, by performing the same calculation routine of Chapter 2, we summarize the main equations of which were altered due to the inclusion of the chemical potential and that are necessaries to analyze the doped regime. Hence, the Lagrangian density reads:

$$\begin{aligned} \mathcal{L}(\tau) \;=\; & \sum_{\boldsymbol{i}\alpha\sigma} a^{\dagger}_{\boldsymbol{i}\alpha\sigma} \left(\partial_{\tau} - \mu \right) a_{\boldsymbol{i}\alpha\sigma} + \sum_{\boldsymbol{i}\alpha\sigma\sigma'} a^{\dagger}_{\boldsymbol{i}\sigma'} (U_{\boldsymbol{i}\alpha})^{\dagger}_{\sigma'\sigma} \partial_{\tau} (U_{\boldsymbol{i}\alpha})_{\sigma'\sigma} a_{\boldsymbol{i}\alpha\sigma} \\ & - t \sum_{\boldsymbol{ij}\alpha\beta\sigma} \left(a^{\dagger}_{\boldsymbol{i}\alpha\sigma} a_{\boldsymbol{j}\beta\sigma} + \text{H.c.} \right) - t \sum_{\boldsymbol{ij}\alpha\beta\sigma\sigma'} \left[a^{\dagger}_{i\alpha\sigma'} \left(U^{\dagger}_{\boldsymbol{i}\alpha} U_{\boldsymbol{j}\beta} - 1 \right)_{\sigma'\sigma} a_{\boldsymbol{j}\beta\sigma} \right. \\ & \left. + \text{H.c.} \right] + \frac{U}{2} \sum_{\boldsymbol{i}\alpha\sigma} (1 - p_{\boldsymbol{i}\alpha}\sigma) a^{\dagger}_{\boldsymbol{i}\alpha\sigma} a_{\boldsymbol{i}\alpha\sigma}. \end{aligned} \quad \text{(B.2)}$$

For simplicity, let us decompose the above equation in two parts:

$$\begin{aligned} \mathcal{L}_0 \;=\; & \sum_{\boldsymbol{i}\alpha\beta\sigma} a^{\dagger}_{\boldsymbol{i}\alpha\sigma} \left(\partial_{\tau} - \mu \right) a_{\boldsymbol{i}\alpha\sigma} - t \sum_{\boldsymbol{ij}\alpha\beta\sigma} \left(a^{\dagger}_{\boldsymbol{i}\alpha\sigma} a_{\boldsymbol{j}\beta\sigma} + \text{H.c.} \right) \\ & + \frac{U}{2} \sum_{i\alpha\sigma} (1 - p_{\boldsymbol{i}\alpha}\sigma) a^{\dagger}_{\boldsymbol{i}\alpha\sigma} a_{\boldsymbol{i}\alpha\sigma}, \end{aligned} \quad \text{(B.3)}$$

and

$$\begin{aligned} \mathcal{L}_n \;=\; & \sum_{\boldsymbol{i}\alpha\sigma\sigma'} a a^{\dagger}_{\boldsymbol{i}\alpha\sigma'} (U_{\boldsymbol{i}\alpha})^{\dagger}_{\sigma'\sigma} \partial_{\tau} (U_{\boldsymbol{i}\alpha})_{\sigma'\sigma} a_{\boldsymbol{i}\alpha\sigma} \\ & - t \sum_{\boldsymbol{ij}\alpha\beta\sigma\sigma'} \left[a^{\dagger}_{\boldsymbol{i}\alpha\sigma'} \left(U^{\dagger}_{\boldsymbol{i}\alpha} U_{\boldsymbol{j}\beta} - 1 \right)_{\sigma'\sigma} a_{\boldsymbol{j}\beta\sigma} + \text{H.c.} \right]. \end{aligned} \quad \text{(B.4)}$$

The Hamiltonian associated with $\mathcal{L}_0$, in Eq.(B.3), takes the form:

$$\mathcal{H}_0 = -t \sum_{\boldsymbol{ij}\alpha\beta\sigma} \left(a^{\dagger}_{\boldsymbol{i}\alpha\sigma} a_{\boldsymbol{j}\beta\sigma} + \text{H.c.} \right) + \frac{U}{2} \sum_{\boldsymbol{i}\alpha\sigma} (1 - p_{\boldsymbol{i}\alpha}\sigma) a^{\dagger}_{\boldsymbol{i}\alpha\sigma} a_{\boldsymbol{i}\alpha\sigma} - \mu \sum_{\boldsymbol{i}\alpha\sigma} a^{\dagger}_{\boldsymbol{i}\alpha\sigma} a_{\boldsymbol{i}\alpha\sigma}. \quad \text{(B.5)}$$

Moreover, in $\boldsymbol{k}$-space, $\mathcal{H}_0$:

$$\mathcal{H}_0 = \sum_{\boldsymbol{k}\sigma} \left[\left(-E_{\boldsymbol{k}} + \frac{U-\mu}{2} \right) \alpha^{\dagger}_{\boldsymbol{k}\sigma} \alpha_{\boldsymbol{k}\sigma} + \left(E_{\boldsymbol{k}} + \frac{U-\mu}{2} \right) \beta^{\dagger}_{\boldsymbol{k}\sigma} \beta_{\boldsymbol{k}\sigma} \right], \tag{B.6}$$

where

$$u_{\boldsymbol{k}} = \frac{1}{\sqrt{2}} \sqrt{1 + \frac{|\epsilon_{\boldsymbol{k}}|}{E_{\boldsymbol{k}}}} \quad \text{and} \quad v_{\boldsymbol{k}} = \frac{1}{\sqrt{2}} \sqrt{1 - \frac{|\epsilon_{\boldsymbol{k}}|}{E_{\boldsymbol{k}}}}, \tag{B.7}$$

with

$$E_{\boldsymbol{k}} = \sqrt{\epsilon^2_{\boldsymbol{k}} + \frac{(U-\mu)^2}{4}}, \tag{B.8}$$

and

$$\epsilon_{\boldsymbol{k}} = t \sqrt{3 + 2\cos\left(\sqrt{3}k_y\right) + 4\cos\left(\frac{3k_x}{2}\right)\cos\left(\frac{\sqrt{3}k_y}{2}\right)}. \tag{B.9}$$

Notice that at half-filling the chemical potential $\mu = 0$.

In the strong-coupling regime, the Hamiltonian $\mathcal{H}_0$ in Eq. (B.5) becomes:

$$\begin{aligned} \mathcal{H}_0 \;=\; & -(J-\mu) \sum_{\boldsymbol{i}} \alpha^{\dagger}_i \alpha_i + (J+\mu) \sum_{\boldsymbol{i}} \beta^{\dagger}_{\boldsymbol{i}} \beta_{\boldsymbol{i}} - \frac{J}{8} \sum_{ij} \Big(\alpha^{\dagger}_i \alpha_{i+\hat{\boldsymbol{e}}_j} \\ & - \beta^{\dagger}_{\boldsymbol{i}} \beta_{i+\hat{\boldsymbol{e}}_j} + \text{H.c.} \Big) + U \sum_{\boldsymbol{i}} \beta^{\dagger}_{\boldsymbol{i}} \beta_{\boldsymbol{i}}. \end{aligned} \tag{B.10}$$

Correspondingly, the Lagrangian density related to the above equation reads:

$$\begin{aligned} \mathcal{L}_0 \;=\; & \alpha^{\dagger}_i \partial_\tau \alpha_i - \beta^{\dagger}_{\boldsymbol{i}} \partial_\tau \beta_{\boldsymbol{i}} - (J-\mu) \sum_{\boldsymbol{i}} \alpha^{\dagger}_i \alpha_i - \frac{J}{8} \sum_{ij} \Big(\alpha^{\dagger}_i \alpha_{i+\hat{\boldsymbol{e}}_j} \\ & - \beta^{\dagger}_{\boldsymbol{i}} \beta_{i+\hat{\boldsymbol{e}}_j} + \text{H.c.} \Big) + (U+J+\mu) \sum_{\boldsymbol{i}} \beta^{\dagger}_{\boldsymbol{i}} \beta_{\boldsymbol{i}}. \end{aligned} \tag{B.11}$$

Therefore, we find that the effective low-energy Lagrangian of the honeycomb Hubbard model in the large-U limit, up to J order, is given by

$$\begin{aligned} \mathcal{L} \;=\; & \sum_{\boldsymbol{i}} \alpha^{\dagger}_{\boldsymbol{i}} \left(\partial_\tau - \mu \right) \alpha_{\boldsymbol{i}} + \sum_{\boldsymbol{i}\alpha\sigma} \theta(\sigma) \left(U^{\dagger}_{\boldsymbol{i}\alpha} \partial_\tau U_{\boldsymbol{i}\alpha} \right)_{\sigma\sigma} \alpha^{\dagger}_{\boldsymbol{i}} \alpha_{\boldsymbol{i}} - \frac{J}{8} \sum_{\boldsymbol{i}j\alpha\beta\sigma} \theta(\sigma) \\ & \left[\left| \left(U^{\dagger}_{\boldsymbol{i}\alpha} U_{\boldsymbol{i}+\hat{\boldsymbol{e}}_j\beta} \right)_{\sigma\sigma} \right|^2 + \left| \left(U^{\dagger}_{\boldsymbol{i}\alpha} U_{\boldsymbol{i}-\hat{\boldsymbol{e}}_j\beta} \right)_{\sigma\sigma} \right|^2 \right] \alpha^{\dagger}_{\boldsymbol{i}} \alpha_{\boldsymbol{i}} + \frac{J}{8t} \sum_{\boldsymbol{i}j\alpha\sigma} \left(U^{\dagger}_{\boldsymbol{i}\alpha} \partial_\tau U_{\boldsymbol{i}\alpha} \right)_{\sigma,-\sigma} \\ & \Big[\theta(\sigma) \alpha^{\dagger}_{\boldsymbol{i}} \left(\alpha_{\boldsymbol{i}+\hat{\boldsymbol{e}}_j} + \alpha_{\boldsymbol{i}-\hat{\boldsymbol{e}}_j} \right) + \theta(-\sigma) \left(\alpha^{\dagger}_{\boldsymbol{i}+\hat{\boldsymbol{e}}_j} + \alpha^{\dagger}_{\boldsymbol{i}-\hat{\boldsymbol{e}}_j} \right) \alpha_{\boldsymbol{i}} \Big] - t \sum_{\boldsymbol{i}j\alpha\beta\sigma} [\theta(\sigma) \\ & \left(U^{\dagger}_{\boldsymbol{i}\alpha} U_{\boldsymbol{i}+\hat{\boldsymbol{e}}_j\beta} \right)_{\sigma,-\sigma} \alpha^{\dagger}_{\boldsymbol{i}} \alpha_{\boldsymbol{i}+\hat{\boldsymbol{e}}_j} + \text{H.c.} \Big]. \end{aligned} \tag{B.12}$$

Further, by performing the Legendre transform:

$$\mathcal{H} = -\sum_{\boldsymbol{i}} \frac{\partial \mathcal{L}}{\partial \left(\partial_\tau h_{\boldsymbol{i}}\right)} \partial_\tau h_{\boldsymbol{i}} + \mathcal{L}, \tag{B.13}$$

where

$$\frac{\partial \mathcal{L}}{\partial \left(\partial_\tau h_{\boldsymbol{i}}\right)} = h_{\boldsymbol{i}}^{\dagger}, \tag{B.14}$$

we can write down the corresponding Hamiltonian as:

$$\begin{aligned}
\mathcal{H} \;=\; & \sum_{\boldsymbol{i}\alpha\sigma} \theta(\sigma) \left(U_{\boldsymbol{i}\alpha}^{\dagger} \partial_\tau U_{\boldsymbol{i}\alpha}\right)_{\sigma\sigma} \left(1 - h_{\boldsymbol{i}}^{\dagger} h_{\boldsymbol{i}}\right) - \frac{J}{8} \sum_{\boldsymbol{i}j\alpha\beta\sigma} \theta(\sigma) \Big[\Big| \left(U_{\boldsymbol{i}\alpha}^{\dagger} U_{\boldsymbol{i}+\hat{\boldsymbol{e}}_j\beta}\right)_{\sigma\sigma} \Big|^2 \\
& + \Big| \left(U_{\boldsymbol{i}\alpha}^{\dagger} U_{\boldsymbol{i}-\hat{\boldsymbol{e}}_j\beta}\right)_{\sigma\sigma} \Big|^2 \Big] \left(1 - h_{\boldsymbol{i}}^{\dagger} h_{\boldsymbol{i}}\right) + \frac{J}{8t} \sum_{\boldsymbol{i}j\alpha\sigma} \left(U_{\boldsymbol{i}\alpha}^{\dagger} \partial_\tau U_{\boldsymbol{i}\alpha}\right)_{\sigma,-\sigma} \Big[\theta(\sigma) h_{\boldsymbol{i}}^{\dagger} \left(h_{\boldsymbol{i}+\hat{\boldsymbol{e}}_j}\right. \\
& \left. + h_{i-\hat{\boldsymbol{e}}_j}\right) + \text{H.c.}\Big] - t \sum_{\boldsymbol{i}j\alpha\beta\sigma} \Big[\theta(\sigma) \left(U_{\boldsymbol{i}\alpha}^{\dagger} U_{\boldsymbol{i}+\hat{\boldsymbol{e}}_j\beta}\right)_{\sigma,-\sigma} \\
& h_{\boldsymbol{i}}^{\dagger} h_{\boldsymbol{i}+\hat{\boldsymbol{e}}_j} + \text{H.c.}\Big] - \mu \sum_{\boldsymbol{i}} \left(1 - h_{\boldsymbol{i}}^{\dagger} h_{\boldsymbol{i}}\right).
\end{aligned} \tag{B.15}$$

Let us now introduce the SU(2)-matrix, $U_{\boldsymbol{i}\alpha}^{SC}$, in the form :

$$U_{\boldsymbol{i}\alpha}^{\text{SC}} = \begin{bmatrix} \sum_j \chi_{\hat{\boldsymbol{e}}_j} & -\sum_j \Delta_{\hat{\boldsymbol{e}}_j} \\ \sum_j \Delta_{\hat{\boldsymbol{e}}_j} & \sum_j \chi_{\hat{\boldsymbol{e}}_j} \end{bmatrix}, \tag{B.16}$$

where $\Delta_{\hat{\boldsymbol{e}}_j}$ is the nearest-neighbor spin-singlet pairing correlation and $\chi_{\hat{\boldsymbol{e}}_j}$ is the nearest-neighbor single-particle hopping correlation.

In the sequence, we explicit the elements of the matrix product that appears in Eq.(B.15), for instance, for the diagonal and off-diagonal terms:

$$\left(U_{\boldsymbol{i}\alpha}^{\dagger} U_{i+\hat{\boldsymbol{e}}_j\beta}\right)_{\sigma\sigma} = \sum_j \left(\chi_{\hat{\boldsymbol{e}}_j} + \Delta_{\hat{\boldsymbol{e}}_j}\right), \tag{B.17}$$

$$\left(U_{\boldsymbol{i}\alpha}^{\dagger} U_{\boldsymbol{i}+\hat{\boldsymbol{e}}_j\beta}\right)_{\sigma,-\sigma} = \sum_j 2\chi_{\hat{\boldsymbol{e}}_j} \Delta_{\hat{\boldsymbol{e}}_j}, \tag{B.18}$$

Now, by inserting the Eq. (B.17) and (B.18) into Eq. (B.15), we obtain that the Hamiltonian, $\mathcal{H}$, in $\boldsymbol{k}$-space, assumes the form:

$$\begin{aligned}
\mathcal{H} \;=\; & -\frac{J}{4} \sum_{\boldsymbol{k}} \left\{ \left[\left(\Delta_{\boldsymbol{k}}^{c} + \Delta_{\boldsymbol{k}}^{s}\right) w_{\boldsymbol{k}}\right]^2 b_{\boldsymbol{k}}^{\dagger} b_{\boldsymbol{k}} + \text{H.c.} \right\} - \frac{J}{2} \sum_{\boldsymbol{k}j} |\Delta_{\hat{\boldsymbol{e}}_j}|^2 \left(1 - a_{\boldsymbol{k}}^{\dagger} a_{\boldsymbol{k}}\right) \\
& - 2t \sum_{\boldsymbol{k}j} \chi_{\hat{\boldsymbol{e}}_j} \left[\left(\Delta_{\boldsymbol{k}}^{c} + \Delta_{\boldsymbol{k}}^{s}\right) w_{\boldsymbol{k}} a_{\boldsymbol{k}}^{\dagger} b_{\boldsymbol{k}} + \text{H.c.}\right] - \mu \sum_{\boldsymbol{k}} \left(1 - a_{\boldsymbol{k}}^{\dagger} a_{\boldsymbol{k}}\right),
\end{aligned} \tag{B.19}$$

where we defined:

$$\Delta_{\boldsymbol{k}}^{c} \equiv \sum_{j} \Delta_{\hat{\boldsymbol{e}}_j} \cos\left(\boldsymbol{k}\cdot\hat{\boldsymbol{e}}_j\right), \tag{B.20}$$

$$\Delta_{\boldsymbol{k}}^{s} \equiv i\sum_{j} \Delta_{\hat{\boldsymbol{e}}_j} \sin\left(\boldsymbol{k}\cdot\hat{\boldsymbol{e}}_j\right), \tag{B.21}$$

and

$$w_{\boldsymbol{k}} \equiv \sum_{j} \exp\left(i\boldsymbol{k}\cdot\hat{\boldsymbol{e}}_j\right). \tag{B.22}$$

At this stage, let us introduce the new set of fields:

$$A_{\boldsymbol{k}} = \frac{a_{\boldsymbol{k}}}{\sqrt{2}} + \frac{w_{\boldsymbol{k}}}{\sqrt{2}|w_{\boldsymbol{k}}|} b_{\boldsymbol{k}}, \tag{B.23}$$

$$B_{\boldsymbol{k}} = \frac{a_{\boldsymbol{k}}}{\sqrt{2}} - \frac{w_{\boldsymbol{k}}}{\sqrt{2}|w_{\boldsymbol{k}}|} b_{\boldsymbol{k}}. \tag{B.24}$$

So that, by placing the Eqs. (B.23) and (B.24) into Eq. (B.19), we get

$$\begin{aligned}
\mathcal{H} \;=\; \sum_{\boldsymbol{k}} \Bigg\{ & \left[-\epsilon_{\boldsymbol{k}}\chi_{\boldsymbol{k}}\Delta_{\boldsymbol{k}}^{c} - \frac{J|w_{\boldsymbol{k}}|^2\left[(\Delta_{\boldsymbol{k}}^{c})^2 + (\Delta_{\boldsymbol{k}}^{s})^2\right]}{4} - \frac{J|w_{\boldsymbol{k}}|^2\chi_{\boldsymbol{k}}^2}{4} + \frac{J\chi_{\boldsymbol{k}}\Delta_{\boldsymbol{k}}^{c}|w_{\boldsymbol{k}}|^2}{2} - \frac{\mu}{2} \right] A_{\boldsymbol{k}}^{\dagger}A_{\boldsymbol{k}} \\
& + \left[\epsilon_{\boldsymbol{k}}\chi_{\boldsymbol{k}}\Delta_{\boldsymbol{k}}^{s} + \frac{J|w_{\boldsymbol{k}}|^2\left[(\Delta_{\boldsymbol{k}}^{c})^2 + (\Delta_{\boldsymbol{k}}^{s})^2\right]}{4} + \frac{J|w_{\boldsymbol{k}}|^2\chi_{\boldsymbol{k}}^2}{4} - \frac{J\chi_{\boldsymbol{k}}\Delta_{\boldsymbol{k}}^{c}|w_{\boldsymbol{k}}|^2}{2} + \frac{\mu}{2} \right] A_{\boldsymbol{k}}^{\dagger}B_{\boldsymbol{k}} \\
& + \left[\epsilon_{\boldsymbol{k}}\chi_{\boldsymbol{k}}\Delta_{\boldsymbol{k}}^{s} + \frac{J|w_{\boldsymbol{k}}|^2\left[(\Delta_{\boldsymbol{k}}^{c})^2 + (\Delta_{\boldsymbol{k}}^{s})^2\right]}{4} + \frac{J|w_{\boldsymbol{k}}|^2\chi_{\boldsymbol{k}}^2}{4} - \frac{J\chi_{\boldsymbol{k}}\Delta_{\boldsymbol{k}}^{c}|w_{\boldsymbol{k}}|^2}{2} + \frac{\mu}{2} \right] B_{\boldsymbol{k}}^{\dagger}A_{\boldsymbol{k}} \\
& + \left[\epsilon_{\boldsymbol{k}}\chi_{\boldsymbol{k}}\Delta_{\boldsymbol{k}}^{c} - \frac{J|w_{\boldsymbol{k}}|^2\left[(\Delta_{\boldsymbol{k}}^{c})^2 + (\Delta_{\boldsymbol{k}}^{s})^2\right]}{4} - \frac{J|w_{\boldsymbol{k}}|^2\chi_{\boldsymbol{k}}^2}{4} + \frac{J\chi_{\boldsymbol{k}}\Delta_{\boldsymbol{k}}^{c}|w_{\boldsymbol{k}}|^2}{2} - \frac{\mu}{2} \right] B_{\boldsymbol{k}}^{\dagger}B_{\boldsymbol{k}} \Bigg\},
\end{aligned} \tag{B.25}$$

with $\epsilon_{\boldsymbol{k}} \equiv t|w_{\boldsymbol{k}}|$.

Let us introduce the Bogoliubov transformation:

$$A_{\boldsymbol{k}} = u_{\boldsymbol{k}}\alpha_{\boldsymbol{k}} - v_{\boldsymbol{k}}\beta_{\boldsymbol{k}}, \quad B_{\boldsymbol{k}} = v_{\boldsymbol{k}}\alpha_{\boldsymbol{k}} + u_{\boldsymbol{k}}\beta_{\boldsymbol{k}}, \tag{B.26}$$

restricted to the canonical constraint $(u_{\boldsymbol{k}})^2 + (v_{\boldsymbol{k}})^2 = 1$. Furthermore, it is convenient to use the Nambu spinor representation [36]

$$\Psi_{\boldsymbol{k}} = \begin{pmatrix} \alpha_{\boldsymbol{k}} \\ \beta_{\boldsymbol{k}} \end{pmatrix}, \tag{B.27}$$

such that, by plugging the Eqs. (B.26) and (B.27) into Eq. (B.25), after a pretty long calculation, we obtain:

$$\mathcal{H} = \sum_{\boldsymbol{k}} \Psi_{\boldsymbol{k}}^{\dagger} \tilde{E}_{\boldsymbol{k}}^{SC} \Psi_{\boldsymbol{k}} + \frac{3JN_c\chi^2}{2} + \sum_j \frac{JN_c\Delta_{\hat{\boldsymbol{e}}_j}^2}{2} - N_c\mu, \tag{B.28}$$

with

$$\tilde{E}_{\boldsymbol{k}}^{SC} = \begin{pmatrix} -E_{\boldsymbol{k}}^{SC} & 0 \\ 0 & E_{\boldsymbol{k}}^{SC} \end{pmatrix}, \tag{B.29}$$

and $E_{\boldsymbol{k}}^{SC}$, that defines the band spectrum of the superconducting phases, is given by

$$E_{\boldsymbol{k}}^{SC} = \left\{ \left[\epsilon_{\boldsymbol{k}}\chi_{\boldsymbol{k}}\Delta_{\boldsymbol{k}} + \frac{J}{4t^2}\chi_{\boldsymbol{k}}^2\epsilon_{\boldsymbol{k}}^2 - \frac{\mu}{2} + \frac{J}{4t^2}\chi_{\boldsymbol{k}}\Delta_{\boldsymbol{k}}\epsilon_{\boldsymbol{k}}^2 \right]^2 + (\epsilon_{\boldsymbol{k}}\chi_{\boldsymbol{k}}\Delta_{\boldsymbol{k}})^2 \right\}^{1/2}, \tag{B.30}$$

in which

$$\Delta_{\boldsymbol{k}} \equiv \sum_j \Delta_{\hat{\boldsymbol{e}}_j} \cos\left(\boldsymbol{k}\cdot\hat{\boldsymbol{e}}_j\right), \tag{B.31}$$

$$\chi_{\boldsymbol{k}} \equiv \sum_j \chi_{\hat{\boldsymbol{e}}_j} \cos\left(\boldsymbol{k}\cdot\hat{\boldsymbol{e}}_j\right). \tag{B.32}$$

C. Tight-Binding Density of States

The non-interacting density of states per unit cell $\rho(\varepsilon)$ is defined by

$$\rho(\varepsilon) = \lim_{N_c \longrightarrow \infty} \frac{1}{N_c} \sum_{\boldsymbol{k},s} \delta\left(\frac{\epsilon_{\boldsymbol{k},s}}{t} - \varepsilon\right), \tag{C.1}$$

in the thermodynamic limit, Eq. C.1 can be written in the convenient form:

$$\rho(\varepsilon) = \frac{1}{4\pi^2} \sum_{s=\pm} \int_0^{2\pi} dx \int_0^{2\pi} dy \delta\left[s\sqrt{3 + 2\cos(x) + 2\cos(y) + 2\cos(x+y)} - \varepsilon\right], \tag{C.2}$$

where we have used the tight-binding spectrum:

$$\epsilon_{\boldsymbol{k}} = t\sqrt{3 + 2\cos(\sqrt{3}k_y) + 4\cos\left(\frac{3k_x}{2}\right)\cos\left(\frac{\sqrt{3}k_y}{2}\right)}. \tag{C.3}$$

We now proceed by calculating the number of frequencies whose squared-values lie between ε^2 and $\varepsilon^2 + d\varepsilon^2$, i.e., we search the frequency distribution $g\left(\varepsilon^2\right) d\varepsilon^2$, such that $\rho(\varepsilon) = 2 \mid \varepsilon \mid g\left(\varepsilon^2\right)$. We thus have

$$g\left(\varepsilon^2\right) = \frac{1}{\pi^2} \int_0^{\pi} d\theta \int_0^{\pi} \delta\left[1 + 4\cos(2\theta)\cos(\phi) + 4\cos^2(2\theta) - \varepsilon^2\right], \tag{C.4}$$

in which we employed the substitutions:

$$x = 2\theta + \phi; \quad y = 2\theta - \phi, \tag{C.5}$$

where $0 \leq \theta$ and $\phi \leq \pi$. Moreover, upon using the following substitutions:

$$u = \cos(2\theta); \quad \upsilon = \cos(\phi), \tag{C.6}$$

we can rewrite Eq. (C.4) in the form:

$$g\left(\varepsilon^2\right) = \frac{2}{\pi^2} \int_{-1}^{1} du \int_{-1}^{1} d\upsilon \frac{\delta\left(1 + 4u\upsilon + 4u^2 - \varepsilon^2\right)}{2\sqrt{1-u^2}\sqrt{1-\upsilon^2}}. \tag{C.7}$$

At this stage, we define:

$$\mathcal{I}\left(u, \varepsilon^2\right) \equiv \int_{-1}^{1} d\upsilon \frac{\delta\left(1 + 4u\upsilon + 4u^2 - \varepsilon^2\right)}{\sqrt{1-\upsilon^2}}, \tag{C.8}$$

and applying the substitution $z = u\,(u+\upsilon)$, we can write down Eq. (C.8) as:

$$\mathcal{I}\left(u,\varepsilon^2\right) = \int_{u(u-1)}^{u(u+1)} dz \frac{\operatorname{sgn}(u)\,\delta\left(1+4z-\varepsilon^2\right)}{\sqrt{(z-u\,(u-1))\,(u\,(u+1)-1)}}. \tag{C.9}$$

The integral in Eq. (C.9) is of form:

$$\mathcal{I} = \int_a^b f\,(z)\,\delta\left[p\,(z)\right] dz. \tag{C.10}$$

It can be calculated by defining $w \equiv p\,(z)$ and the solution $z = q\,(w)$, such that $dz = q^{'}\,(w)\,dw$ in which $q^{'}\,(w) = dq\,(w)\,/dw$ [94]. Thus, by using the following property of Dirac delta function:

$$\int_\alpha^\beta \mathcal{F}\,(w)\,\delta\,(w)\,dw = \begin{cases} \mathcal{F}\,(0)\,, & \text{for} \quad \alpha\beta < 0, \\ 0, & \text{otherwise,} \end{cases} \tag{C.11}$$

we get

$$I = \begin{cases} f\left[q\,(0)\right] q^{'}\,(0)\,, & p\,(a)\,p\,(b) < 0, \\ 0, & \text{otherwise.} \end{cases} \tag{C.12}$$

In order to relate the above result to the integral in Eq.(C.9), we write down:

$$f\,(z) = \frac{1}{\sqrt{(z-a)\,(b-z)}}, \tag{C.13}$$

with

$$a = \begin{cases} u\,(u-1)\,, & \text{for} \quad u > 0, \\ u\,(u+1)\,, & \text{for} \quad u < 0, \end{cases} \tag{C.14}$$

and

$$b = \begin{cases} u\,(u+1)\,, & \text{for} \quad u > 0, \\ u\,(u-1)\,, & \text{for} \quad u < 0, \end{cases} \tag{C.15}$$

as well as

$$q\,(w) = \frac{1\left[w-\left(1-\varepsilon^2\right)\right]}{4}, \tag{C.16}$$

and

$$p\,(z) = 1 + 4z - \varepsilon^2. \tag{C.17}$$

Thus, by substituting Eqs. (C.13) (C.14), (C.15), (C.16) and (C.17) into Eq. (C.9), we obtain:

$$I = \begin{cases} \frac{1}{4\sqrt{[q(0)-a][b-q(0)]}}, & [q\,(0)-a]\,[b-q\,(0)] > 0 \\ 0, & \text{otherwise.} \end{cases} \tag{C.18}$$

In the sequence, we define $\xi \equiv u^2$, so that $[q\,(0)-a]\,[b-q\,(0)]$ we can be written as $(\xi_+ - \xi)\,(\xi_- - \xi)$, where

$$\xi_\pm = \frac{(\mid \xi \mid \pm 1)^2}{4}. \tag{C.19}$$

At this point, to evaluate $g\left(\varepsilon^2\right)$, it is important to use the following identity [74]:

$$\int_{\alpha}^{\beta} \frac{dx}{x\left(\gamma-x\right)\left(\beta-x\right)\left(\alpha-x\right)} = \frac{2}{\sqrt{\beta\left(\alpha-\gamma\right)}}\mathbb{F}\left(\frac{\pi}{2},\sqrt{\frac{\alpha\left(\beta-\gamma\right)}{\beta\left(\alpha-\gamma\right)}}\right), \tag{C.20}$$

in which $\alpha \geq \beta \geq \gamma \geq 0$ and $\mathbb{F}\left(\pi/2,k\right)$ is the complete elliptical integral of the first kind. Thus, for $\mid \xi \mid \leq 1$, we have $1 \geq \xi_{+} \geq \xi_{-} \geq 0$, while we have $\xi_{+} \geq 1 \geq \xi_{-} \geq 0$, when $1 \leq \mid \xi \mid \leq 3$.

Now, let us take $Z_0 = 4\beta\left(\alpha-\gamma\right)$ and $Z_1 = 4\alpha\left(\beta-\gamma\right)$, such that substituting Eqs. (C.18) and (C.20) into Eq. (C.7) yields:

$$g\left(\xi^2\right) = \frac{1}{\pi^2\sqrt{Z_0}}\mathbb{F}\left(\frac{\pi}{2},\sqrt{\frac{Z_1}{Z_0}}\right). \tag{C.21}$$

Correspondingly,

$$\rho\left(\epsilon\right) = \frac{4 \mid \varepsilon \mid}{\pi^2 t^2\sqrt{Z_0}}\mathbb{F}\left(\frac{\pi}{2},\sqrt{\frac{Z_0}{Z_1}}\right), \tag{C.22}$$

in which

$$Z_0 = \begin{cases} \left(1+\mid \varepsilon \mid\right)^2 - \frac{1}{4}\left(\mid \varepsilon \mid^2 -1\right)^2, & \text{for} \quad \mid \varepsilon \mid \leq 1, \\ 4 \mid \varepsilon \mid, & \text{for} \quad 1 \leq \mid \varepsilon \mid \leq 3, \end{cases} \tag{C.23}$$

and

$$Z_1 = \begin{cases} 4 \mid \varepsilon \mid, & \text{for} \quad \mid \varepsilon \mid \leq 1, \\ \left(1+\mid \varepsilon \mid\right)^2 - \frac{1}{4}\left(\mid \varepsilon \mid^2 -1\right)^2, & \text{for} \quad 1 \leq \mid \varepsilon \mid \leq 3, \end{cases} \tag{C.24}$$

with

$$\mathbb{F}\left(\frac{\pi}{2},k\right) = \int_{0}^{\frac{\pi}{2}} \frac{d\theta}{\sqrt{1-k^2\sin^2\left(\theta\right)}}. \tag{C.25}$$